Designing an Inhibitor for AAC(6')-Ii by Fragment-based Drug Design using SAR by NMR

Eric Habib

Department of Chemistry
McGill University
Montreal, Quebec, Canada
H3A 0B8

July 2013

A thesis submitted to McGill University in the partial fulfillment of the requirements of the degree of Master of Science

To my wife Elisabeth.

Table of Contents

TABLE OF CONTENTS	III
LIST OF FIGURES	VII
LIST OF SCHEMES	X
LIST OF TABLES	XI
LIST OF ABBREVIATIONS	XII
ABSTRACT	XIV
RÉSUMÉ	XVI
ACKNOWLEDGEMENTS	XVIII
CHAPTER 1 INTRODUCTION	1
1.1 Research Motivation	2
1.2 Aminoglycoside N-6'-Acetyltransferase Ii	
1.2.1 Mechanistic and Structural Studies	8
1.2.2 Inhibitors	10
1.3 Fragment-based Drug Design	11
1.4 Protein-Ligand Screening	15
1.4.1 Nuclear Magnetic Resonance (NMR) Spectroscopy	15
1.4.2 Protein-Observe NMR Methods	16
1.4.3 Ligand-Observe Experiments	20
1.4.4 Comparison of NMR Methods for Screening	27
1.4.5 Differential Scanning Fluorimetry	29
1.5 Protein-Ligand Complex Characterization	31
1.5.1 Circular Dichroism Spectroscopy	31
1.5.2 Measurements of Enzyme Kinetics	33
1.5.3 Interligand Nuclear Overhauser Effect NMR	
1.6 Thesis Goals	37
CHAPTER 2 FRAGMENT SCREENING	39
2.1 Preface	40
2.2 Introduction	40
2.3 HSQC Ligand Screening	41
2.3.1 Initial HSQC Screening of Mixtures	42
2.4 SATURATION TRANSFER DIFFERENCE SCREENING AND COMPETITION ASSAYS	46
2.5 STRUCTURAL INFORMATION FROM HSQCs	
2.6 OTHER NMR METHODS	54
2.7 CONCLUSION	54

CHAPTER 3 - BIOLOGICAL ACTIVITY	56
3.1 Preface	57
3.2 Introduction	
3.3 SYNTHESIS AND DERIVATIVES	58
3.3.1 Derivatives of 2.1	
3.3.2 Derivatives of 2.2	
3.3.3 Hybrids	
3.4 T _M OF AAC(6')-II	
3.4.1 T_m of AAC(6')-Ii in the Presence of Natural Substrates and Known Inhibitors	
3.4.2 Fragments	
3.4.3 Hybrids	
3.5 KINETIC STUDIES OF AAC(6')-II	74
3.5.1 Derivatives of 2.1	
3.5.2 Derivatives of 2.2	
3.5.3 Hybrids	77
3.6 Conclusion	77
CHAPTER 4 CONTRIBUTIONS AND FUTURE DIRECTION	79
4.1 Contributions	80
4.2 Future Directions	81
CHAPTER 5 EXPERIMENTAL	83
5.1 Instruments	84
5.2 BIOLOGICAL STUDIES	85
5.2.1 Materials	85
5.2.2 Expression of Aminoglycoside N-6'-Acetyltransferase Ii	85
5.2.3 Expression of ¹⁵ N labeled AAC(6')-Ii	86
5.2.4 Purification of AAC(6')-Ii	86
5.2.5 NMR:HSQC, STD, STD-TOCSY, TOCSY, ILOE	89
5.2.6 HSQC	89
5.2.7 STD and STD-TOCSY	89
5.2.8 ILOE	89
5.2.9 Circular Dichroism (CD)	89
5.2.10 Differential Scanning Fluorimetry (DSF)	90
5.2.11 Kinetics Studies – UV-vis, Stopped-flow	90
5.2.12 Docking	91
5.3 Synthesis	91
5.3.1 Chemicals	91
5.3.2 Compound characterization	92
REFERENCES	106

APPENDIX A	. 112
APPENDIX R – COMPONENT COMPOUNDS OF MIXTURES	124

List of Figures

Figure 1.1- Structures of six antibacterial compound classes a) Aminoglycoside
(neomycin); b) Ansamycin (geldanamycin); c) Carbapenem (imipenem); d)
Cephalosporin (cefacetril); e) Macrolide (erythromycin); f) Quinolone (nalidixic acid) 3
Figure 1.2 - Antibiotic resistance mechanisms: a) normal antibiotic binding b) efflux c)
permeability decrease d) target modification e) drug modification (molecular bypass not
shown)
Figure 1.3 - Crystal structure of AAC(6')-Ii bound to coenzyme A [19]
Figure 1.4 - AAC(6')-Ii catalyzed reaction. Shown with AcCoA and Neomycin B 9
Figure 1.5 – First and second generation of AAC(6')-Ii inhibitors
Figure 1.6 - Fragment screening and fragment buildup approaches for fragment
improvement
Figure 1.7 - 1-4) fragments Lombès found to bind with micromolar affinity, 5)
bisubstrate extension with best fragment showed 950nM binding [28]
Figure 1.8 - (top) HSQC spectrum of the apo form of AAC(6')-Ii (bottom) Correlation
between amide proton and nitrogen on the peptide backbone
Figure 1.9 - NMR signal exchange rates affect peak position and broadening
Figure 1.10 - Example of T1ρ experiment with FK506 binding protein and a mixture of
9 compounds. A) nine compound mixture without protein B) with FK506 binding
protein. A clear decrease is observed in the residues indicated by dotted lines. Figure
adapted from [1]
Figure 1.11 - Saturation transfer mechanics for STD reference and on-resonance spectra.
The reference spectrum saturates away from any molecules in solution, such that nothing
is saturated in solution. The on-resonance spectrum saturates the protein. Upon ligand
is saturated in solution. The on-resonance spectrum saturates the protein. Opon figuria
binding (circles), saturation transfers to them. Non-binding ligands (squares) are not
•
binding (circles), saturation transfers to them. Non-binding ligands (squares) are not
binding (circles), saturation transfers to them. Non-binding ligands (squares) are not affected. Blue colour indicates saturation
binding (circles), saturation transfers to them. Non-binding ligands (squares) are not affected. Blue colour indicates saturation
binding (circles), saturation transfers to them. Non-binding ligands (squares) are not affected. Blue colour indicates saturation
binding (circles), saturation transfers to them. Non-binding ligands (squares) are not affected. Blue colour indicates saturation
binding (circles), saturation transfers to them. Non-binding ligands (squares) are not affected. Blue colour indicates saturation
binding (circles), saturation transfers to them. Non-binding ligands (squares) are not affected. Blue colour indicates saturation
binding (circles), saturation transfers to them. Non-binding ligands (squares) are not affected. Blue colour indicates saturation
binding (circles), saturation transfers to them. Non-binding ligands (squares) are not affected. Blue colour indicates saturation
binding (circles), saturation transfers to them. Non-binding ligands (squares) are not affected. Blue colour indicates saturation

Figure 1.18 - Michaelis-Menten plot and the values that can be extracted from it.
Independent axis is substrate concentration, while the dependent axis is Initial enzyme
reaction rate
Figure 1.19 - ILOE shows positive resonances for bound ligand and negative resonances
for unbinding ligand
Figure 2.1 HSQC spectrum of AAC(6')-Ii alone (black) and with Neomycin B (red)42
Figure 2.2 - A sample spectrum comparing protein alone with protein with mixture 1
(spectrum in black), with positive changes highlighted in yellow and negative changes
highlighted in aqua44
Figure 2.3 - Structures of the two hits: N-(3-aminopropyl) morpholine (APM) and b. 4-
hydroxyphenethyl alcohol (2.2)
Figure 2.4 - Comparing the (top) STD spectrum (on-resonance spectrum – reference
spectrum) to the (bottom) reference proton spectrum of 2.2
Figure 2.5 - Interligand NOE spectrum of 2.1 and 2.2 with the protein a. full spectrum b.
zooming in on the circled region. Negative peaks (red) indicate intramolecular relaxation
while positive peaks (blue) indicate intermolecular relaxation between 2.1 and 2.2 while
in the ternary protein-bound complex
Figure 2.6 - Competition STD experiment showing that residues both from 2.2 and 2.1
are still visible at when at high concentrations (> $10 \times K_d$). Top blue off-resonance
spectrum corresponds to the ¹ H pre-saturation spectrum, bottom blue spectrum is the
STD spectrum. 50
Figure 2.7 - Overlay of ¹⁵ N/ ¹ H HSQC spectra of AAC(6')-Ii bound to CoA (black) and
the protein bound to CoA and 2.1 (red).
Figure 2.8 - Crystal structure of AAC(6')-Ii with the 2.1 spectral shifts shown in red
space fill and 2.2 spectral shifts shown in blue space fill a. view showing the binding site
b. view showing alpha helix residues c. view showing distant changes53
Figure 3.1 – Commercial and synthetic derivatives of 2.1 and 2.2, Synthetic targets are
highlighted in boxes. 59
Figure 3.2 – Tm measurements of AAC(6')-Ii in 300 mM ionic strength by A) DSF,
three replicates are shown (blue, red, yellow) with an arithmetic mean T_m = 49.0 ± 0.5 °C.
B) Circular dichroism at 222 nm with increasing temperature. The trace shown is one of
three with an arithmetic mean $T_m = 49.4 \pm 0.4$ °C
Figure 3.3 - Protein Tm was measured by DSF. Ionic strength was calculated from
buffer concentration, pKa and solution pH in addition to added NaCl to adjust for higher
ionic strengths
Figure 3.4 - Structures of product CoA and substrate neomycin c
Figure 3.5 – AAC(6')-Ii (5 μ M) T_m was investigated using natural substrates as a
function of ionic strength. A) The Tm shift induced by CoA (0.8 mM) changed greatly
with increasing ionic strength. B) With neomycin c (0.8 mM), there is no effect with
increasing ionic strength71

Figure 3.6 - Structure of the bisubstrate NC1	. 72
Figure 3.7 - DSF measurements of Tm with each natural substrate alone, a combination	on
of both, and the bisubstrate inhibitor.	. 72
Figure 3.8 - DSF melting point difference from protein only for fragment hits and	
hybrids.	. 74
Figure 3.9 - Michaelis-Menten curve of 2.1 substrate activity. This curve measured a	K_{M}
of 33.4 mM and k_{cat} of 0.15 s ⁻¹	. 75
Figure 3.10 - Derivatives activity as substrate for AAC(6')-Ii, replacing neomycin c	. 76
Figure 3.11 - Inhibition by derivatives of 2.2, compound 2.2 shows 54% activity (68	
mM) while both 3.16 and 3.31 show 78% activity at much higher concentration (250	
mM)	. 77

List of Schemes

Scheme 3.1 – Synthetic scheme for 3.8 and 3.9	60
Scheme 3.2 - Synthetic scheme of compounds 3.10 and 3.11	61
Scheme 3.3 – Synthetic scheme for compound 3.12.	61
Scheme 3.4 - Synthetic scheme of compound 3.14.	61
Scheme 3.5 – Synthetic scheme for compound 3.13	62
Scheme 3.6 – Synthetic scheme for 3.15	63
Scheme 3.7 – Synthetic scheme for 3.24.	63
Scheme 3.8 – Synthetic scheme for 3.25.	64
Scheme 3.9 - Synthetic scheme for compounds 3.30 and 3.31.	65
Scheme 3.10 – Synthetic scheme for compounds 3.28 and 3.29.	66
Scheme 3.11 - Synthetic scheme for compound 3.32.	66

List of Tables

Table 1 - Changes in HSQC spectra of AAC(6')-Ii with different ligands and mixtures.	
The content of the mixtures is defined in Appendix B	.45

List of Abbreviations

Å Ångstrom

AAC(6')-Ii aminoglycoside N-6'-acetyltransferase Ii

APM aminopropylmorpholine

CD circular dichroism

DCM dichloromethane

DMF dimethylformamide

DMSO dimethylsulfoxide

DSC differential scanning calorimetry

DSF differential scanning fluorimetry

DTDP 4,4'-dithiodipyridine

DTNB 5,5'-dithiobis-(2-nitrobenzoic acid)

EDC 1-ethyl-3-(3-dimethylaminopropyl)carbodiimide

EDTA ethylenediaminetetraacetic acid

ESI electrospray ionization

FPLC fast protein liquid chromatography

HEPh 4-hydroxyethyl phenol

HEPES 4-(2-hydroxyethyl)-1-piperazineethanesulfonic acid

HRMS high resolution mass spectrometry

HSQC heteronuclear single quantum coherence

IC₅₀ inhibitory constant (50%)

ILOE interligand nuclear Overhauser effect

IPTG isopropyl β-D-1-thiogalactopyranoside

ITC isothermal titration calorimetry

K_M Michaelis constant

k_{cat} catalytic constant

LB Luria-Bertani

LDL low density lipoprotein

MES 2-(*N*-morpholino)ethanesulfonic acid

MOM methoxymethyl

NMWL nominal molecular weight limit

NOE nuclear Overhauser effect

NOESY nuclear Overhauser effect Spectroscopy

NMR nuclear magnetic resonance

OD optical density

PCR polymerase chain reaction

PFG pulsed field gradient

RF radio frequency

SAR structure-activity relationship

SDS-PAGE sodium dodecylsulfate polyacrylamide gel electrophoresis

STD saturation transfer difference

THF tetrahydrofuran

TOCSY total correlation spectroscopy

trNOE transferred nuclear Overhauser effect

TROSY transverse relaxation optimized spectroscopy

UV-vis ultraviolet-visible

waterLOGSY water ligand-observe gradient spectroscopy

Abstract

Aminoglycosides are valuable broad-spectrum antibiotics effective in both Gram-positive and Gram-negative bacteria. Antibiotic resistance has however been a scourge since the advent of modern antibiotics. One of the main mechanisms of resistance to aminoglycosides is antibiotic modification by the clinically widespread enzyme aminoglycoside N-6'-acetyltransferase (AAC(6')).

Inhibiting resistance-causing enzymes is an important strategy among the multiple approaches to counter antibiotic resistance. The Auclair lab has previously developed a series of aminoglycoside-coenzyme A bisubstrates that was found to be potent inhibitors of AAC(6')-Ii, but lacked activity in cell-based assays.

In order to combat aminoglycoside resistance, this thesis aims at developing a new class of AAC(6') inhibitors using fragment-based drug design with NMR-based assays for the initial screening. This approach has the advantage of potentially identifying new structural scaffolds that are fundamentally different from those that have been previously developed in the group.

Following the introductory chapter 1, chapter 2 describes the NMR-based screening of a library of fragments against AAC(6')-Ii as well as the characterization of these hits in complex with the protein by NMR methods. Two hits with significant affinity for the enzyme were discovered, and their binding was further defined by HSQC methods. Chapter 3 describes the synthesis of derivatives of these initial hits, including hybrids, as well as the evaluation of their binding to AAC(6')-Ii using differential scanning fluorimetry and kinetic measurements. From the library of modified hits, only one was

found to be an improvement over the initial hits. One of the hybrid molecules was found to have slightly improved affinity over the initial hits, but its activity was still too weak to be useful in further studies.

Résumé

Les aminoglycosides sont une classe importante d'antibiotiques à large spectre, efficaces contre les bactéries Gram-positives et Gram-négatives. La résistance des bactéries envers les antibiotiques demeure un problème depuis leur découverte. Un des mécanismes principaux de résistance aux aminoglycosides est leur modification par l'enzyme aminoglycoside *N*-6'-aminotransférase (AAC(6')).

Inhiber la résistance antibiotique est une stratégie qui a fait ses preuves pour contrer ce problème. Le groupe Auclair a précédemment développé une série de bisubstrats aminoglycoside-coenzyme A qui sont de puissants inhibiteurs *in vitro* mais sont inefficaces dans des essais cellulaires.

Pour combattre la résistance aux aminoglycosides, cette thèse vise le développement d'une nouvelle classe d'inhibiteurs d'AAC(6') en utilisant une approche par fragments avec des essais à base de RMN pour le criblage initial. Cette approche a l'avantage de potentiellement trouver de nouveaux patrons structurels, fondamentalement différents de ceux qui ont été précédemment découverts.

Suivant l'introduction dans le chapitre 1. Le chapitre 2 décrit le criblage par RMN d'une librairie de composés avec l'enzyme AAC(6')-Ii. Les molécules actives ont ensuite été caractérisées en complexe avec la protéine par RMN dont la HSQC. Le chapitre 3 décrit la synthèse de composés modifiés basés sur les résultats du criblage initial aussi bien que la caractérisation de leur complexation avec l'enzyme par DSF et par mesures d'essais cinétiques. Seul un ligand a été trouvé un meilleur ligand que les ligands initiaux. Un

des composés hybrides montrait une légère amélioration dans son affinité pour AAC(6')-
Ii, mais son activité est trop faible pour que cet inhibiteur mérite de plus amples études.

Acknowledgements

First and foremost, I would like to thank: my wife Elisabeth for her constant understanding and support in this undertaking; my parents Marie-José and Nagy for their love and guidance and brother Christian his support despite his apparent cynicism; Dr Tara Sprules for all her time, patience and lessons in NMR; Dr Aaron Larsen for showing how we can have fun as part of our work and life; Dr Amélie Ménard and Kenward Vong for showing me how to be persistent despite adversity; Dr Lee Freiburger for showing me that great minds can still be laid back; Dr Kayode Akinnusi for giving me a high skill level to aim for; Dr Emelia Awuah for reminding me that even very skilled people must be humble and down to earth; Matthew Hachey for his continued kindness; Annabelle Hoegl for her delicious cupcakes and sweet personality; Vanja Polic for her playful disposition; Sylvain Rocheleau for always being open to Q&A sessions; Moes Soliman for keeping me sane with exercise; Dr Bob Zamboni for sharing some advice and giving so many neat tricks.

I would also like to thank my supervisors: Dr Karine Auclair for showing me to always aim high and work as hard as I can; Dr Tony Mittermaier for always giving me great lessons and constructive criticisms when needed and showing me how to deal with problems as they arise.

Of course, a big thank you to all of the McGill chemistry department's support staff without which literally none of this would have been possible.

Chapter 1 Introduction

1.1 Research Motivation

Bacterial infections have been a scourge for as long as long as man has been around. In ancient history, many civilizations used moulds to treat infections without really knowing the source of the curative powers [2]. By the late 17th century, Anton Von Leeuwenhoek was the first to observe bacteria in canal water [3]. With the following development of the germ theory of disease – postulating that some infectious diseases are caused by microorganisms – it was shown that some kind of seed organisms were indeed responsible for sickness in people. Subsequently in the 1880s, Paul Ehrlich noted that certain dyes could selectively colour human, animal, or bacterial cells, bringing forward the possibility that these organisms might be selectively targeted by certain compounds. Many synthetically prepared chemicals were used as treatments, though none were selective for the invading organisms except the sulfonamides. It was not until 1928 with the serendipitous discovery of the antibacterial properties of the *penicillia* moulds that Fleming allowed for a new type of selective antibacterial compounds.

Clinical use of penicillin G (Benzyl penicillin), the active ingredient, allowed selective treatment of infections, significantly decreasing the mortality rate due to bacterial infections. Penicillin G was just the first of many antibacterials to be isolated from natural sources. In the 85 years since the discovery of penicillin G, not only have many other penicillins been discovered, but several other classes of antibacterials have been found including aminoglycosides, ansamycins, carbapenems, cephalosporins, macrolides, quinolones, and many more (Figure 1.1).

Figure 1.1- Structures of six antibacterial compound classes a) Aminoglycoside (neomycin); b) Ansamycin (geldanamycin); c) Carbapenem (imipenem); d) Cephalosporin (cefacetril); e) Macrolide (erythromycin); f) Quinolone (nalidixic acid) Almost immediately following the broad use of antibacterials for treatment of infection, another phenomenon became readily apparent. True to their legacy of survival through

years of natural selection, bacteria started to exhibit resistance to those antibacterials. Originally, it was thought that bacterial resistance to antibacterials was a purely evolutionary phenomenon due to the vulnerability of microbes predating the antibacterial era, but recent studies have shown that many of the genes responsible for antibacterial resistance have in fact been present in the genomes of bacteria dating back as far as 30,000 years [4]. Indeed, since most of the antibacterials used today are natural products [5], co-evolution of organisms would indeed strongly favor the development of counter measures to these compounds, as posited in the Red Queen Hypothesis[6, 7]. Moreover, resistance genes were found for synthetic antibacterials, genes that also spread by horizontal transfer. Thus resistance is an evolutionary phenomenon that has existed for a long time, and we are unlikely to be rid of it in the near future.

One class of antibacterial that has been used extensively is aminoglycosides. These bactericidal antibiotics are composed at least partially of amino-derived sugars (**Figure 1.1a**). They were isolated from bacteria of the *Streptomyces* as well as *Micromonospora* genera. Aminoglycosides have broad spectrum activity against Gram-negative bacteria and are used synergistically in combination with β -lactams and glycopeptides in Grampositive bacteria, but show negligible activity against anaerobes [8-10]. The mechanism of action of this class of antibacterial compounds is through binding to the 30S subunit of the prokaryotic ribosome. While this binding does not prevent the formation of the initiation complex for peptide synthesis, it affects proofreading and thus causes an increase in mistranslation. This in turn causes malformed proteins that lead to leakage in the bacterial membranes, introduction of more aminoglycoside into the cell, and

eventually cell death [11]. Thus the versatility as well as potency of aminoglycosides has led to their widespread use in the last several decades.

Bacterial resistance to antibacterials is not, contrary to popular belief, a single phenomenon. Many different species of bacteria have a multitude of resistance mechanisms to counter an even larger variety of antibacterials. There are five types of resistance mechanisms: efflux, impermeability, molecular bypass, target modification, and drug modification (**Figure 1.2**). Resistance by efflux and impermeability work the same way, preventing the drug from getting in proximity to its target. Molecular bypass consists of amending the inhibited pathway through an alternate enzymatic route either using their natural – if secondary - function, or using a modified reaction as caused by a mutation. With target and drug modification, the molecule gets to its target, but is unable to bind to it efficiently, preventing the desired effect. While all mechanisms have been studied extensively in bacteria and in other organisms, the principal mechanism of interest here is drug modification [12].

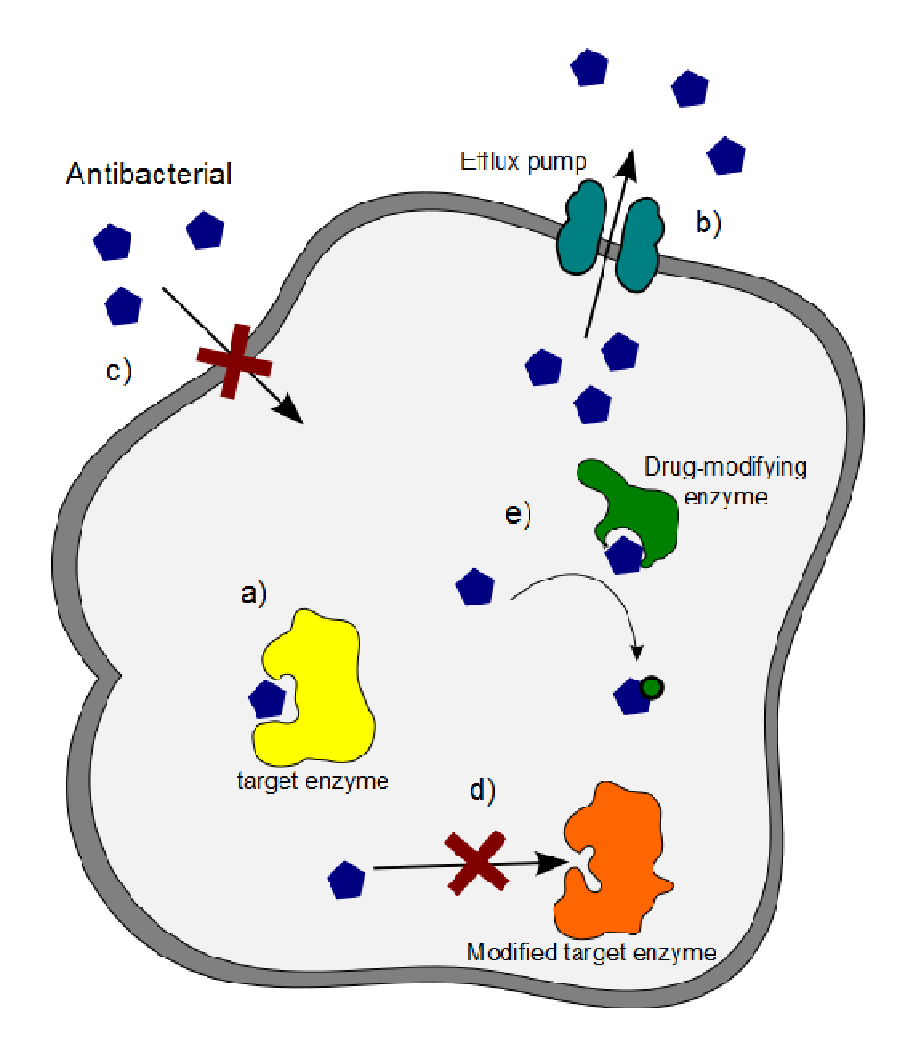


Figure 1.2 - Antibiotic resistance mechanisms: a) normal antibiotic binding b) efflux c) permeability decrease d) target modification e) drug modification (molecular bypass not shown)

1.2 Aminoglycoside N-6'-Acetyltransferase Ii

Among the modification enzymes, resistance to aminoglycosides is problematic as this class is often used as a first-line treatment due to its broad spectrum of activity against most gram-negative aerobes. One resistance-causing enzyme family that is of particular interest to the Auclair group is aminoglycoside acetyltransferase, which has been widely identified as a source of resistance [13-16]. Aminoglycoside 6'-*N*-acetyltransferase-Ii (AAC(6')-Ii) is an enzyme that is chromosomally encoded by *Enterococcus faecium*, to

which it confers mid-level resistance to many aminoglycoside antibacterials. The 42 kDa homo-dimer was first isolated by Wright and Ladak [17] who also measured affinity as well as kinetic constants for the protein with a variety of substrates. In the 15 years since then, much work has been reported, studying the enzyme mechanism and thermodynamics as well as finding new and better ways to inhibit it.

AAC(6')-Ii is a member of the GCN5-related *N*-acetyltransferases (GNAT) super-family of folds, known to have conserved sequence motifs involved in the binding of the acylcoenzyme A substrates (**Figure 1.3**) [18]. This protein is known to catalyze the transfer of the acetyl group of acetyl coenzyme A (CoA) to the 6' amine of most aminoglycosides with concurrent formation of CoA. This newly added acetyl group on the aminoglycoside dramatically lowers the affinity of the aminoglycosides for the ribosome, to the point where they become clinically ineffective.

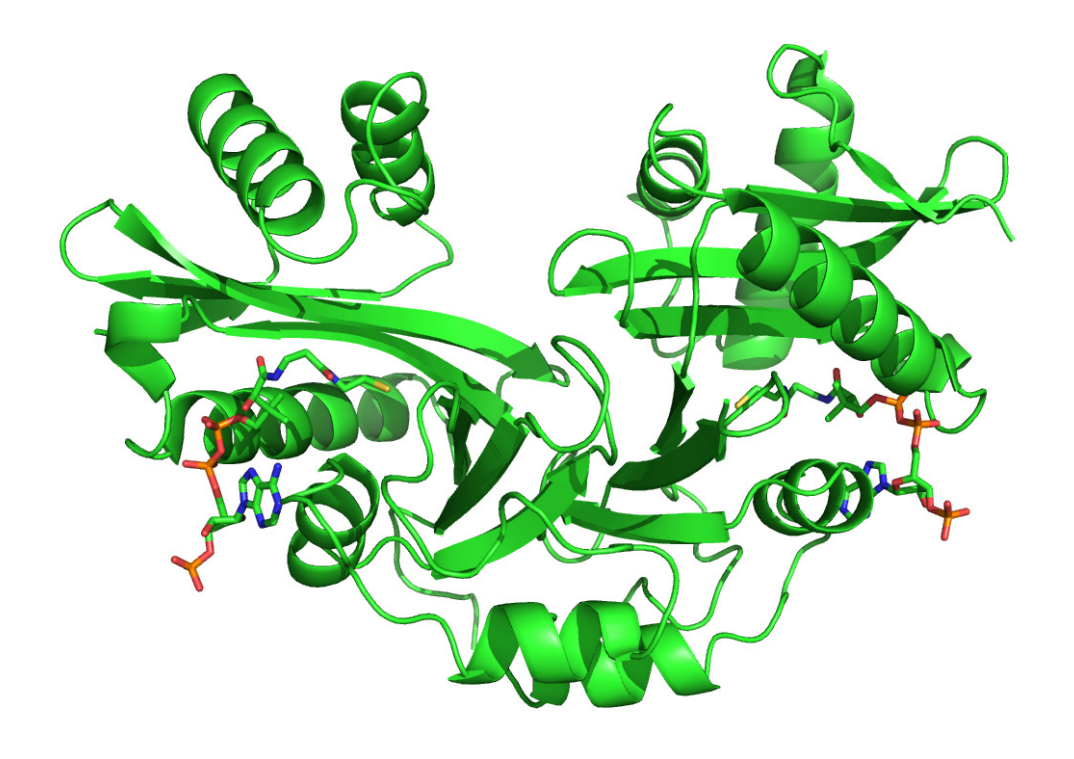


Figure 1.3 - Crystal structure of AAC(6')-Ii bound to coenzyme A [19]

1.2.1 Mechanistic and Structural Studies

The mechanism of AAC(6')-Ii has been extensively studied. Kinetic studies by Draker and Wright [18] have demonstrated that this enzyme operates through an ordered bi-bi kinetic mechanism with the AcCoA binding first, then the aminoglycoside, followed by catalysis and releasing in the opposite order (**Figure 1.4**). Initial Michaelis-Menten constants for the enzyme were established to be 5-36 µM for aminoglycosides, and 24 µM for acetyl-CoA. The catalytic constants (k_{cat} and k_{cat}/K_M) that were determined for this protein were also several orders of magnitude worse than those of many other known aminoglycoside-modifying enzymes. The relatively low affinity of its substrate, coupled with its low catalytic activity and specificity has led to speculation that the enzyme's primary function is or was indeed something other than antibacterial modification [17].

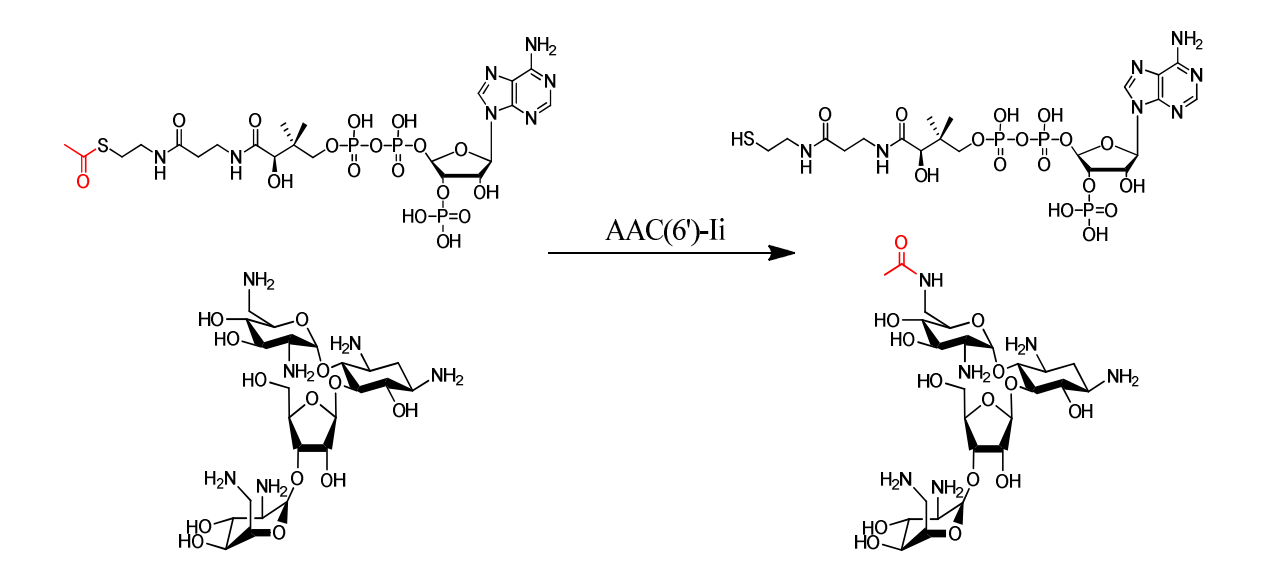


Figure 1.4 - AAC(6')-Ii catalyzed reaction. Shown with AcCoA and Neomycin B Studies suggesting dimer cooperativity were reported based on the loss of activity of some monomeric mutants [18]. Further studies into the interactions between subunits revealed that the cooperative nature of the inter-monomer interactions are quite complex, and do not conform to simple two-state binding thermodynamics. Indeed, for AcCoA, binding events at low temperature as measured by isothermal titration calorimetry (ITC) show positive cooperativity, but as the temperature increases, this tendency fades, eventually giving way to negative cooperativity near the melting temperature of the protein. On the other hand, for aminoglycoside binding to the apo form of the protein, there was positive cooperative behavior at all temperatures measured [20]. Further NMR and circular dichroism studies were combined with ITC data to study the conformational impact of substrate binding to the protein [21]. Therefore the conformational dynamics and thermodynamics of the enzyme are very complex and are subject to further studies in our labs.

1.2.2 Inhibitors

Early attempts to probe and block the activity of AAC(6')-Ii were fairly successful. The compounds that were developed exhibited nanomolar inhibition of the enzyme. These compounds were created in attempts to mimic the catalytic transition state of the enzyme by linking the aminoglycoside moiety to the CoA thiol affording bisubstrates. Though they exhibited nanomolar affinity (e.g. 43 ± 23 nm) in vitro, the polar nature of the molecules caused problems with uptake into the cells, significantly reducing their in vivo usefulness (Figure 1.5) [22]. These bisubstrate inhibitors, while they lacked potency in cells demonstrated a proof of concept. Two approaches were taken to resolve the uptake and polarity issues: 1) modifications of the nucleotide portion of the bisubstrate to noncharged mimics; and 2) making prodrugs to be transformed in the cell to the active bisubstrates. The former approach was based on the knowledge that the negative charge of the phosphate groups was most likely responsible for the lack of activity in cells. Thus the molecule was truncated at the end of the pantoyl moiety, and an acetoacetate group was attached as a diphosphate mimic (Figure 1.5). This modification using a diphosphate bioisostere kept the required interactions with AAC(6')-Ii, but eliminated the deleterious charged moieties that were preventing uptake. For the pro-drug approach, cell penetration was facilitated by cleaving the bisubstrate at the end of the pantothenic acid portion of the molecule. Since the non-natural aminoglycoside portion was far enough to be outside of the active site, this allowed the molecule to be taken as a substrate by the CoA synthesis enzymes of the cells where the pro-drug is further extended to the full bisubstrate[23]. Therefore both the prodrug series and the acetoacetate series of compounds exhibit very promising activity.

Figure 1.5 – First and second generation of AAC(6')-Ii inhibitors.

1.3 Fragment-based Drug Design

The principles behind fragment-based drug design are fairly simple. If we consider a binding site on a protein with a corresponding strong affinity ligand, we can consider this ligand to be a series of functions that confer binding character, with a series of functions that attach these binders together. Individually, each of these binders is non-specific and has a low energy of binding, but taken together the affinities add together to yield strong binding [24].

When performing traditional high throughput screening, a large number of molecules of relatively high molecular weight are screened against a protein in the hopes of finding one or more that bind with medium to high affinity. There are many degrees of freedom for molecule binding: distance, charge, orientation, flexibility, electronic character. The probability of finding a molecule with the desired properties in the screened molecules is low. Furthermore, in order to thoroughly sample the space occupied by all these degrees

of freedom, not only the number of molecules, but also the diversity in these must be extensive. In fragment-based screening, testing smaller molecules (or "fragments"), the degrees of freedom are much more limited, and therefore can be sampled with a smaller number of compounds. The binding affinity of the fragment is however lower.

There are two main approaches to fragment-based drug design: the building up approach, and the fragment linking approach (**Figure 1.6**). In the building up approach, the concept is to screen for a single fragment of small to medium affinity (high μ M to low mM). Using this binder as an anchor, it can then be extended to reach out and bind other interaction sites in its vicinity. In the fragment linking approach, the fragment screening must find multiple binders that attach in non-overlapping nearby regions. Ideally, the binding site of the fragments should be well characterized to allow them to be linked together to optimize placement and obtain a high affinity ligand. Of course, these approaches are not mutually exclusive. The approach will also be largely influenced by the amount of structural data available. In all cases, the more structural data that can be obtained, the easier it is to create a high affinity ligand from fragments.

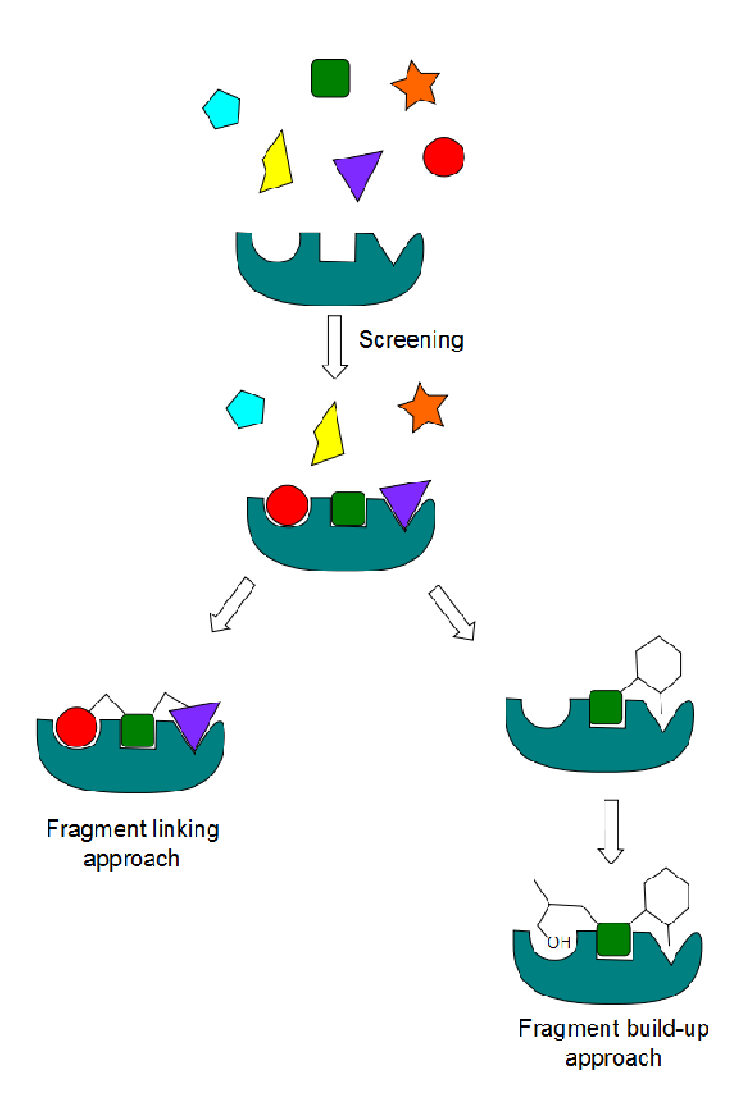


Figure 1.6 - Fragment screening and fragment buildup approaches for fragment improvement

While the beginnings of fragment-based drug-design were fairly high risk, the technique has grown much in the last two decades. Over the last 10 years, many groups have used fragment-based design to find potent inhibitors ($IC_{50} < 100 \text{ nM}$) [25-28]. The targets for these molecules range from matrix metallo-proteases as in the original paper from Fesik [24] to adipocyte lipid-binding protein-2 [29]. Additionally, there is a trend of increasing use of fragment-based design, both in industrial and academic settings [26]. This useful

approach has now proven its usefulness and has become a tool in the arsenal of drug development [26].

A noteworthy effort in fragment-based drug design was performed by Lombès [28] against the AAC(6')-Ib. They found a diamino-cyclopentanol compound that bound to the protein with 41 μ M affinity (**Figure 1.7**). From there, the compound was derivatized with many different aromatic moieties through ester and ether linkages. These were tested against the protein through reverse NOE pumping experiments (further discussed in the NMR section). Once the fragment was optimized, it was linked to a CoA moiety in the same manner as was used to make the Auclair group bisubstrate inhibitors [22]. The affinity of this compound was measured to 950 \pm 190 nM, one order of magnitude stronger than CoA alone (35 μ M) [30], but still 200-fold weaker than the best reported bisubstrate for AAC(6')-Ii [22]. Thus, while their approach was marginally successful, the improvement in binding from the fragment portion of the molecule was only a slight improvement on normal substrate activity.

Figure 1.7 - 1-4) fragments Lombès found to bind with micromolar affinity, 5) bisubstrate extension with best fragment showed 950nM binding [28].

1.4 Protein-Ligand Screening

Finding inhibitors for a protein requires a robust assay. Many methods have been used to test for ligand binding, often having varying effectiveness for different proteins. Two main groups of screening methods will be described: Nuclear Magnetic Resonance (NMR) spectroscopy-based methods, and other methods.

1.4.1 Nuclear Magnetic Resonance (NMR) Spectroscopy

In efforts to measure ligand affinity for a protein, many different NMR methods were tried and tested. These were divided into two main categories: protein-observe experiments and ligand-observe experiments. As suggested by the name, the difference lies with which element of the mixture is observed for changes due to binding. Either type of method has its advantages as well as its disadvantages, in addition to being more amenable to use with proteins that exhibit specific properties, as will be described below.

1.4.2 Protein-Observe NMR Methods

In protein-observe experiments, as the name suggests, parts of the protein are observed in order to assess binding. Changes in the chemical shift for various signals of the protein are observed, which are related to conformational shifts in the protein or changes in protein dynamics. Simple one dimensional NMR spectra of protein do not provide enough information due to heavy overlap and peak broadening to be of any use. In order to obtain any sort of useful information, two-dimensional spectra are required.

The most common experiments are heteronuclear correlation experiments, such as the popular heteronuclear single quantum coherence (HSQC)[31]. N-H HSQC experiments are commonly used with proteins because they detect pairs of ¹⁵N-¹H atoms present in amide peptide links. Besides amide bonds, this technique also detects nitrogencontaining side chains such as those of tryptophan or histidine. The resulting spectra are representative of protein conformation. Changes in the spectrum can be correlated to structural shifts that can occur as a result of ligand binding, assuming controlled conditions for pH, ionic strength, and temperature. Binding of ligand itself can also cause shifts in the HSQC. On the other hand, if binding to the protein does not cause sufficient structural changes to be observed such a ligand could easily be missed.

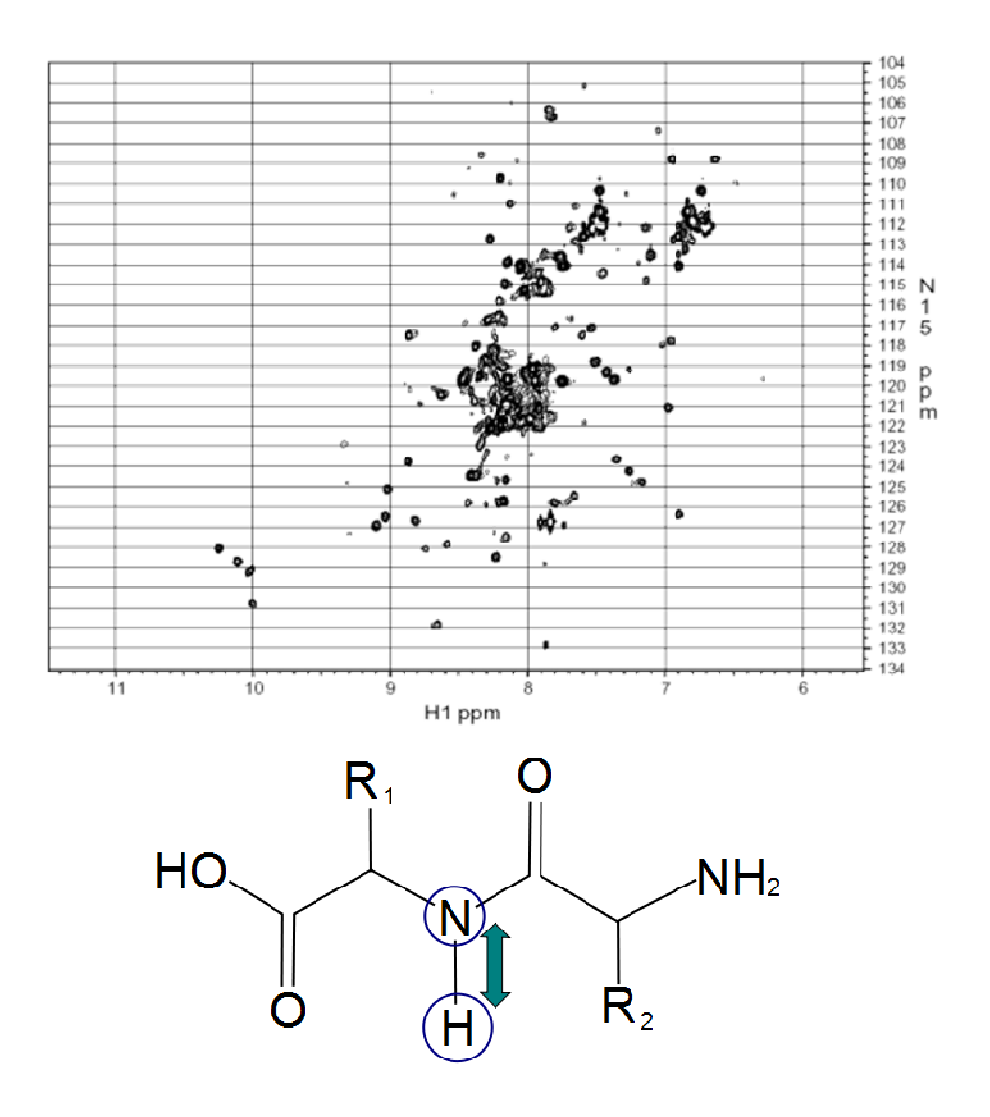


Figure 1.8 - (top) HSQC spectrum of the apo form of AAC(6')-Ii (bottom) Correlation between amide proton and nitrogen on the peptide backbone.

The changes observed in the spectra can often be attributed to changes in the chemical environments of specific residues in the protein. The characteristics of the changes will depend upon the exchange rate between the two observed states. A fast exchange rate will show a peak moving from the coordinates of state A to the coordinates of state B at a position between each signal, representing a population-weighted average of the chemical shifts of the two states. A slow exchange regime will show a peak at position

A, and a peak at position B whose respective intensities are a function of the populations in either state.

$$K_a = \frac{k_{on}}{k_{off}}$$

$$k_{ex} = k_{on} + k_{off}$$

Slow exchange $\Delta \omega \gg k_{ex}$

Intermediate exchange $\Delta \omega \approx 2k_{ex}(f_a f_b)^{\frac{1}{2}}$

Fast exchange $\Delta \omega \ll k_{ex}$

Where K_a is the association constant, k_{ex} is the exchange rate, k_{on} is the ligand on-rate, k_{off} is the ligand off-rate, $\Delta \omega$ is the frequency difference between state a and state b, and f_a and f_b are the fractions of state a and state b.

In terms of the information that can be extracted from titration spectra, fast exchange provides the data that are easiest to interpret due to the proportional movement of the peaks. In principle, this allows affinity constants to be measured in titrations of the protein with ligand [32]. In slow exchange, additional experimentation is required in order to correlate the disappearance of a peak with the appearance of another peak, though the simple disappearance or appearance of peaks can be used to provide some information of structural change. In contrast, in intermediate exchange regimes, a weighted average of the peak positions will be observed with an added broadening effect in the middle regions that can make it difficult to measure at all. Therefore information

is provided regardless of the exchange regime, but fast exchanging processes are easier to analyze due to the progressive nature of the observed changes that occur.

Protein-observe experiments have limitations beyond the structural change of the protein. The major issue is that past a certain size of protein, the very fast relaxation prevents the distinction of peaks. For HSQC experiments, the limit is approximately 30 kDa or 50 kDa depending on whether complete deuteration of the protein is used or not [33, 34]. The reason this experiment works with the AAC(6')-Ii homodimer (of a total weight of ca. 42 kDa) is that each monomer consists of only 21 kDa, which is within the size

limit. There are other NMR experiments that allow for observation of larger proteins such as

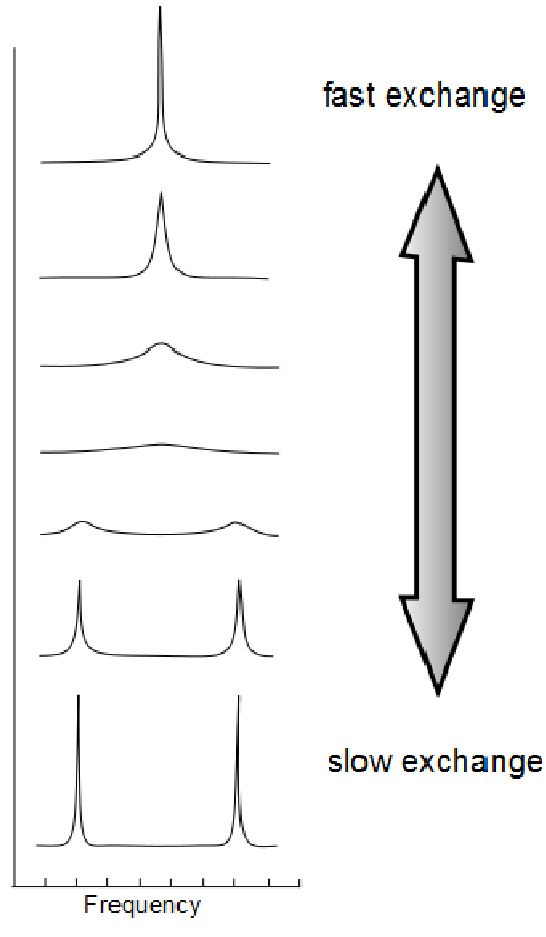


Figure 1.9 - NMR signal exchange rates affect peak position and broadening.

transverse relaxation optimized spectroscopy (TROSY) [34], but that is outside the scope of this thesis.

One caveat of using HSQCs which is of particular note is that given the bi-nuclear nature of the experiment, the sample of protein must be isotopically enriched in ¹⁵N in order for the signal to be visible using practical concentrations of protein. Obtaining isotopically enriched protein involves growing the cells expressing the protein in an enriched

medium. More details can be found in the "Experimental" chapter of this thesis. A sideeffect of isotopic enrichment is that not only is the production of protein somewhat more
costly, but it entails a reduced protein yield for a given amount of medium. In addition to
this, given that the protein itself is being observed, much larger quantities of it are
required to obtain a usable signal to noise ratio. However, these disadvantages can
definitively be offset by the richness of information provided by this method.

1.4.3 Ligand-Observe Experiments

In ligand-observe experiments, rather than looking at the signals assigned to protein residues, signals corresponding to the ligands themselves are directly observed.

Generally, an increase or decrease of the signal intensity indicates binding. There are two main types of ligand-observe experiments: relaxation transfer experiments, and diffusion-ordered experiments.

Cross-relaxation Experiments

In order to understand how this type of experiment works, relaxation must first be understood. Relaxation defines the rate at which the magnetization on the nuclei of interest return to equilibrium values. Relaxation efficiency depends on the distance between interacting spins (nuclei), and the reorientation time of the internuclear vector. The last term depends on the tumbling correlation time of the molecule for perfectly rigid molecules, and otherwise involves the internal motions as well. The tumbling correlation time can be calculated by the following empirically-derived equation:

$$\tau [ns] = \frac{9.18 \times 10^{-3}}{T[K]} \times N^{0.93} \times e^{\frac{2416}{T[K]}}$$

Such that τ is the correlation time in nanoseconds, T[K] is the temperature in Kelvin, and N is the number of residues in the protein. Given that proteins are very large, their tumbling times are very long, which corresponds to very fast transverse relaxation. Conversely, when compared to proteins, ligands are generally very small, and therefore relax very slowly. Interestingly, while a ligand is bound to a protein, it will tumble at the speed of the protein, causing it to relax much more quickly than it would in the free state.

If we were to directly observe the ligand when bound to protein, distance and tumbling correlation time would be the only factor of import, but unfortunately this is not possible. In order to measure bound ligand, the concentration of protein would have to be comparable to that of the ligand in question. Given the large variety of functional groups, the proton spectrum for proteins cover a large frequency range (-2 to 8 ppm would be a conservative estimate), which makes it impossible to differentiate between protein and ligand. This problem can be circumvented by having a large excess of ligand when compared to protein and observing the free ligand rather than the bound. In such a scheme, the intensity of the signal observed relies heavily on the exchange rate between the free and the bound states of the ligand. Free ligand binds to protein; the effective increase in size causes it to relax much faster; it then releases from the protein. Given fast enough exchange between the bound and free states of the ligand, the observed relaxation will be equal to the weighted average between the free and bound forms, which results in a decrease in spectral intensity.

The observed decrease in signal intensity is a product of both the exchange rate, and the distance between the bound ligand and the protein. For smaller distances, relaxation occurs much more efficiently and therefore the signal will relax more than for longer

range interactions. This will play a role in experiments that are used to define compound binding to protein.

Experiments that use relaxation to measure ligand binding are T_{1p} , saturation transfer difference (STD), water ligand observed gradient spectroscopy (water LOGSY), and transferred nuclear Overhauser effect (trNOE). While they all use similar principles, many of them use different mechanics.

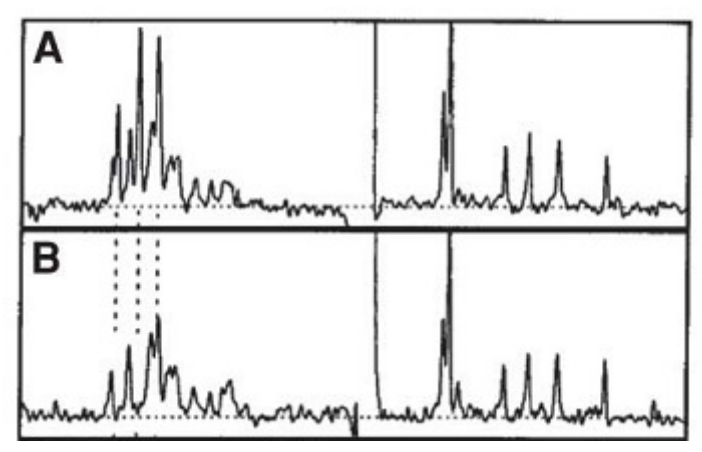


Figure 1.10 - Example of T1ρ experiment with FK506 binding protein and a mixture of 9 compounds. A) nine compound mixture without protein B) with FK506 binding protein. A clear decrease is observed in the residues indicated by dotted lines. Figure adapted from [1]

The T_{1p} experiment is traditionally a method of measuring the transverse relaxation rates of the nuclei in question. Due to the physics stated above, the relaxation rate increases for ligands bound to protein. In a normal proton spectrum, this appears as peak broadening. Through a series of spectra with varying acquisition delays, the relaxation rate can be measured. For screening purposes, normally, rather than recording a series of spectra, only one spectrum is obtained with a short acquisition delay (10-200 ms) [35]. This acquisition delay accentuates the intensity change that is normally seen with delay

in the proton spectrum, resulting in decreased intensity. The result is that binding molecules have decreased intensity in the presence of protein when compared to the small molecules alone.

The saturation transfer difference (STD) experiment works by taking the difference of two spectra. The first spectrum is referred to as the reference, or off-resonance spectrum. This spectrum is collected following a saturating pulse that is at a frequency where there are no protein or ligand signals. Normally, the reference spectrum should be identical to a 1D proton spectrum of the mixture. The second spectrum, known as the on-resonance spectrum uses an RF pulse to saturate only the signal of the protein in a narrow bandwidth. Given the high ¹H relaxation rate of protein, this saturation diffuses over protons within the entire protein and any bound ligands. Thus, when ligand binds to protein, they acquire this saturation and their spectral intensities decreases as described above. For a ligand that binds to protein, the on-resonance spectrum would be a spectrum of the ligand that has been heavily attenuated. For a ligand that does not bind to the protein, no extra relaxation will have occurred, and thus the spectrum will be identical to a 1D proton spectrum of the ligand. The final step is to subtract the onresonance spectrum from the reference spectrum. The resulting spectrum will effectively show a 1D spectrum of the ligand, modulated by that ligand's proximity to the protein.

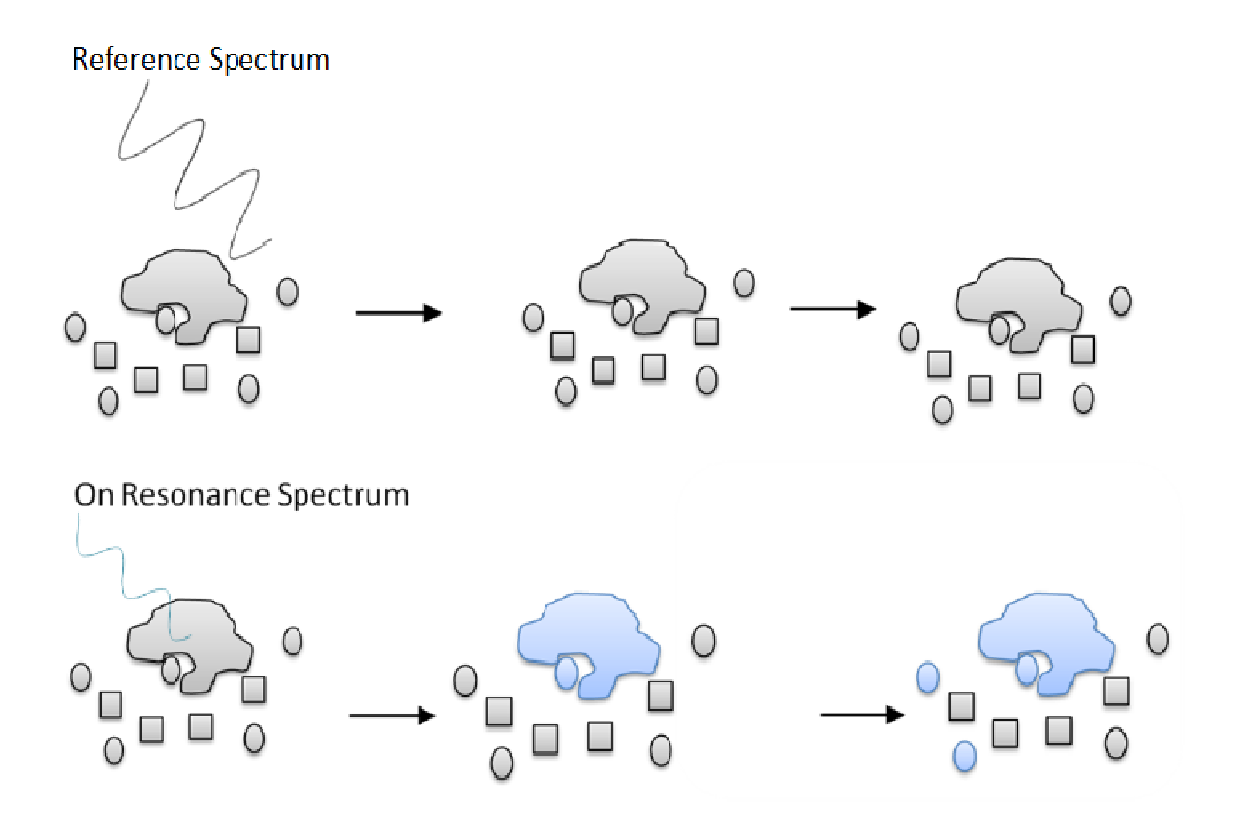


Figure 1.11 - Saturation transfer mechanics for STD reference and on-resonance spectra. The reference spectrum saturates away from any molecules in solution, such that nothing is saturated in solution. The on-resonance spectrum saturates the protein. Upon ligand binding (circles), saturation transfers to them. Non-binding ligands (squares) are not affected. Blue colour indicates saturation.

When used in mixtures composed of several organic compounds, where signals start to overlap, a method such as STD starts to lose some of its usefulness for high throughput screening. One solution to this is simply to select mixtures of compounds in such a way as to minimize spectral overlap. Different NMR experiments can be modulated using the STD pulse sequence, leading to STD spectra, spread into a second dimension in such a way as to further distinguish peaks that would otherwise overlap in the proton dimension. Most commonly used is the STD-TOCSY sequence, which leads to 2D ¹H-¹H spectrum where only signals from binding ligands appear.



Figure 1.12 – WaterLOGSY saturation transfer from active site water to bound ligands.

The waterLOGSY experiment works similarly to the STD experiment with several important differences [36]. Rather than saturating the protein resonance, bulk water in the medium is excited. For the same reason as the STD works (relaxation rate and correlation time), protein-bound water molecules impart their saturation to the protein. Additionally, chemical exchange of the protons of water with acidic and basic groups can do the same to further aid in protein saturation. Given that the saturating pulse hits all water molecules, both the free water and the bound water impart their saturation to adjacent molecules. In the case of free water however, the correlation time causes a reversal in signal intensity. The final spectrum shows bound ligands as positive peaks on

the spectrum, and unbinding ligands as negative peaks, resulting in a clear distinction between the two.

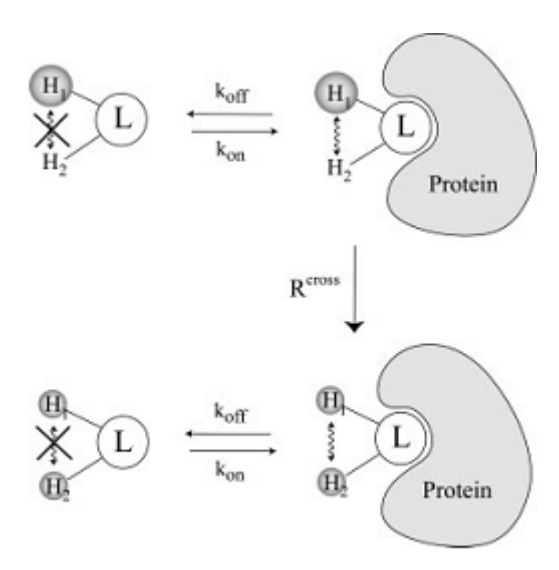


Figure 1.13 - trNOE mechanics. Free ligand has negligible cross-relaxation. Bound ligand exhibits cross-relaxation between H1 and H2.

The transferred nuclear Overhauser effect (trNOE) is similar to the other experiments with the exception that the saturation specifically targets a site on the ligand. One nucleus of the ligand is irradiated. When free in solution, due to the very fast tumbling time, there is negligible cross-relaxation between the different parts of the molecule. As the ligand binds to the protein and the tumbling time significantly increases, the cross-relaxation takes effect and the intensities of the other peaks for the ligand are diminished. The binding ligands will show decreased intensity in the spectrum, while non-binding ligands will exhibit no change (Figure 1.14). In the 1D version of this experiment, a specific atom of the ligand must be selected for monitoring. Alternatively, a 2D version of this experiment can be run (more commonly called nuclear Overhauser effect

spectroscopy NOESY) where all the resonances are interrogated in turn to yield a full picture of the interactions between the different parts of the ligands in the presence of absence or protein. In the 2D version, rather than seeing signal decrease, the signal transfer appears as cross-peaks.

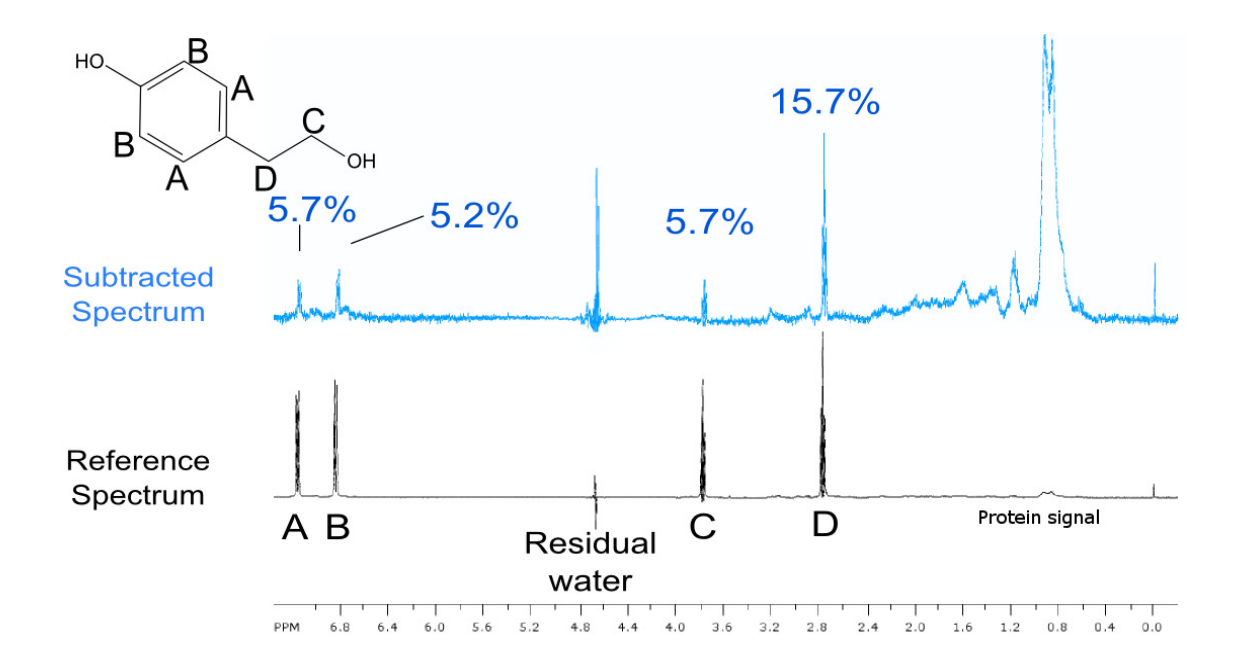


Figure 1.14 - STD spectrum showing the difference (subtracted) spectrum and reference spectrum.

Diffusion-editing Experiments

Diffusion-editing experiments were not used for this thesis and will not be described here. Readers are referred to literature for diffusion-ordered spectroscopy (DOSY) ligand screening [35, 37].

1.4.4 Comparison of NMR Methods for Screening

HSQCs being the most viable option for protein-observe screening, there are several advantages and disadvantages linked to this experiment when compared to ligand-observe experiments. Given that we are observing protein structure directly, as

previously stated, this limits screening to molecules that induce a conformational shift, which means three things: firstly, conformational shifts are indicative of a binding event or a reaction; second, lack of chemical shift does not necessarily indicate lack of binding; and third, proteins that exhibit little conformational change may be more difficult to screen using this method. The information provided upon binding is much greater than that provided by the ligand-observe methods by the very nature of the assay, given the residue shift information. In the context of fragment screening, where the hit rate in initial screening is very high (usually around 5%), missing some positives is not much of an issue whereas it might be for more traditional high throughput screening methods.

For ligand-observe methods in general, given that the association constant K_a is a function of both the on-rate (k_{on}) and the off-rate (k_{off}) , this will lead to certain limitations in this ligand-observe methods. In order for the experiment to yield useful information, the exchange rate must be sufficiently high as to maximize the fraction of free ligand that can bind to the protein and then relax. In most cases, this means that these experiments work optimally for weakly bound ligands (millimolar to high micromolar concentrations) since these tend to have higher exchange rates.

As a final consideration, simply in terms of resource use, ligand-observe experiments are much more economical. Having to use low milli-molar amounts of protein that is ¹⁵N labelled ends up being much more expensive and time-consuming than using low micromolar amounts of non-labelled protein, both in terms of resources and in the time invested to synthesize that protein [38].

1.4.5 Differential Scanning Fluorimetry

While certain methods for measuring ligand binding can be used with the majority of proteins, specific methods for ligand binding must often be developed for a new enzyme. These methods can take advantage of changes in absorbance or fluorescence (such as substrate turnover or tryptophan fluorescence), which are popular because of their high throughput. Only one such method was used in the context of this project.

Differential scanning fluorimetry (DSF) is a method whose approach involves monitoring the unfolding of the protein of interest in the presence of a fluorescent dye. Historically, the measurement of unfolding has been done using calorimetric methods such as differential scanning calorimetry (DSC), but this method requires very precise instrumentation in a thermally isolated system and experiments can only be performed one sample at a time.

Already in the 1950s, several naphthalene derivatives had been found that manifested little fluorescence in aqueous environments, but became highly fluorescent in apolar organic solvents. Additionally, it was found that interaction with hydrophobic binding sites also caused an increase in fluorescence accompanied by a blue shift of the peak maximum [39]. There are a variety of factors that can affect the quantum yield of a dye, but in this case, the factor of interest involves the change of dielectric constant of the solvent [40]. Given that the fluorescence of the dye is related to hydrophobicity of the medium, and that protein unfolding generally exposes hydrophobic residues from the protein core, there is a dramatic increase in fluorescence of the dye when this happens.

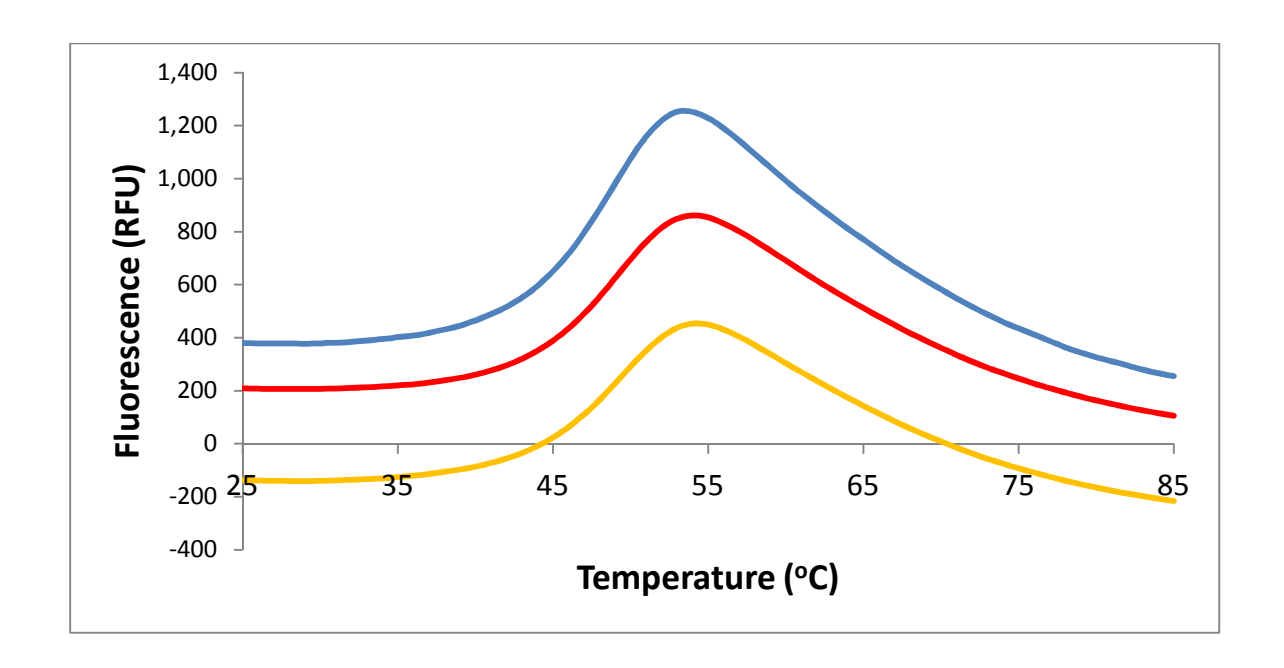


Figure 1.15 - Typical DSF plot showing protein melting at 47°C.

The usefulness of this method comes from the physics of protein unfolding. The thermostability of the protein is related to its Gibbs free energy of unfolding ΔG_u , which is temperature dependent. The temperature dependence of the component elements of the free energy is related to the heat capacity change ΔC_p between the native and denatured states as given by the following relationship:

$$\Delta G_{\rm u}(T) = \Delta H + T \Delta S = \Delta H_{\rm m} \left(1 - \frac{T}{T_m} \right) + \Delta C_p \left[(T - T_{\rm m}) - T * \ln \left(\frac{T}{T_m} \right) \right]$$

Where ΔG_u (T) is the free energy of unfolding as a function of temperature T, ΔH_m is the enthalpy of unfolding at the melting temperature, and T_m is the melting temperature [40]. When a ligand binds to the protein, the change in the free energy of binding results in an increase in the ΔG_u , which in turn causes an increase in T_m . In terms of reaction equilibria, the ligand can only bind to the native state of the protein. Following Le Chatelier's principle, this causes shifts in the equilibrium towards the native state,

consequently increasing the T_m . Thus, by monitoring the melting temperature of the protein in the presence of potential ligands, binders can be distinguished from non-binders simply by monitoring fluorescence as temperature increases.

1.5 Protein-Ligand Complex Characterization

While the methods described above can be used to screen mixtures composed of many different compounds, the techniques described below are more suited to use with single ligands. Once a ligand is identified, these methods are used to further define the parameters of the protein-ligand interaction in order to allow further modifications of the compound to improve affinity or specificity as the case may be. Three methods will be discussed: circular dichroism spectroscopy, enzyme kinetics measurements, and the interligand NOE NMR experiment.

1.5.1 Circular Dichroism Spectroscopy

Circular dichroism (CD) refers to the differential absorption of left- and right-handed circularly polarized light as a function of wavelength. When circularly polarized light passes through optically active media, the degree to which it is absorbed can differ between the two directions of polarization. Circular dichroism is considered to be the difference in absorbance between right- and left-handed circularly polarized light as described by $\Delta \epsilon = \epsilon_L - \epsilon_R$. For historical reasons, most CD instruments give molar ellipticity $[\theta]$:

$$\tan(\theta) = \frac{E_R - E_L}{E_R + E_L}$$

$$[\theta] = 3298.2 \Delta \varepsilon$$

Where E_R is the absorbance of right-handed polarized light and E_L is the absorbance of left-handed polarized light.

Most biological molecules including proteins and nucleic acids are chiral and show circular dichroism in their ultraviolet absorption bands, which is often used as an indication of secondary structure. As such, changes in the CD spectrum can serve as quantitative measurement of protein conformational change upon ligand binding [41].

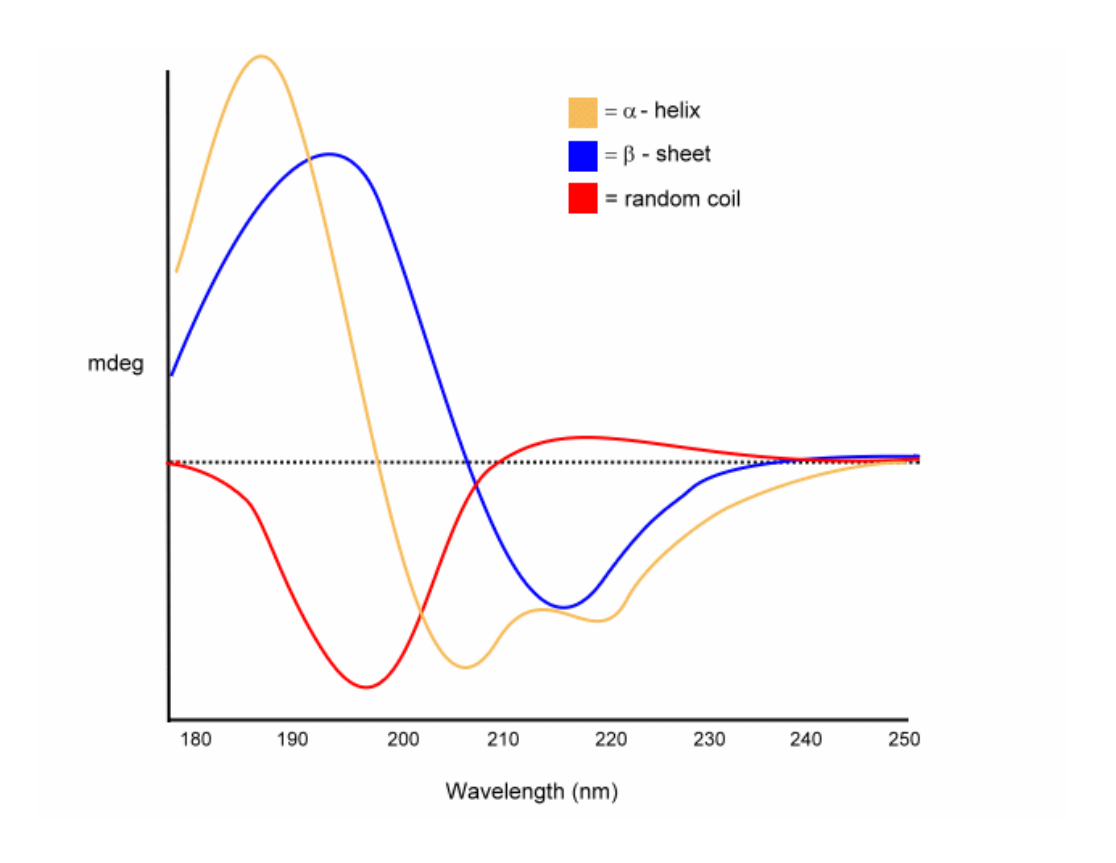


Figure 1.16 - Circular dichroism reference spectra for poly-lysine chain in different conformations (adapted from [42])

In studies of protein structure, far-ultraviolet wavelength scans are acquired (190-250 nm). The resulting spectrum represents the weighted average of the secondary structural motifs (Figure 1.16), the most prominent being alpha helices, beta sheets, and random coils. While these motifs each have a relatively distinct spectrum, when fitting data to

estimate the content of each one, there are many reference sets that can be used, ideally using one that is most similar to the protein of interest [43]. Given that CD acts as described by the Beer-Lambert law, when multiple species are in solution, the observed spectrum will be a weighted average of the different forms. Therefore if an appropriate reference set is available, and a ligand induces sufficient structural changes in the protein, binding to the protein can be measured with high accuracy.

1.5.2 Measurements of Enzyme Kinetics

Kinetic measurements of enzyme activity are the most accurate estimate of a ligand's propensity to bind to the protein in the binding site or an allosteric site for inhibitors or substrates. In kinetics studies, the turn-over rate of the enzyme is observed (indirectly in the case of AAC(6')-Ii). In the presence of a ligand, perturbations in the turnover rate can be observed, that will indicate the affinity of the ligand, and its overall effect on the catalytic reaction of the enzyme.

Figure 1.17 - After AAC(6')-Ii catalyzes the transfer from AcCoA to neamine, the CoA thiol reacts with DTDP to yield the disulfide the thiopyridine chromatophore.

As described above, AAC(6')-Ii catalyzes the transfer of an acetyl group from acetyl CoA to the 6' amine of aminoglycosides, yielding an acetylated aminoglycoside and CoA with a free thiol (Figure 1.17). Given that none of the starting materials or products exhibit detectable changes in their optical properties, an indirect method is used to monitor the appearance of the CoA thiol product. A fluorogenic disulfide such as 4,4'-dithiodipyridine or 5,5'-dithiobis(2-nitrobenzoic acid) is added to the mixture. As CoA is generated, it reacts in a disulfide exchange reaction, generating a new thiol with modified absorption properties (4-thiopyridine (Figure 1.17), or 2-nitro-4-thiobenzoic acid). Compared to the reaction rate of the enzyme, the disulfide exchange is many orders of magnitude faster when an excess of fluorogenic disulfide is used. Thus the appearance of product can be monitored by the absorbance of the indirect reporter.

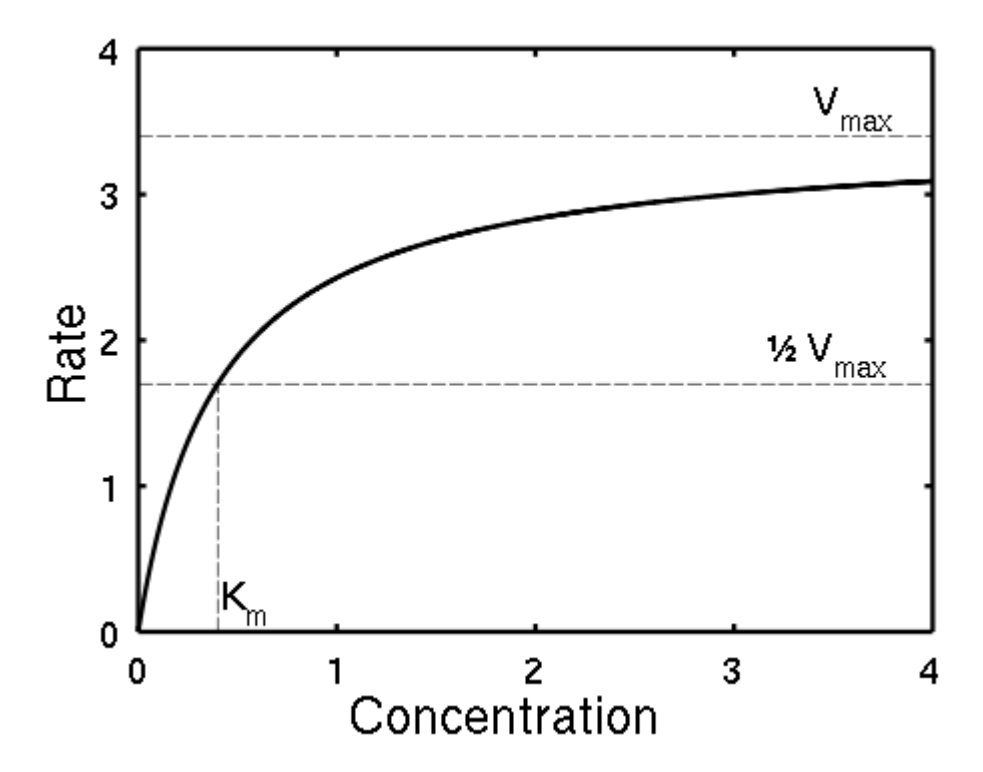


Figure 1.18 - Michaelis-Menten plot and the values that can be extracted from it. Independent axis is substrate concentration, while the dependent axis is Initial enzyme reaction rate.

The parameters of enzyme catalysis are approximated using the Michaelis-Menten equation as shown below:

$$v = \frac{V_{max}[S]}{K_M + [S]}$$

Where v is the initial reaction rate, [S] is the substrate concentration, K_m is the Michaelis constant, and V_{max} is the maximum reaction rate of the enzyme

This equation can be further expanded by defining V_{max} as the product of the catalysis constant k_{cat} and the enzyme concentration [E].

$$V_{max} = k_{cat} [E]$$

An important distinction must be made between measuring binding, and measuring detectable activity differences. Oftentimes compounds that induce a conformational shift will affect catalysis one way or another, but it is feasible that a binding event causes structural changes that have no effect on catalysis. Thus inhibitory activity of a compound implicates binding, but binding of a compound does not necessarily indicate inhibition of any sort.

1.5.3 Interligand Nuclear Overhauser Effect NMR

Interligand NOE (ILOE) works on the same principle as the trNOE discussed in the section about ligand-based screening methods. In this experiment, the objective is to observe cross-relaxation between residues of two separate ligands to ascertain proximity of these when bound to protein (**Figure 1.19**). The mechanics of the experiment are in fact the same as a 2D trNOE (NOESY), with the single difference that the mixing times are much longer (on the order of 700-900 ms). This method is particularly useful in the context of fragment-based drug design, as the second step after finding binding fragments is to link them together. Thus ILOE provides proximity information of two or more ligands when bound to protein [44].

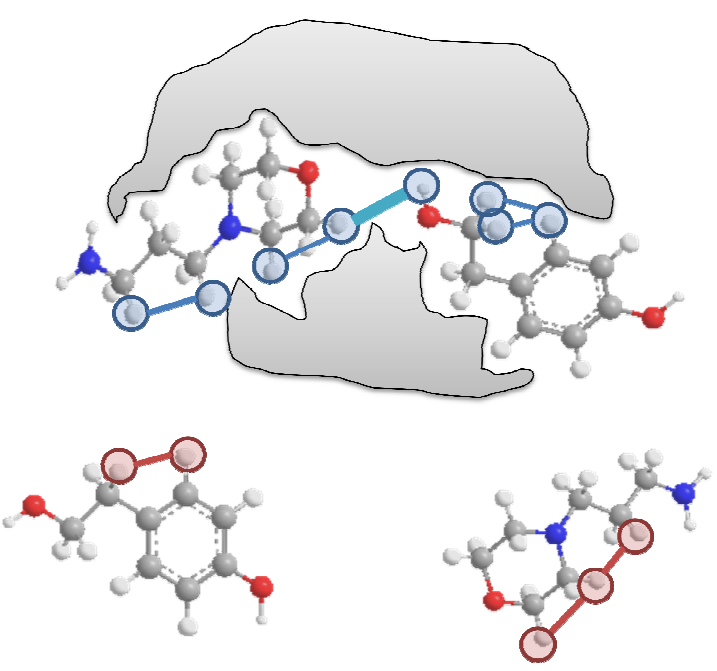


Figure 1.19 - ILOE shows positive resonances for bound ligand and negative resonances for unbinding ligand

1.6 Thesis Goals

The goal of this thesis is to identify new inhibitors of AAC(6')-Ii in a new structural class. Chapter 2 will discuss the multiple NMR-based screening methods, and the results observed with known binders as well as known non-binders. Furthermore, the active fragments that were found using NMR methods were then further characterized by kinetic assays.

Chapter 3 will discuss the synthesis that was carried out as well as the docking results and rationale that went into the synthetic planning. Beyond simple fragment modification, linked fragments that were synthesized will be discussed.

In Chapter 4, the biological activity of the compounds will be discussed. The activity of the compounds was ascertained by enzyme kinetics analysis and DSF.

The method analysis performed in this thesis will help future efforts to identify ligands for slow-exchanging proteins, and further defined some of the structure-activity relationships that govern binding of ligands to AAC(6')-Ii.

Chapter 2 Fragment Screening

2.1 Preface

Ligand screening has historically been a tool of choice for finding new protein ligands. The difficulty in ligand screening arises from the fact that proteins differ in their properties: size, fold, dynamics, physical properties, and composition. Due to these differences, screening methods vary from simple fluorescence measurements to detection of complex changes in protein dynamics by NMR [45-47].

In addition to screening in the wet lab, many different groups have developed computational tools that use structural information from the protein's crystal structures in order to virtually screen molecules [47-49]. The quality of the docking information is however largely dependent on the properties of the protein. Very rigid proteins tend to produce very high quality docking results due to the high predictability of the conformation of their active sites. Conversely, highly flexible proteins tend to produce poor docking results.

The goal of this chapter is to perform initial screening on the fragment library and further define the initial hits that were found by a variety of NMR experiments. I performed the great majority of the protein purification required for the experiments. Protein purified by Siqi Zhu, Kenward Vong and Lee Freiburger was also occasionally used. I ran all of the screening experiments with the help of Dr Tara Sprules in the QANUC NMR facility for NMR-based experiments and the help of Dr Robert Zamboni for DSF studies.

2.2 Introduction

Fragment screening is one of the recent strategies in ligand screening, it is characterized by small sizes and low affinities that these compounds typically exhibit. Protein-based methods generally do not work as well in fragment screening given the weak affinity [46, 50]. For AAC(6')-Ii however, the large conformational changes upon ligand binding allows ligand binding to be easily seen by changes in the NMR protein spectra.

In this thesis, many different screening methods were investigated for fragment screening. NMR was selected as the method of choice given the dynamics of AAC(6')-Ii. In previous NMR studies of AAC(6')-Ii using HSQC experiments, it was shown that the apo state the protein is very disordered. Once bound to a ligand, the protein takes on a more ordered state, resulting in a large, observable change in the NMR spectrum (Figure 2.1 compares the apo state and the neomycin-bound state).

Many previous examples of NMR screening use ligand-based methods. The challenge, however comes in selecting potential ligands with non-overlapping NMR signals. Several software packages are available that are designed to predict chemical shifts of compounds and design mixtures to minimize the overlapping signals. Such packages become more crucial as the number of compounds in the screening mixtures increases. This chapter describes initial NMR screening of 4 compound mixtures and further describes the additional information that was obtained concerning the bound ligands by using NMR methods.

2.3 HSQC Ligand Screening

Previous literature on the subject of ligand screening using HSQC spectra suggest that up to 100 compounds can be screened simultaneously [35]. Given the small number of compounds available to us, the HSQC screening was nevertheless performed in groups of 10 compounds. Groups of compounds that were shown to affect the HSQC spectrum of

AAC(6')-Ii were separated into their component parts and tested individually for binding. In HSQC ligand screening, even weak binding can cause structural changes.

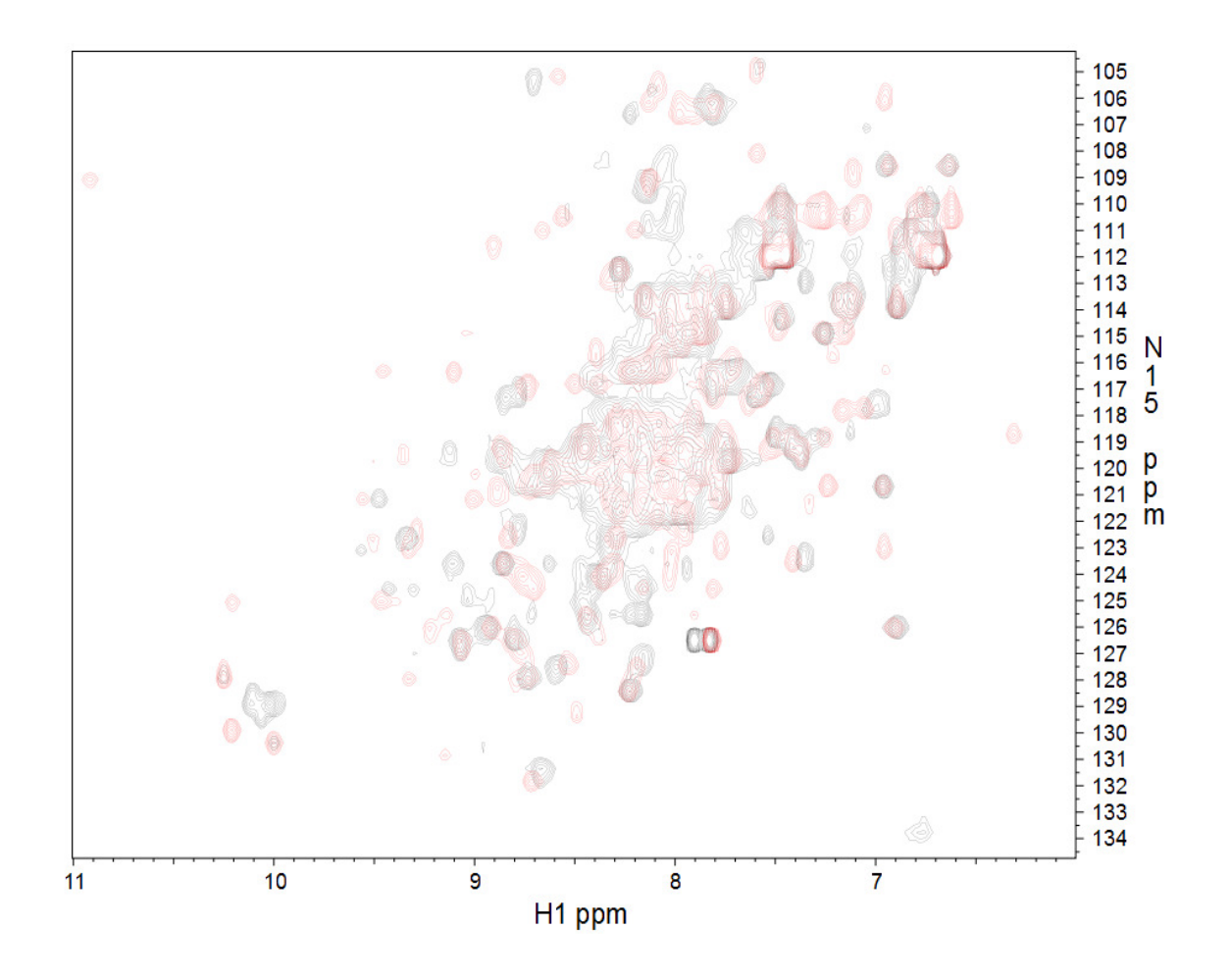


Figure 2.1 HSQC spectrum of AAC(6')-Ii alone (black) and with Neomycin B (red).

2.3.1 Initial HSQC Screening of Mixtures

After initial spectra of AAC(6')-Ii were collected, compound mixtures were tested with different protein concentrations. While higher concentrations of protein (300-400 μ M) were more effective given the higher signal to noise ratio in the NMR spectra, lower concentrations (100 μ M) were used in order to preserve protein. While the lower concentrations had much more noise, the changes in the spectra that were indicative of binding were still visible.

The first obstacle in ligand screening was to distinguish binding from non-binding compounds. In proteins with large flexible regions such as AAC(6')-Ii, solvent conditions can cause changes in the spectrum. In order to ascertain the significance of changes, controls such as different concentrations of DMSO were used to look at baseline changes in protein spectra. In addition to DMSO, some negative non-ligand controls were tested such as glucose and fluorobenzene. These negative controls yielded very small changes in the protein spectrum.

When HSQCs are used for ligand binding experiments, peak shifts are used to measure ligand binding and protein saturation. All binding events that have been studied in this protein thus far have been shown to be in slow exchange. Given that slow-exchanging systems exhibit peak appearance/disappearance rather than the peak shifting that occurs during fast exchange, traditional methods of peak tracking would not work. This peak movement is often used to calculate binding constants by titrating a ligand [32]. Realistically, individual peak tracking is of little use in ligand screening since only a semi-quantitative binding measurement is important during the screening step.

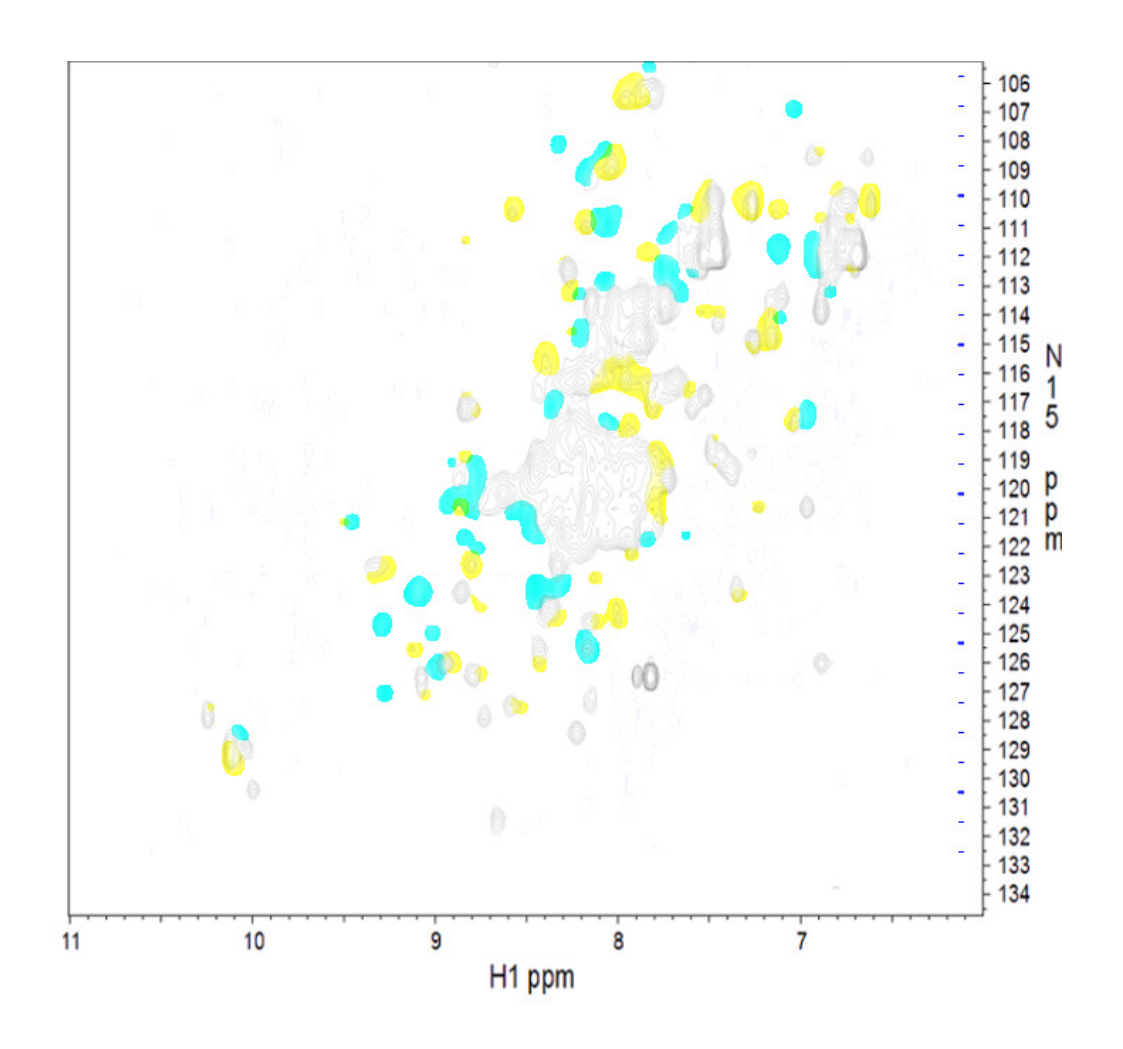


Figure 2.2 - A sample spectrum comparing protein alone with protein with mixture 1 (spectrum in black), with positive changes highlighted in yellow and negative changes highlighted in aqua.

In order to have a semi-quantitative method of measuring changes in protein spectra, image manipulation techniques were used, providing a quantitation of the percentage change from one spectrum to another (The script is in Appendix A). The script works as follows: two HSQC spectra are taken, one containing only protein, and one containing the protein and the compound(s) to be tested. Each script is passed through a threshold operation which separates signal from noise. The signal areas of the compound are subtracted from that of the protein alone. A blurring operation is used to show only

significant peak changes rather than small slivers. Finally, the area of the difference image is divided by the total area of the image, yielding the percentage spectral change.

 $\begin{tabular}{l} \textbf{Table 1} - Changes in HSQC spectra of AAC(6')-Ii with different ligands and mixtures. \\ The content of the mixtures is defined in Appendix B \\ \end{tabular}$

Compound	Spectral Change
1 mM DMSO	0 %
2 M DMSO	0.1 %
Glucose	0 %
Fluorobenzene	0 %
Neomycin C	2.7 %
Coenzyme A	5.1 %
Mixture 1	3.8 %
Mixture 2	0.8 %
Mixture 3	3.3 %
Mixture 4	0.3 %

The different mixtures (contents shown in Appending B) were tested using HSQC spectra as stated above, and two of the mixtures exhibited significant changes when compared to a protein-only reference. Mixture 1 was found to show significant changes. When the compounds of the mixture were tested individually, one of them - *N*-3-aminopropyl morpholine (APM, **2.1**, Figure 2.3) was found to bind to the protein with 30 mM affinity as measured by circular dichroism titration and kinetic assays. The same process was used for mixture 3, where another compound, 4-hydroxyphenethyl alcohol (HEPh, **2.2**, Figure 2.3) was found to bind with similar affinity.

a. b.
$$HO \longrightarrow OH$$
 APM APM 2.1 LEPh 2.2

Figure 2.3 - Structures of the two hits: *N*-(3-aminopropyl) morpholine (APM) and b. 4-hydroxyphenethyl alcohol (**2.2**)

While there was no report of biological activity for **2.1**, **2.2** has been previously studied. This compound is also known under the name of tyrosol and is a natural product found in olive oil and argan oil [51, 52]. It is an antioxidant that has been shown to be effective at offsetting the oxidative damage caused by oxidized LDL in Caco-2 cells (small intestine). Therefore one of the fragments has been widely studied and should not cause toxicity *in vivo*, while the other's biological effect remains to be seen. Naturally, the toxicity of the fragments cannot be used determine the toxicity of the final linked compounds.

2.4 Saturation Transfer Difference Screening and Competition Assays

Attempts were made to test ligand mixtures using saturation transfer difference (STD) experiments. While different mixing times and different ligand and protein concentrations and ratios were tested to minimize the appearance of non-specific interactions, the experiment was too sensitive when compared to the HSQC method. Even ligands of negligible affinity as measured by HSQC titrations were indicated as binders and so the method could not be used for initial fragment screening.

While STD experiments were of little use for initial screening, once ligands had been identified by HSQC screening, the binding mode could be further defined by STD experiments. Given that the cross-relaxation between the protein and the ligand is a function of distance, atoms in the ligand that are closer to the protein show larger peaks than atoms that are further away. This method gave some information about the binding distances of **2.1** and **2.2** to AAC(6')-Ii. In the presence of protein (**Figure 2.4**), the intensity of some signals of **2.1** in the difference spectrum are increased; those of the aminoalkyl chain are affected most. For **2.2** with protein, the methylene adjacent to the phenol ring demonstrates a signal 3-fold stronger than all the others, suggesting greater proximity to the protein. Therefore STD experiments yielded information about the importance of the different regions of the fragment in protein binding.

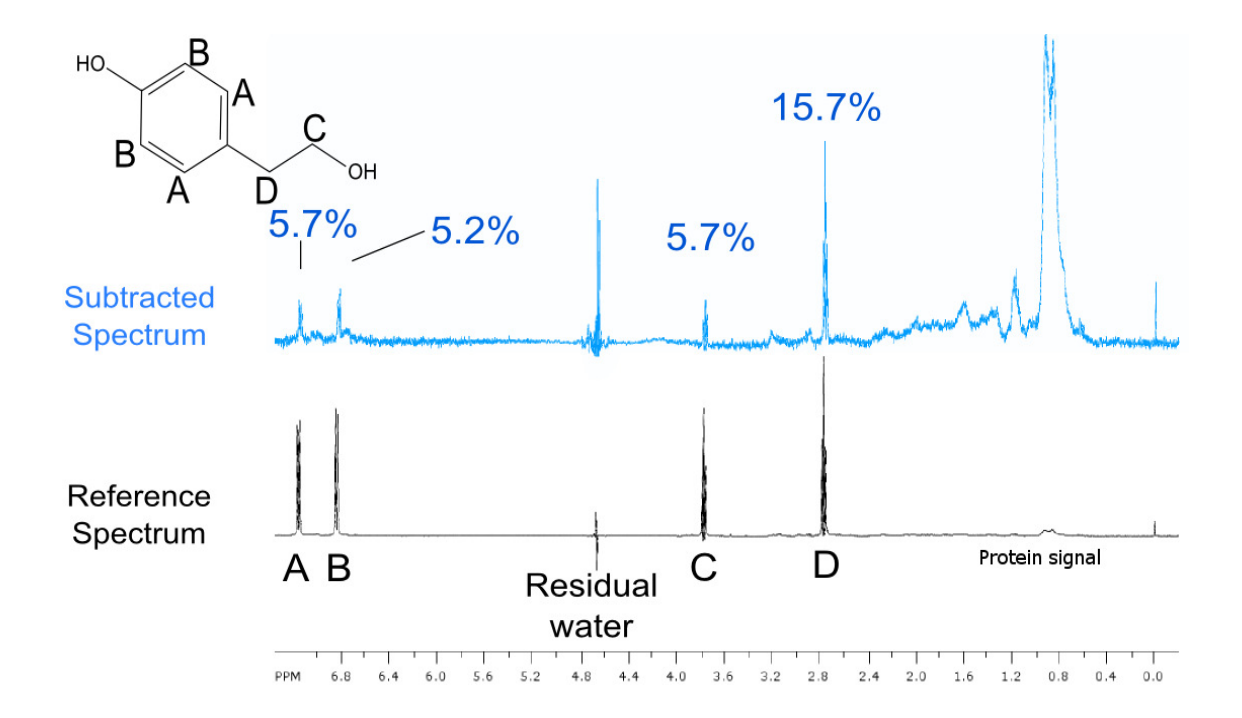


Figure 2.4 - Comparing the (top) STD spectrum (on-resonance spectrum – reference spectrum) to the (bottom) reference proton spectrum of **2.2**.

Furthermore, STD experiments were used to test for concurrent binding or competition of **2.1** and **2.2** to get an idea of the binding sites of the ligands. In competition experiments, one ligand is titrated into a solution of both the second ligand and the protein. As the titration progresses, the spectral signals produced by the first ligand start to disappear as the second ligand displaces it from the protein in the difference spectrum. This only happens if there is a displacement effect, if both ligands bind to the protein simultaneously, then the signals of both compounds appear in the spectrum simultaneously.

2.1 was tested for competition with either of the natural substrates, and was found to bind to the protein in the presence of CoA, but not in the presence of neomycin c. The structure of **2.1** contains two amines, which would be positively charged under the conditions of the experiment (pH 6.5). This would likely allow binding to the aminoglycoside binding pocket of the enzyme, which contains several negative charges.

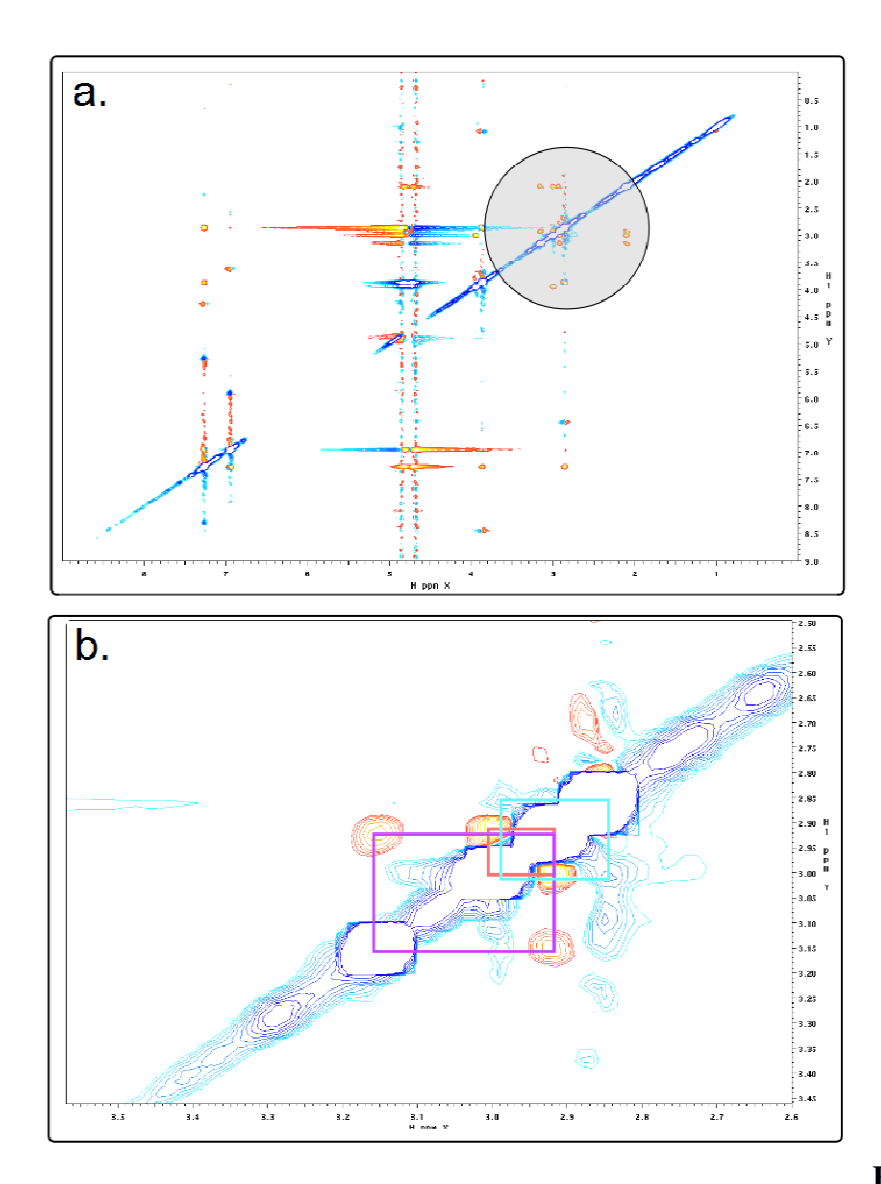


Figure 2.5 - Interligand

NOE spectrum of **2.1** and **2.2** with the protein a. full spectrum b. zooming in on the circled region. Negative peaks (red) indicate intramolecular relaxation while positive peaks (blue) indicate intermolecular relaxation between **2.1** and **2.2** while in the ternary protein-bound complex.

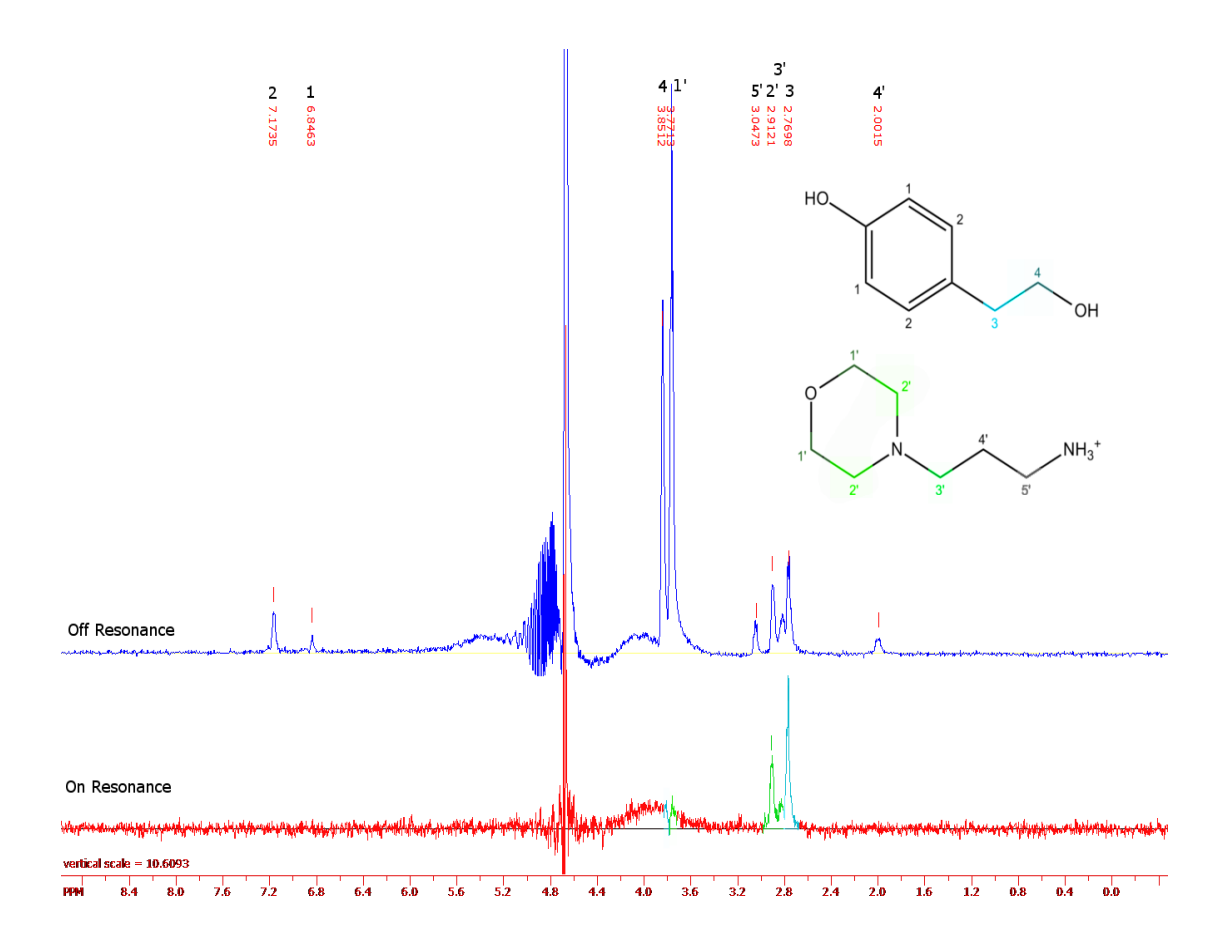


Figure 2.6 - Competition STD experiment showing that residues both from **2.2** and **2.1** are still visible at when at high concentrations (> $10 \times K_d$). Top blue off-resonance spectrum corresponds to the 1H pre-saturation spectrum, bottom blue spectrum is the STD spectrum.

Both ligands were next tested for concurrent binding. In STD competition experiments, both **2.1** and **2.2** were shown to bind without competing each other off (**Figure 2.6**), suggesting that they could bind together and thus could potentially be linked together to form a high affinity ligand. Further testing using ILOE experiments showed cross-peaks between nuclei of **2.1** and **2.2** as shown in **Figure 2.5**, suggesting that they are within 5 Å of each other when bound to protein [35]. This further supported our plan to covalently link them to make a higher affinity ligand.

2.5 Structural Information from HSQCs

In traditional methods of drug design, once a ligand is found, attempts are made to obtain a crystal structure of the ligand bound to protein. Given the weak affinity of the fragments identified in this study and the large degree of disorder in this protein, this was deemed challenging. Since a partial NMR assignment of the AcCoA-bound form of AAC(6')-Ii had already been obtained, this structure was used as a starting point for obtaining structural information by NMR. Experimentally, this was done by taking a HSQC spectrum of the protein fully bound to CoA [19] and then titrating in a secondary ligand (2.2 or 2.1 as shown in Figure 2.7). Since the ligand binding events occur in slow exchange, the changes could only be tracked by monitoring disappearance of the peaks of the CoA bound form. Those changes were then mapped onto the structure of the protein (Figure 2.8).

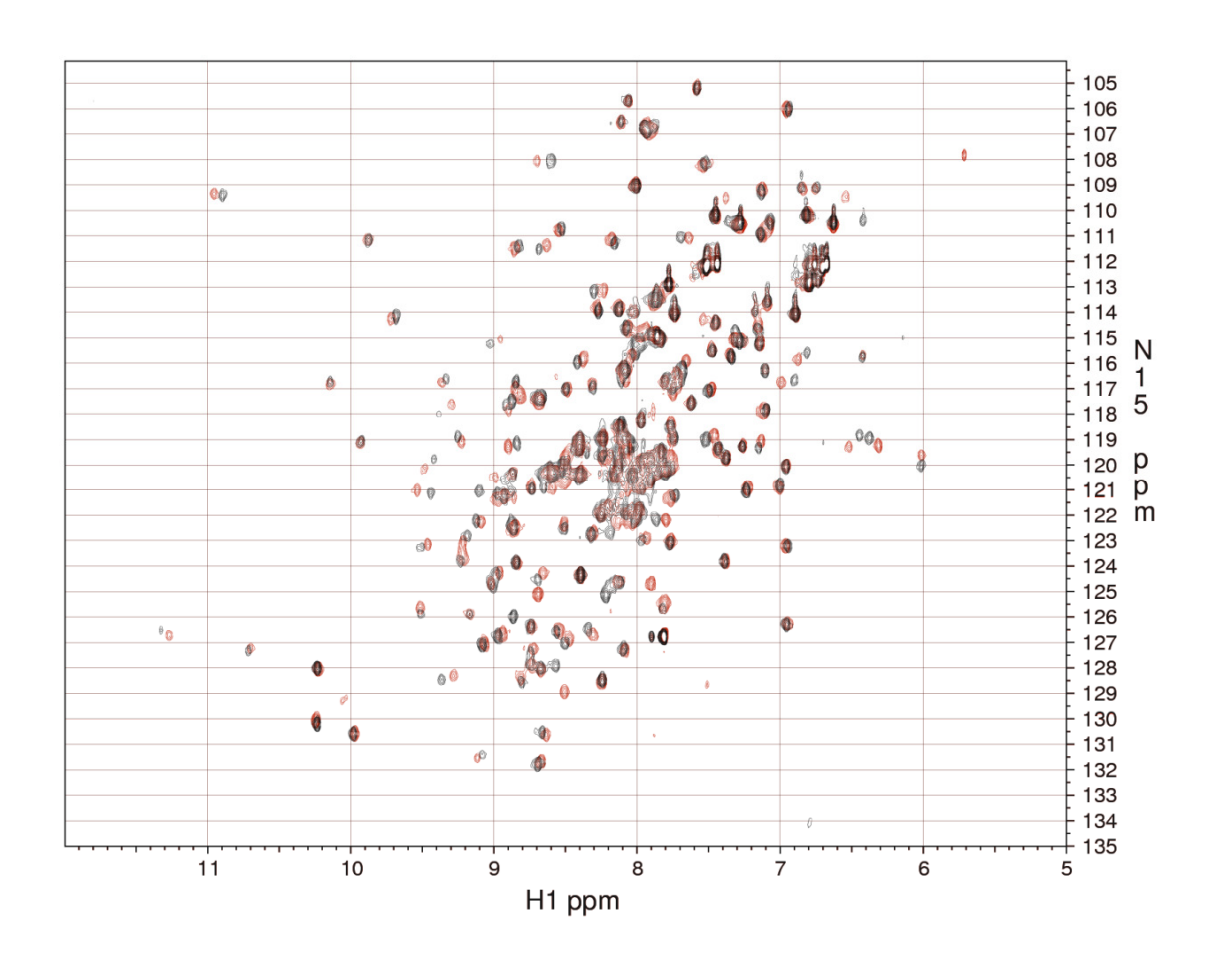


Figure 2.7 - Overlay of ¹⁵N/¹H HSQC spectra of AAC(6')-Ii bound to CoA (black) and the protein bound to CoA and **2.1** (red).

The changes associated with **2.1** and **2.2** are non-overlapping as expected for two ligands binding in different sites. Peaks shifting due to **2.1** localize mostly in the aminoglycoside binding site (E27, E28, D112, **Figure 2.7**a), and the adjacent α-helix (S32, A34, **Figure 2.7**b), which is unsurprising considering the positive charge that is present on this fragment at the assay pH. There are four additional peak shifts (D52, Q53, S81, Q122, Figure 2.7c) away from the binding site in random coil regions that may change due to protein conformational shifts upon binding, possibly in an open-close mechanism. Thus **2.1** binding seems to cause changes mostly in the active site, but also induces minor changes in a distant site.

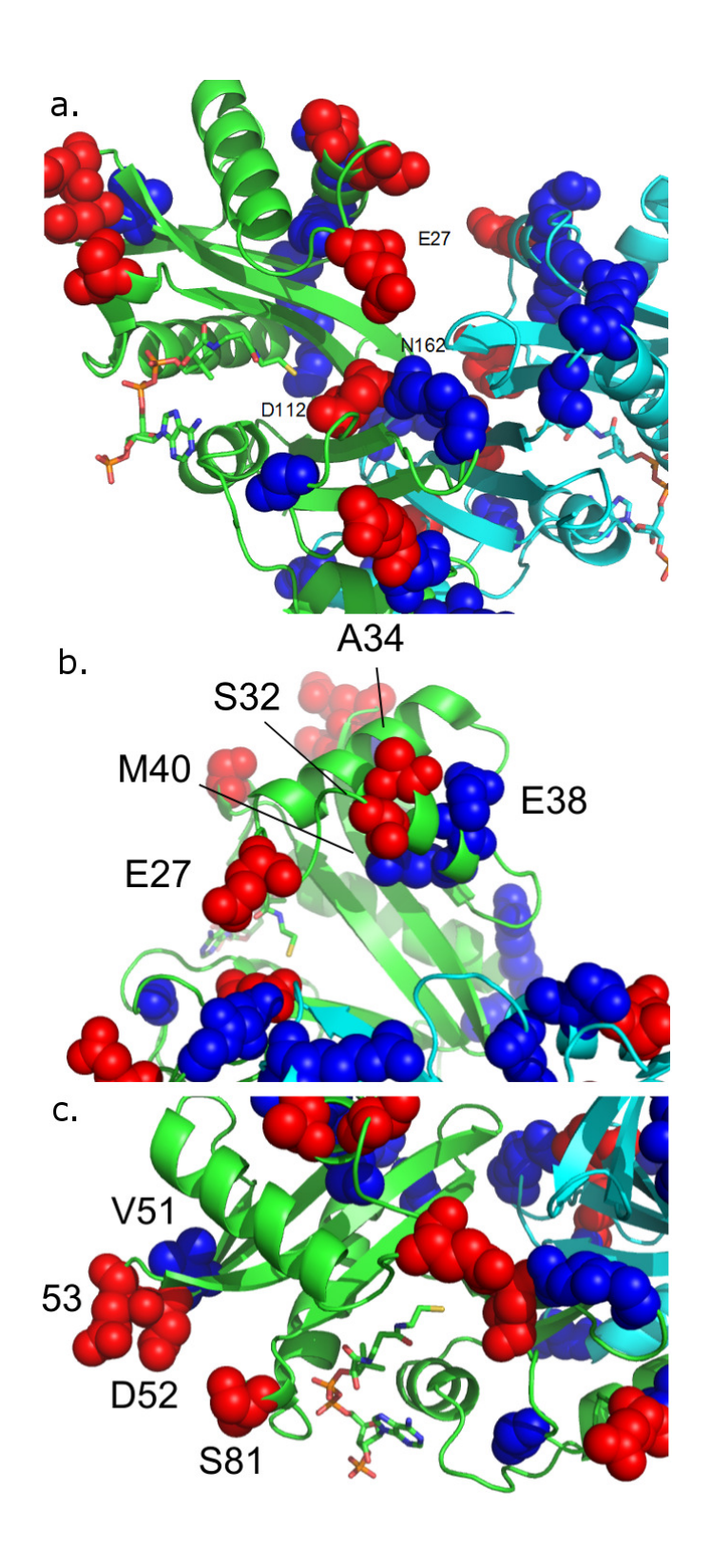


Figure 2.8 - Crystal structure of AAC(6')-Ii with the **2.1** spectral shifts shown in red space fill and **2.2** spectral shifts shown in blue space fill a. view showing the binding site b. view showing alpha helix residues c. view showing distant changes.

Upon binding to **2.2**, most of the peaks observed to shift correspond to residues outside of the active site. Two of the residues observed to shift (E38, M40) lie in the same α -helix as **2.1** does. One of the peak movements (V51) also matches the region of **2.1** binding for putative opening-closing. The remaining few shifts seem to correspond to movements in hinge regions adjacent to secondary structure elements, suggesting a rearrangement of the protein upon binding. The lack of changes in the active site may be due to the binding of **2.2** outside of the binding site or simply because of the presence of a bound CoA molecule, such that the changes caused by **2.2** are the same as those caused by CoA. Therefore binding of **2.2** appears to be complimentary to the binding of **2.1** to AAC(6')-Ii.

2.6 Other NMR Methods

HSQC and STD experiments yielded the bulk of the information that was used in initial screening, two additional experiments were attempted to identify ligands: T1p and waterLOGSY. While T1p experiments worked as well as expected, they had similar advantages and disadvantages as STDs and therefore were not used. The waterLOGSY experiment presented problems that we could not resolve. After much time and effort put into getting this technique to work, its use was abandoned in favor of more robust methods.

2.7 Conclusion

A series of 42 compounds was tested in four groups for binding to AAC(6')-Ii using a variety of NMR methods. HSQCs proved to be the most effective assay to test for binding with this protein due to its good sensitivity and the fact that non-specific binding is not detected. While STD could not be used for screening due to its tendency to

produce false positives, it was put to good use in testing for competition between the fragments that were found to bind by HSQC and the natural substrates. Additionally, structural information was obtained for both **2.2** and **2.1** by titrating them into a CoA-saturated protein, whose NMR spectrum has already been assigned, allowing the spectral changes to be mapped to the crystal structure of the protein.

Chapter 3 -	Biological A	Activity		

3.1 Preface

The goal of this chapter is to define the inhibitory properties of the previously discovered hits and further define the molecular properties that determine binding of these compounds to AAC(6')-Ii through chemical modifications and binding measurements using differential scanning fluorimetry and enzyme kinetics.

Simple, well known methodologies were used to vary the functionality of the fragments in different ways to provide variability as will be described below. In addition to the fragment modifications, several hybrid molecules synthesized in an attempt to combine the fragments into a high affinity binder. A series of commercial molecules also complemented the library

The author performed all of the experiments reported in this chapter for synthesis, differential scanning fluorimetry testing and kinetic assays.

3.2 Introduction

In the previous chapter, a small library of compounds was screened by NMR methods and two hits (**2.1** and **2.2**) were found to bind to AAC(6')-Ii with weak affinity. These two hits were further characterized for their binding to the protein by NMR HSQC experiments. Here chemical modifications of these hits are explored. The methods used to evaluate the relative binding affinity of the derivatives compared to the initial hits were differential scanning fluorimetry (DSF) and enzymatic kinetic measurements.

As described in chapter 1, DSF has been used extensively for screening small molecules against protein targets [53, 54], but also for measuring the thermal stability of mutants or protein complex variants [55]. DSF has the advantages of being simple to use and

allowing medium-to-high throughput. It also generates data that permit rapid calculation of melting temperature (T_m) . While DSF allows comparisons of the affinity of different ligands for a biomolecule, it does not allow measurements of enzyme inhibition. To get a complete picture of binding and inhibition, enzyme kinetics were also performed to complement the DSF data.

3.3 Synthesis and Derivatives

N-(3-Aminopropyl)morpholine (**2.1**) and 4-hydroxyphenethyl alcohol (**2.2**) were both established to bind to AAC(6')-Ii by NMR in the previous chapter. In order to get a structure-activity relationship for these compounds many derivatives were either synthesized or obtained from commercial sources. The derivatives were designed to encompass various sizes and shapes, hydrogen bonding and electronic properties as shown in Figure 3.1. Some derivatives were also designed to incorporate elements of both **2.1** and **2.2** (hybrid molecules, Section 3.3.3).

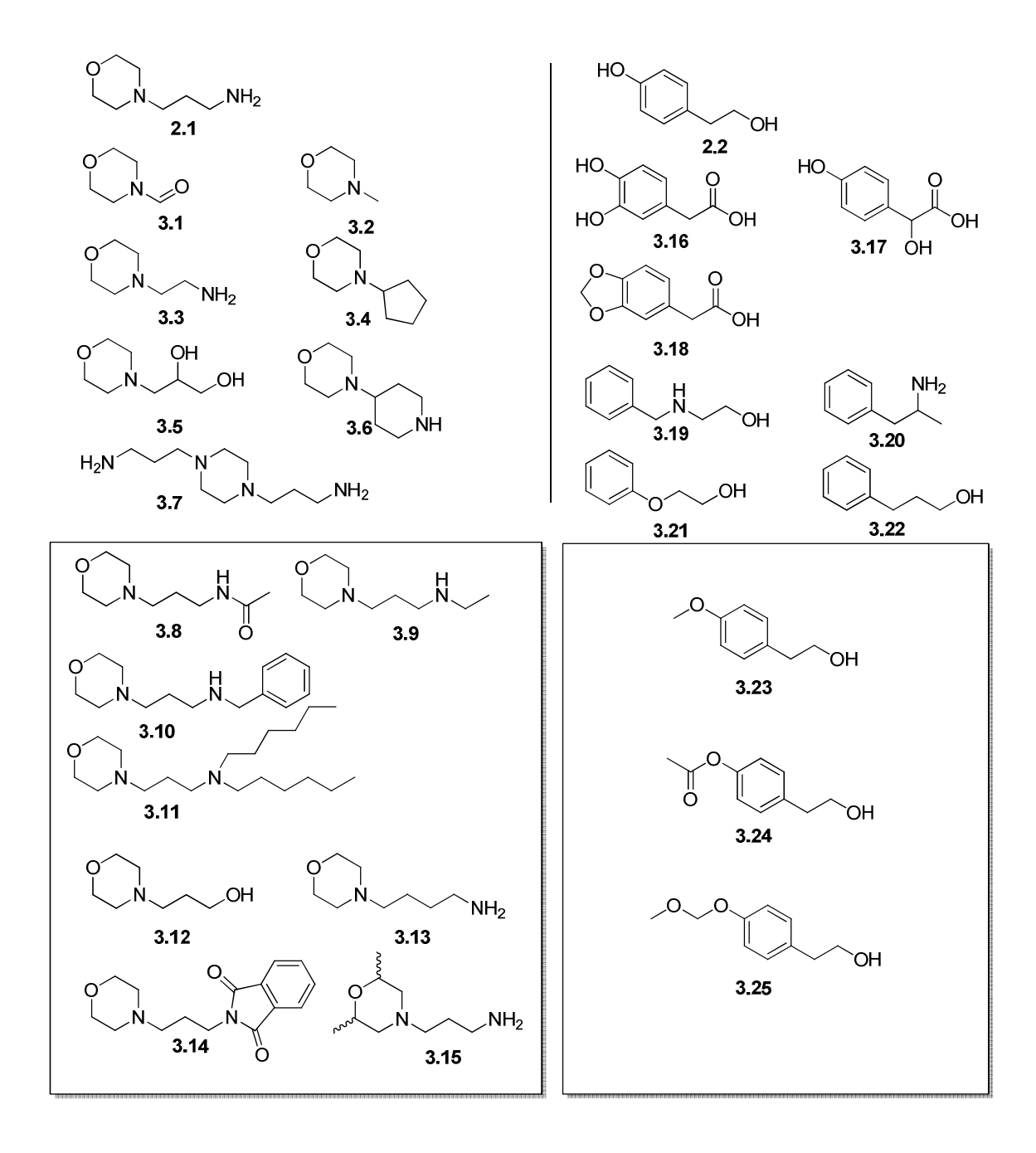


Figure 3.1 – Commercial and synthetic derivatives of **2.1** and **2.2**, Synthetic targets are highlighted in boxes.

3.3.1 Derivatives of 2.1

Previous screening and NMR characterization suggested that the best point of modification for **2.1** to link to another hit such as **2.2** might be at a carbon adjacent to the ether on the morpholine ring. This was indicated by proximity of those carbons to **2.2** in

NMR protein assays of the ternary complex (see Section 2.4). Such derivatives tend however to be only accessible via ≥ 4 step syntheses with low efficiency [56, 57]. Modifications at the primary amine or alkyl chains position, however offered rapid access to a large library of compounds.

The *N*-ethylated molecule **3.9** was a priority target to measure the effect of adding a small alkyl group at the primary amine position. Efforts to synthesize it by reductive amination failed due to a competing polymerization reaction with acetaldehyde. Thus, acetylation of commercially available **2.1** was first carried out to yield acetamide **3.8**. This compound was reduced with lithium aluminum hydride to afford the second product, **3.9**.

Scheme 3.1 – Synthetic scheme for 3.8 and 3.9

In order to measure the effect of hydrophobic groups of both alkyl and aromatic types, compounds **3.10** and **3.11** were obtained as outlined in

Scheme 3.2. While benzyl substitution yielded both the singly (**3.10**) and doubly benzylated compounds, reaction with bromohexane yielded exclusively the doubly hexylated amine, **3.11**.

Scheme 3.2 - Synthetic scheme of compounds 3.10 and 3.11

In order to measure the effect of a group lacking the positive charge while retaining hydrogen-bonding character, alcohol **3.12** was synthesized according to Scheme 3.3. Given the low nucleophilicity of morpholine, conventional heating gave low yield (8%), but microwave irradiation afforded much higher yield (69%).

Scheme 3.3 – Synthetic scheme for compound 3.12.

Compound **3.14** was designed to incorporate an aromatic moiety while maintaining some hydrogen-bonding capacities. The simple reaction of the primary amine **2.1** with phthalic anhydride afforded the phthalimide in excellent yield (Scheme 3.4).

Scheme 3.4 - Synthetic scheme of compound 3.14.

Compound **3.13** was meant to test the effect of a longer chain length. Thus morpholine was reacted with 2-(4-bromobutyl)isoindoline-1,3-dione to yield intermediate **3.32**. As with compound **3.12**, this reaction proceeded more efficiently under microwave irradiation (75%) than with conventional heating (30-44%). The phthalimide protecting group was removed using the Ing-Manske procedure [58] with ethanolic hydrazine to afford target **3.13**.

Scheme 3.5 – Synthetic scheme for compound **3.13**.

Finally, in order to evaluate the binding of derivatives of **2.1** with modifications on the morpholine ring, the *syn* and *anti* diastereomers **3.15** were made in two steps (Scheme 3.6). 2,6-Dimethylmorpholine was reacted with 2-(4-bromopropyl)isoindoline-1,3-dione under microwave irradiation to afford a mixture of *syn* and *anti* isomers **3.26** and **3.27** which were separated by chromatography. Deprotection was performed for each **3.26** and **3.27** separately using the Ing-Manske procedure [58] once again to yield **3.15** *syn*, and the mixture of enantiomers **3.15** *anti*.

Scheme 3.6 – Synthetic scheme for **3.15**

3.3.2 Derivatives of 2.2

NMR studies suggested that **2.2** might tolerate derivatives at the methylene group alpha to the aromatic ring (including STD and ILOE experiments in section 2.4). Most derivatives were obtained from commercial sources; two of them were also synthesized.

Compound **3.24** was synthesized by acetylation of **2.2** using acetic anhydride as shown in Scheme 3.7 to test for the effects of modifications at the phenolic hydroxyl.

Scheme 3.7 – Synthetic scheme for 3.24.

The synthesis of compound **3.25** followed Scheme 3.8. Starting material **2.2** was modified with methoxymethyl chloride to afford the MOM-protected **2.2**. Both compounds **3.24** and **3.25** were designed to incorporate a hydrogen-bond acceptor without the acidity and instability of a phenol group.

Scheme 3.8 – Synthetic scheme for **3.25**.

Many derivatives were obtained which did not include the phenolic hydroxyl such as 3.18-3.23 yet incorporated variations in the chain as replacements of the alcohol such as amines, ethers, hydroxyls or combinations of these. These different groups on the chain were designed to affect the electronic properties.

Another subset of derivatives of **2.2** varied in the oxidation state, both on the chain (**3.17**) and the aromatic group (**3.16-3.18**). Such modifications on the phenyl ring can largely influence the electron density of the ring, as well as its redox potential. Addition of an alcohol on the chain (**3.17**) also allowed variation in the orientation and number of H-bond donors and acceptors. Oxidation of the terminal alcohol to a carboxylic acid also allowed study of the effect of charge at this position (**3.16**, **3.18**).

3.3.3 Hybrids

A large number (120) of potential hybrid molecules of hits **2.1** and **2.2** were first tested *in silico* with the Molecular Forecaster suite of software using the bisubstrate-bound crystal structure of AAC(6')-Ii. While it was not expected that the docking would necessarily be representative of the binding affinity *in vitro*, it was taken as a guideline for the magnitude of interactions between ligand and protein. Some of the docked compounds scored very well when compared to natural ligand, but were more challenging to synthesize. Instead, it was decided to synthesize some of the compounds with slightly

worse docking score, yet easier synthetic routes. Thus target compounds **3.28-3.32** showed good docking scores, though not the best, and were accessible in few steps.

Five hybrid molecules (3.28-3.32) combining features of 2.1 and 2.2 were synthesized in order to sample different orientations and distances between the two.

Synthesis of compound **3.30** involved the EDC peptide coupling of compounds **2.1** and **3.18** (Scheme 3.9). Compound **3.31**, on the other hand was synthesized by transforming acid **3.16** into the acid chloride with oxalyl chloride and this acid chloride was reacted with compound **2.1** to yield hybrid **3.31**.

Scheme 3.9 - Synthetic scheme for compounds 3.30 and 3.31.

The synthesis of compounds **3.28** and **3.29** is shown in Scheme 3.10. Propyldimorpholide (**3.28**) was synthesized by double substitution of malonyl chloride with morpholine. The other hybrid molecule **3.29** was synthesized by double substitution of 1,3-ditosylpropane with morpholine.

Scheme 3.10 – Synthetic scheme for compounds 3.28 and 3.29.

In order to make 2-benzyl-1,3-dimorpholinopropane (3.32), the commercially available diethylbenzyl malonate was reduced to the diol by lithium aluminum hydride reduction (Scheme 3.11). This diol was then mesylated using mesyl chloride. The mesylate was then doubly substituted with morpholine to yield the desired hybrid product (3.32) after purification by chromatography on neutral alumina.

Scheme 3.11 - Synthetic scheme for compound 3.32.

3.4 T_m of AAC(6')-Ii

Differential scanning fluorimetry (DSF) was used as a quick screening assay to evaluate the relative affinity of compounds 3.1-3.32 for AAC(6')-Ii. As discussed in chapter 1, an increase in the protein T_m in the presence of a molecule suggests that it is a ligand for the biomolecule. As a reference point, the T_m of AAC(6')-Ii was measured in the absence of ligand using Sypro orange as the indicator dye. Representative data are shown in Figure 3.2A. When used with AAC(6')-Ii alone in buffer conditions (300 mM ionic strength) a T_m of 49.0 ± 0.5 °C was calculated. In order to validate DSF for T_m determination, CD was also used with free AAC(6')-Ii. A wavelength of 222 nm was selected as it is the λ_{max} for α -helical patterns in protein CD spectra. The melting point obtained by CD was 49.4 ± 0.4 °C, which matched the DSF measurement, confirming the dye had negligible effect on the melting temperature.

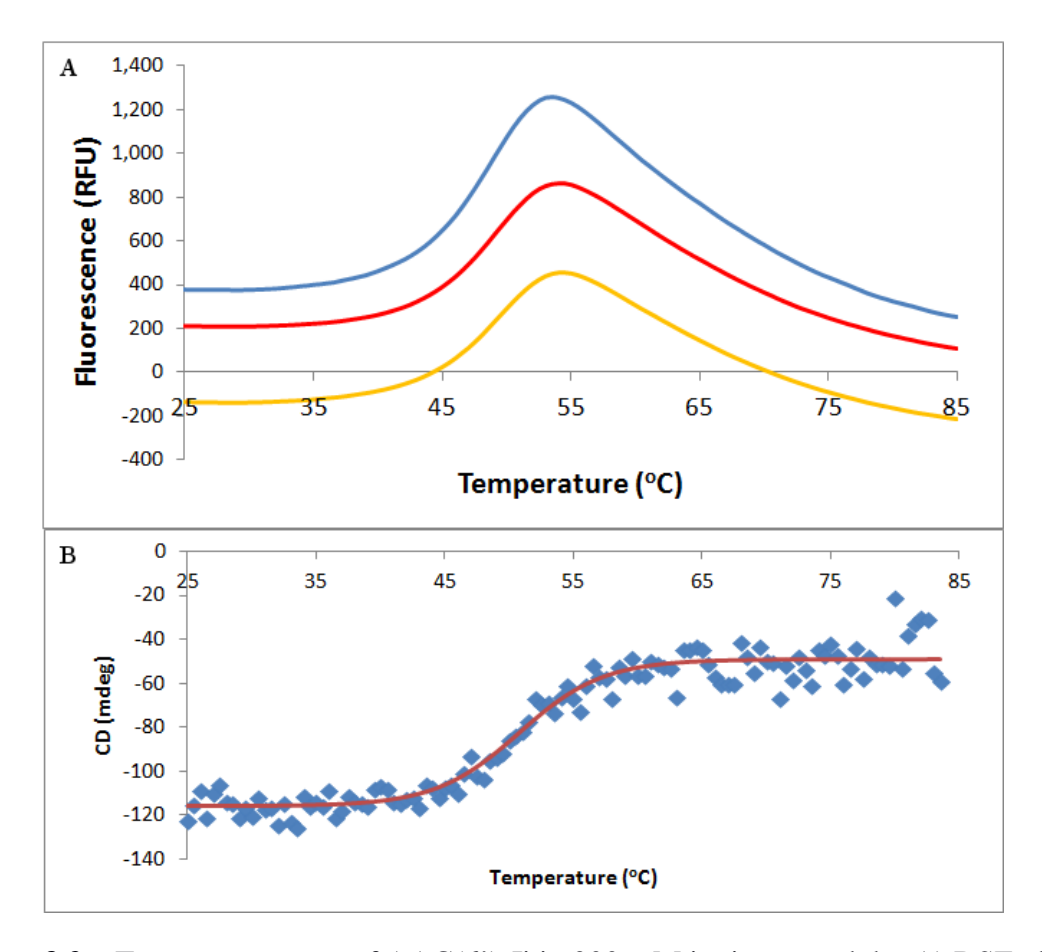


Figure 3.2 – T_m measurements of AAC(6')-Ii in 300 mM ionic strength by A) DSF, three replicates are shown (blue, red, yellow) with an arithmetic mean $T_m = 49.0 \pm 0.5$ °C. B) Circular dichroism at 222 nm with increasing temperature. The trace shown is one of three with an arithmetic mean $T_m = 49.4 \pm 0.4$ °C.

When measured under low salt conditions (200 mM buffer, no salt), T_m for AAC(6')-Ii was measured to be $36 \pm 1^{\circ}$ C. Given the observed variability in the protein's T_m , it was also measured in a variety of ionic strength and pH conditions, and was found to depend empirically on the log of the ionic strength of the assay medium (Figure 3.3). Therefore when measuring the T_m of AAC(6')-Ii in the presence of small molecules, controls had to be used to account for changes in ionic strength.

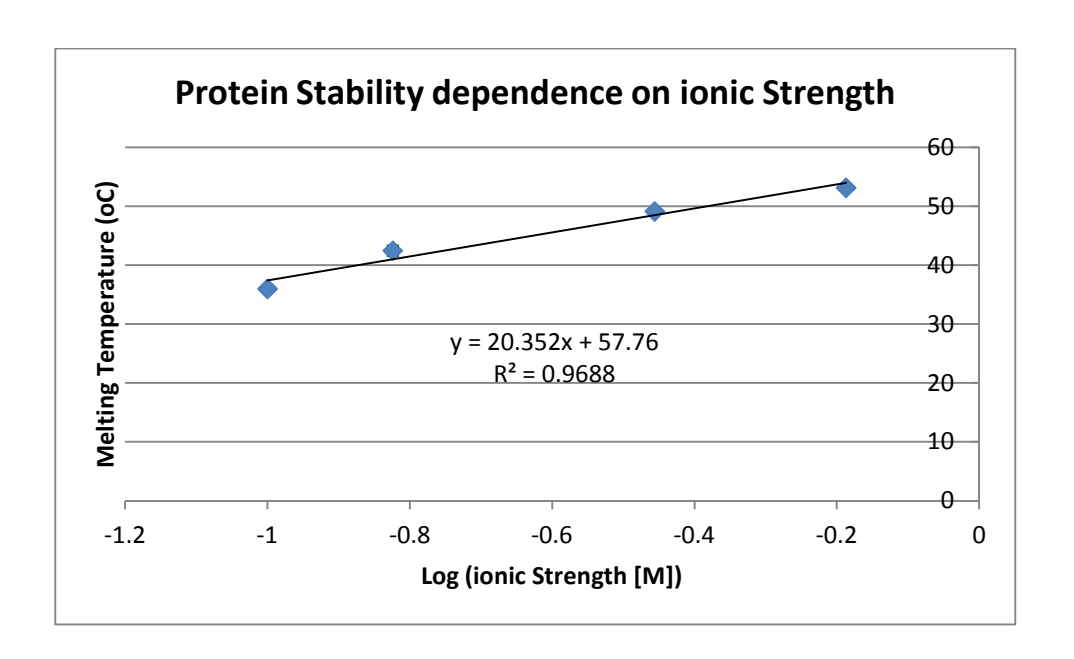


Figure 3.3 - Protein Tm was measured by DSF. Ionic strength was calculated from buffer concentration, pKa and solution pH in addition to added NaCl to adjust for higher ionic strengths.

$3.4.1\ T_m$ of AAC(6')-Ii in the Presence of Natural Substrates and Known Inhibitors

With a reference T_m established for free AAC(6')-Ii, the next step was to look at the effect of known AAC(6')-Ii ligands on the T_m of this protein. In the presence of neomycin c (0.8 mM, 150 × K_M [18], Figure 3.4), the T_m was found to increase by 22°C, while with the product CoA (0.8 mM), the T_m was found to increase by 8°C. This large difference between natural substrates was somewhat surprising given the similarity in K_M and k_{cat}/K_M for these two compounds.

The natural substrates were also tested in combination and with varying salt concentrations. Given the positive charge on aminoglycosides and the highly charged binding pocket on AAC(6')-Ii, increased shielding due to increasing ionic strength

should reduce the affinity of the compound, causing a decrease in T_m (Figure 3.5). However, with increasing ionic strength, the T_m in the presence of neomycin c remains unchanged, suggesting either that shielding has no effect on binding or that the electrostatic interactions of the aminoglycoside substrate can be substituted by a high salt concentration. Conversely, while AcCoA carries approximately three negative charges (on the phosphate groups), the electrostatic interactions are thought to contribute a smaller part of the binding affinity. Unexpectedly however, increasing ionic strength seems to increase the apparent affinity of CoA for AAC(6')-Ii, hinting at a the involvement of electrostatic interactions related to protein thermo-stability away from the CoA binding site. One possible explanation for this might be related to the established binding cooperativity [20, 21]. Therefore increasing ionic strength in the buffer caused an increased ΔT_m in CoA while having no effect for neomycin c.

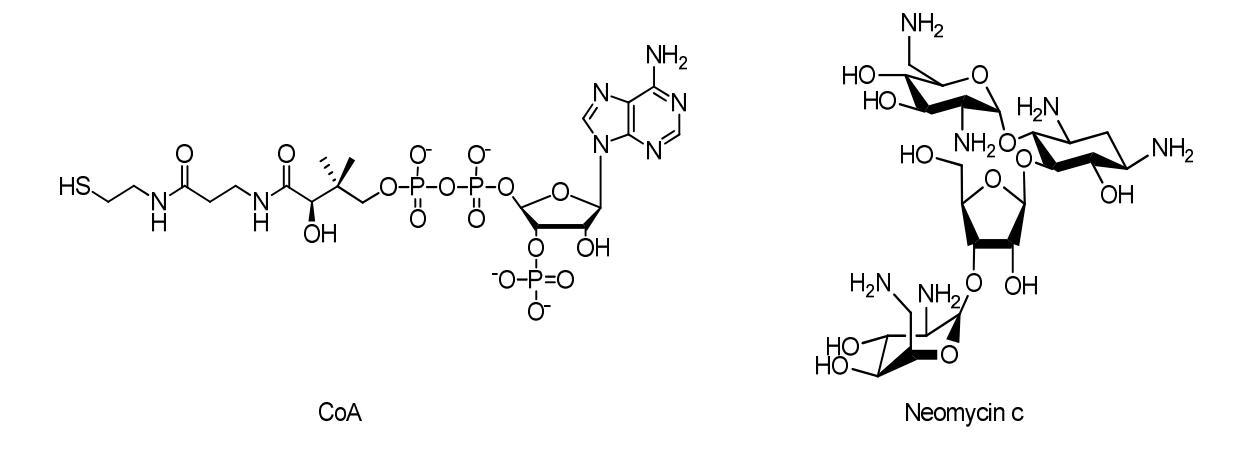


Figure 3.4 - Structures of product CoA and substrate neomycin c.

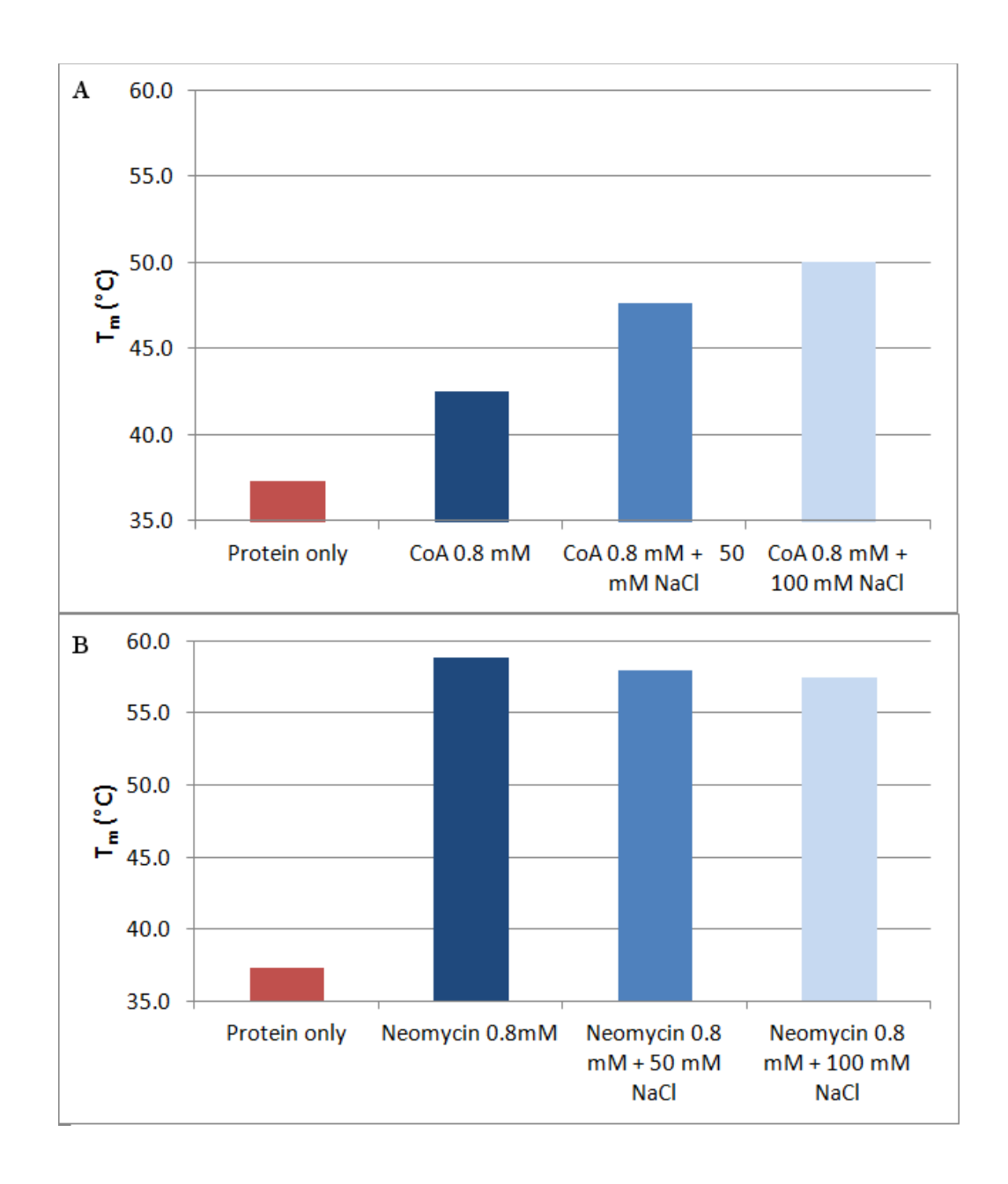


Figure 3.5 – AAC(6')-Ii (5 μ M) T_m was investigated using natural substrates as a function of ionic strength. A) The Tm shift induced by CoA (0.8 mM) changed greatly with increasing ionic strength. B) With neomycin c (0.8 mM), there is no effect with increasing ionic strength.

In addition to comparing the free protein to the bound protein, AAC(6')-Ii in complex with a known bisubstrate inhibitor (**NC1**, Figure 3.6) was another important positive control. As expected from the K_i (76 nM [22]), the measured T_m is greater with **NC1**

than with either substrate individually, and greater even than the sum of both as shown in Figure 3.7.

Figure 3.6 - Structure of the bisubstrate NC1

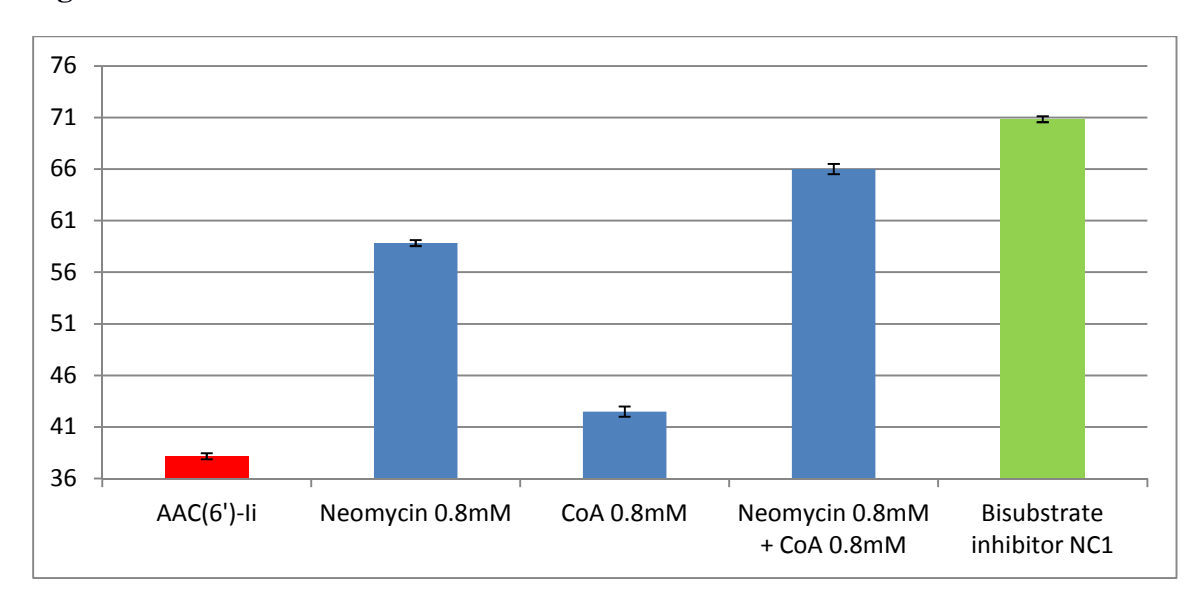


Figure 3.7 - DSF measurements of $T_{\rm m}$ with each natural substrate alone, a combination of both, and the bisubstrate inhibitor.

3.4.2 Fragments

All commercial and synthetic derivatives of **2.1** and **2.2** (Figure 3.1) as well as the hybrids **3.28-3.32** were tested for binding by DSF. Fourteen derivatives of **2.1** were

tested, but none showed a larger ΔT_m than **2.1** itself, whereas the most promising of the ten derivative of **2.2** was 3,4-dihydroxyphenylacetic acid (**3.16**), with a concentration dependent increase in T_m of 4.4°C (2 mM). Most other modifications to fragments yielded little to no T_m difference when compared to protein sample with an equivalent ionic strength.

3.4.3 Hybrids

The hybrid molecules (3.28-3.32) were expected to show enhanced activity compared to 2.1 and 2.2. When compared to the initial hits, 3.28, 3.29, and 3.32 had no effect on the protein melting temperature. The end-linked hybrid 3.30 interfered with DSF such that the no melting temperature could be measured with the compound in the mixture. Finally, 3.31 produced a marginally increased T_m compared to that of 3.16, indicating that the linking increased affinity to the protein. The small T_m increase (0.9°C) though suggests only a very small increase in affinity. Thus, of all 32 derivatives tested only 3.16 and 3.31 showed increased activity compared to the fragment hits 2.1 and 2.2.

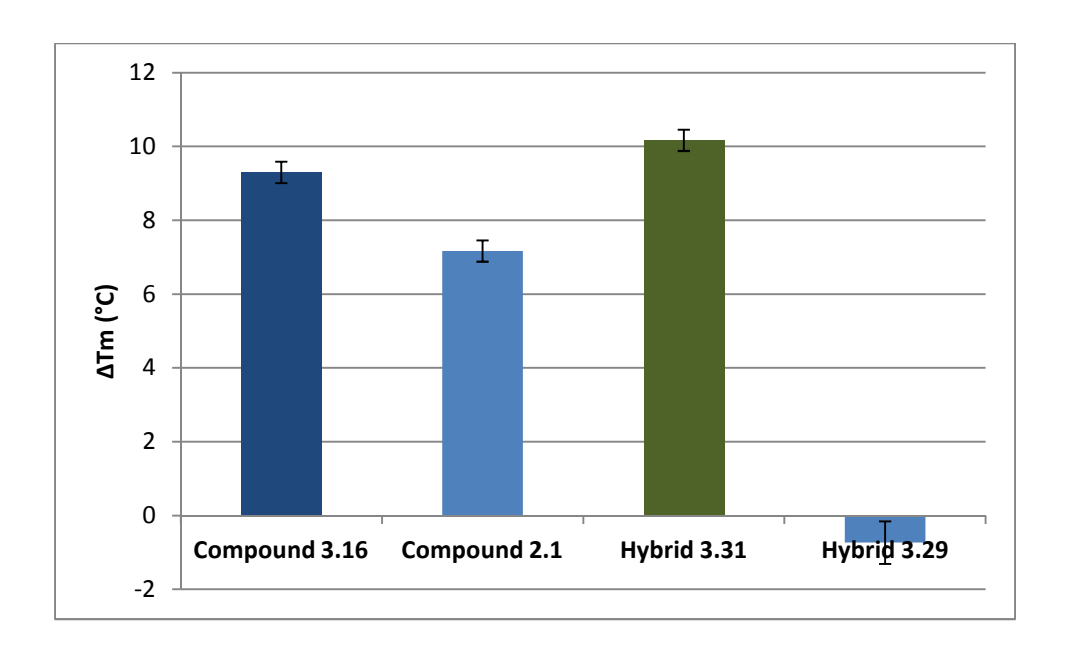


Figure 3.8 - DSF melting point difference from protein only for fragment hits and hybrids.

3.5 Kinetic Studies of AAC(6')-Ii

3.5.1 Derivatives of 2.1

When tested in the kinetic assay, **2.1** was found to be a substrate for AAC(6')-Ii (Figure 3.9). The kinetic parameters that were measured for **2.1** were $K_M = 33.4$ mM and $k_{cat} = 0.15 \text{ s}^{-1}$ for a $k_{cat}/K_M = 4.49 \text{ M}^{-1}\text{s}^{-1}$, which is almost four orders of magnitude weaker than neomycin ($k_{cat}/K_M = 3.9 \times 10^4 \text{ M}^{-1}\text{s}^{-1}$) and AcCoA ($k_{cat}/K_M = 1.7 \times 10^4 \text{ M}^{-1}\text{s}^{-1}$)[18]. Given the competition that was observed with aminoglycosides and given the positive charge on the molecule at neutral pH, this result was not totally unexpected.

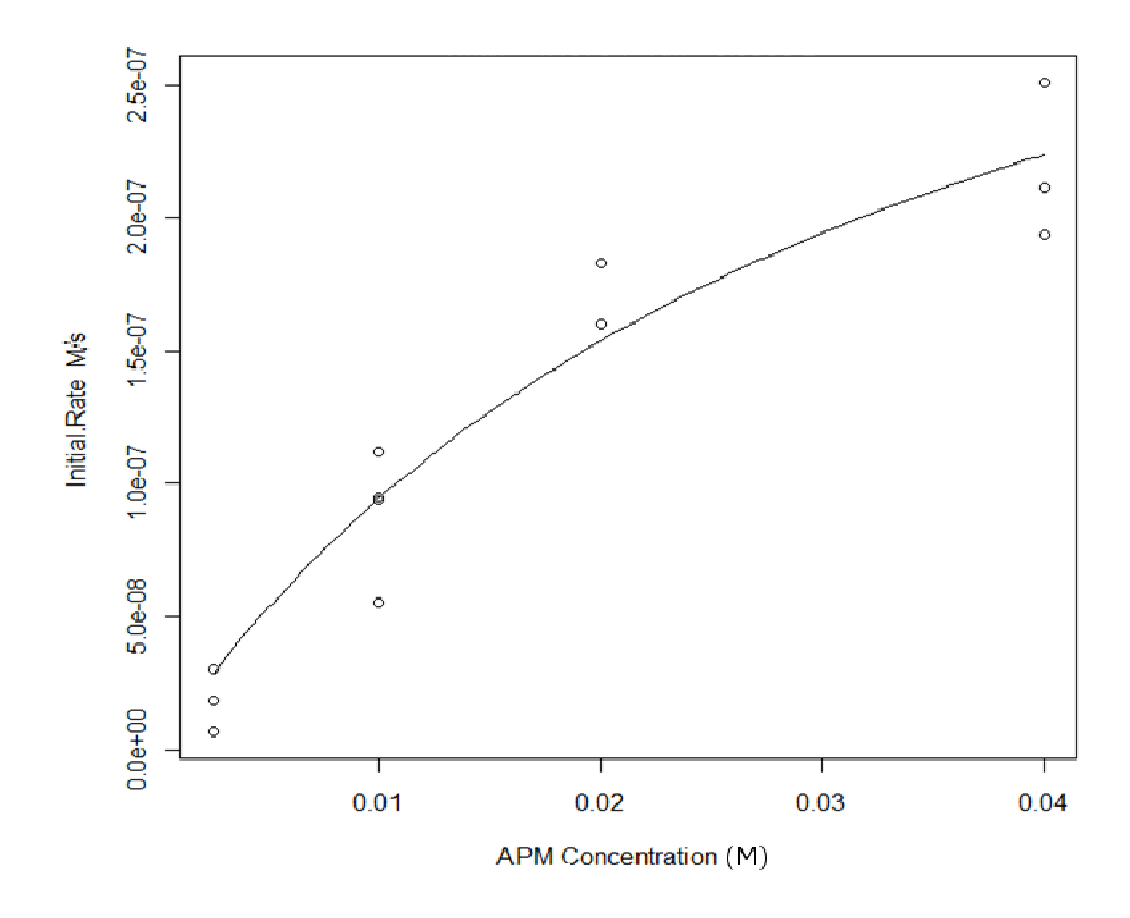


Figure 3.9 - Michaelis-Menten curve of **2.1** substrate activity. This curve measured a K_M of 33.4 mM and k_{cat} of 0.15 s⁻¹.

Compound **3.3** with the n = 2 chain length (N-(2-aminoethyl)morpholine) showed negligible kinetic activity (Figure 3.10), indicating that a minimum chain length of three is required for substrate activity. The rigidified derivative N-(4-piperidinyl)morpholine (**3.6**), showed no substrate activity and only marginal inhibition ($IC_{50} > 100 \text{ mM}$). Another derivative, N-3-(1,2-dihydroxypropyl)morpholine (**3.5**) also had negligible activity, with no inhibition with concentrations up to 12.5 mM, suggesting an amine is necessary at the terminal position for binding.

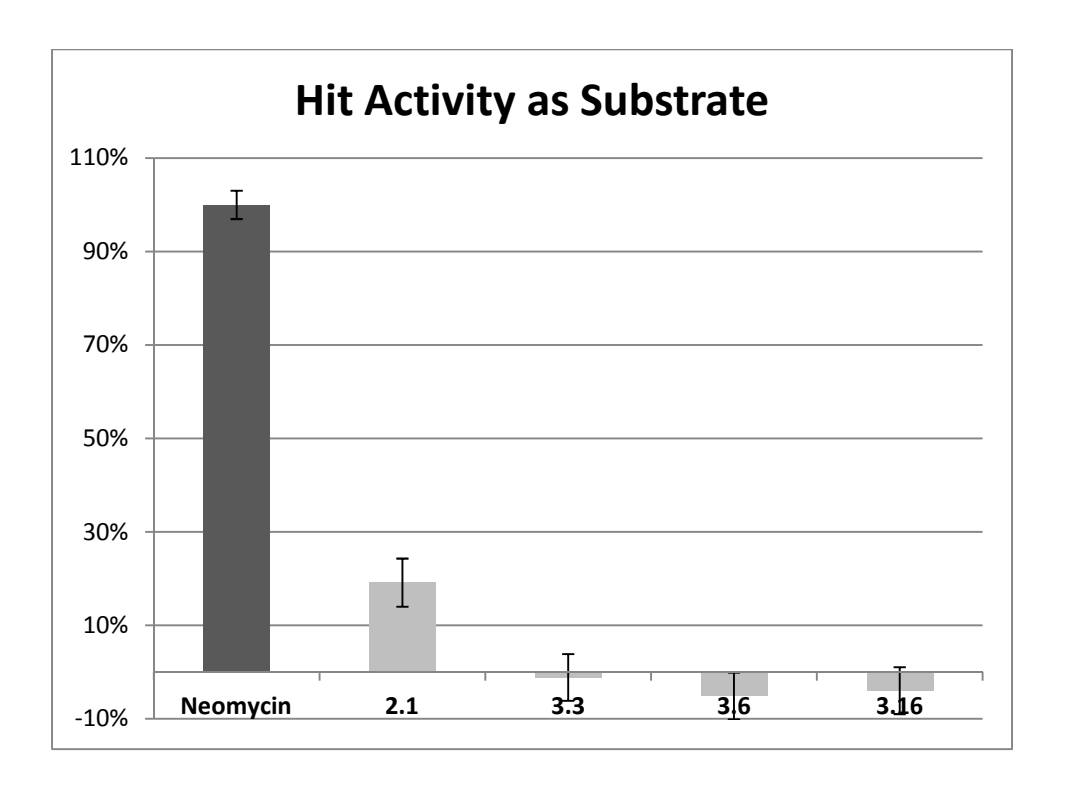


Figure 3.10 - Derivatives relative rate of hydrolysis of AcCoA with AAC(6')-Ii, using derivatives to replace neomycin c.

3.5.2 Derivatives of 2.2

In the AAC(6')-Ii kinetic assay, compound **2.2** showed no substrate activity, but inhibited enzyme activity with $IC_{50} = 70$ mM (Figure 3.11). For derivative **3.23-3.25** however, all inhibitory activity was lost, suggesting a key interaction between the phenolic OH and enzyme. Thus modification at this phenolic hydroxyl was not well tolerated.

3,4-Dihydroxyphenylacetic acid (**3.16**) was tested for AAC(6')-Ii inhibitory activity, but even at high concentrations (250 mM), only a small decrease in protein activity (20% reduction in activity) was observed.

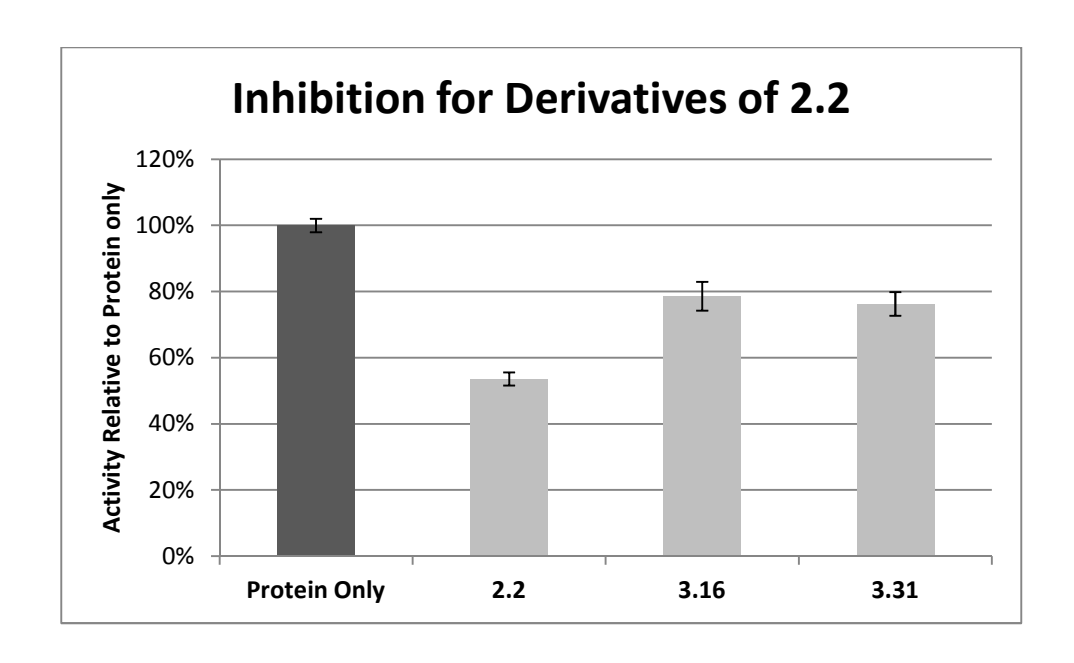


Figure 3.11 - Inhibition by derivatives of **2.2**, compound **2.2** (68 mM) shows 54% relative turnover rate while both **3.16** and **3.31** show 78% activity at much higher concentration (250 mM).

3.5.3 Hybrids

Of all hybrid compounds (3.28-3.32), only 3.31 showed activity and hence only this one was tested for inhibition. Here again, even at high concentration (250 mM), this compound exhibited only a mild inhibition (31%) under standardized kinetic assay conditions, even at such a high concentration.

3.6 Conclusion

After the initial screening by NMR, many derivatives of the initial hits **2.1** and **2.2** were tested for binding to AAC(6')-Ii by DSF and with a kinetic assay. None of the derivatives of **2.1** were more active than the original hit, while a few were equivalent. One of the derivatives of **2.2** (**3.16**) was slightly more active than **2.2** in the DSF binding assay, however when tested by kinetics, it showed decreased activity. Finally, while

hybrid compound 3.31 showed slightly improved binding than 2.1 or 3.16 using DSF, the						
kinetic inhibition profile of the compound is still far too weak to be a useful inhibitor.						

Chapter 4 Contributions and Futu	re Direction	

4.1 Contributions

The work described in this thesis contributes to the advancement of science in the following way. Flexible proteins have always been an obstacle for inhibitor design due to the lack of structural information. Given their flexibility, these proteins can be immune to highly informative methods such as X-Ray crystallography or computational modelling [59-61]. Additionally, the more commonplace screening methods can be ineffective due to the slow-exchanging nature of the protein-ligand complexes (Section 1.4.2) [35].

In this thesis, many screening methods were attempted on the highly flexible resistance-causing enzyme AAC(6')-Ii. Using NMR to identify ligands with HSQC and STD experiments, the changes brought on by this binding event were further characterized. Many fragments were tested for binding and these allowed for an exploration of the chemical space that favored binding to the enzyme. While no high affinity ligands were identified from these NMR assays, it allowed the identification of fragments that bind to the protein.

Through the modifications of the hits described in chapter 3, derivatives of the original hits were synthesized and their study offered more thorough SAR for protein binding. Further measurements were performed that confirmed inhibitory activity for some hits, and revealed the substrate activity for another. Using the information from the NMR assays in combination with that of the DSF binding studies, several hybrid molecules were synthesized and tested, one of which also showed some inhibitory activity. While none of the hybrid molecules had optimal binding, maintaining inhibition in one of them suggests that linking two fragments is a viable strategy for the system.

Design of new inhibitors through the fragment-based approach was only marginally successful and the newly designed inhibitors hold little likelihood of ever becoming as good as the bisubstrate inhibitors or prodrugs that were previously reported by the group. Their study, however provided useful information into the mechanics of binding and inhibition of the resistance-causing AAC(6')-Ii. The salt-dependence on the protein's stability should not be overlooked and studying this relationship further would likely yield some insight into the role of protein binding charged species and the physics that determine protein fold and structure.

Overall, this thesis is a functional study of ligand binding to and inhibition of AAC(6')-Ii and a proof of concept for the application of fragment-screening and the fragment-based approach to inhibitor design in this system.

This work has been presented in the form of a poster at a variety of conferences including ACFAS (2011, 2012), CBGRC (2010-2011), and ENC (2010, 2012). In addition, part of this work was disclosed by the author in oral presentations at CBGRC (2012) and MOOT (2012).

4.2 Future Directions

Given the ligands that were found to be effective, another interesting avenue of research would be the use of these fragments to determine a moiety that could be used to replace parts of the bisubstrate inhibitors in order to improve their biological activity.

Finally, given a large enough library of compounds, the techniques that were used to obtain structural information on fragment binding could be used to obtain a more precise SAR via principle component analysis [62]. This information could lead to more

informed decisions on future modifications to these compounds rather than the computer
modelling approach that has not proven to be particularly effective in this system.

Chapter 5 Experimental

5.1 Instruments

Flash chromatography on silica was performed with 60 Å silica gel from Silicycle (Quebec, Canada). Flash chromatography with acidic, basic, or neutral alumina was performed with aluminum oxide, Brockman Activity grade I of the corresponding type, from Sigma-Aldrich Canada, Ltd (Oakville, Ontario, Canada). Automated flash chromatography was performed on a Combiflash system from Teledyne Isco (Lincoln, NE, USA), using the Rf gold cartridge of the specified size from the same manufacturer. Reactions performed under microwave irradiation were performed using Biotage Initiator microwave synthesizer.

High resolution mass spectrometry (HR-MS) spectra were recorded on a Thermo Fisher Scientific Inc Extractive Orbitrap system. The NMR spectrometers used were one of the following: Varian Mercury 300 MHz with 5 mm PFG switchable probe, Varian Mercury 400 MHz with 5 mm PFG ID probe, Varian Unity Inova 500 MHz with HCN cold probe, or 800 MHz Varian Unity Inova with either room temperature or HCN cold probe. ¹H NMR spectra were obtained on one of those spectrometers as specified. The peak patterns are indicated as follows: s, singlet; d, doublet; t, triplet; q, quartet; m, multiplet; dd, doublet of doublets; td, triplet of doublets. Chemical shifts are reported relative to residual protons in the solvent in parts per million (ppm, 7.26 ppm for CDCl₃, 3.31 ppm for CDOD₃, 4.79 ppm for D₂O) downfield from tetramethylsilane for small molecule experiments or relative to 4,4-dimethyl-4-silapentane-1-sulfonic acid in the case of the protein experiments using water or D₂O as solvent. ¹³C NMR spectra were obtained with the 300 MHz NMR spectrometer. Chemical shifts for these spectra are reported in ppm relative to the center peak of the triplet of 77 ppm corresponding to deuterochloroform or

the heptet of 49 ppm corresponding to tetradeuteromethanol. All protein-related NMR experiments were recorded on either the 500MHz or 800MHz spectrometer listed above.

5.2 Biological Studies

5.2.1 Materials

The pET-22b(+) plasmid containing AAC(6')-Ii was generously provided by Dr. Gerry D. Wright, McMaster University, Canada. The HEPES buffer and broth reagents were obtained from Fisher Scientific (Whitby, ON, Canada). The Q-Sepharose Fast Flow and Superdex 75 chromatography resins were obtained from GE Healthcare (Waukesha, WI, USA). The activated Affi-Gel 15 was purchased from Bio-Rad (Mississauga, ON, Canada). The *Escherichia coli* strain BL21(DE3) competent cells were obtained from Invitrogen (Carlsbad, CA, USA). The ¹⁵NH₄Cl was purchased from Isotech, a subsidiary of Sigma-Aldrich (Oakville, ON, Canada). The SDS-PAGE were run using the Phastsystem and 'Phastgel Homogeneous 20' SDS-PAGE precast gels from GE Healthcare (Waukesha, WI, USA). Concentration of protein was achieved using Amicon Ultra-15 Centrifugal Filter Units – 10,000 NMWL from EMD Millipore (Billerica, MA, USA).

5.2.2 Expression of Aminoglycoside N-6'-Acetyltransferase Ii

BL21(DE3) cells were transformed using the One Shot protocol developed by Invitrogen with the plasmid containing the AAC(6')-Ii gene. The cells were grown on Luria-Bertani (LB) agar plate (15 g/L agar) containing ampicillin (100 μ g/mL). LB (40 mL of 10 g/L NaCl, 10 g/L tryptone, and 5 g/L yeast extract, autoclaved at 120°C for 20 minutes) containing ampicillin (100 μ g/mL) in a 50 mL Falcon tube was inoculated from a single

colony and grown overnight at 37°C and 250 RPM. A culture sample (5 mL) was used to inoculate a larger LB volume (1 L with ampicillin). The cell cultures were grown at 37° C and 250 RPM until the OD_{600nm} reached 0.6. Expression was then induced using isopropyl- β -D-thiogalactoside (IPTG, 1 mM) and the culture was allowed to grow at 37° C and 250 RPM for another 3-4 hours. The cells were collected by centrifugation ($4000 \times g$ for 20 min). The cell pellet (typically 3 g/L) was frozen and stored for at least one night at -80°C.

5.2.3 Expression of ¹⁵N labeled AAC(6')-li

The expression protocol for labeled proteins was adapted from literature [17, 63]. The beginning of the expression matches that of unlabelled protein expression. Once the cells reached $OD_{600nm} = 0.6$, the cells were collected by centrifugation (4000 × g for 10 min). Cells were re-suspended in M9 minimal medium (1 L for 4 L culture, 6 g/L Na_2HPO_4 , 3 g/L KH_2PO_4 , 0.5 g/L NaCl, 0.01 M $CaCl_2$, 0.1 M $MgSO_4$, 10 μ g/mL thiamine, 10 μ g/mL d-biotin, 100 μ g/mL ampicillin, and 1 g/L NH_4Cl , 3 g/L glucose) and allowed to grow for 30-45 min at 37°C and 250 RPM. Cells were again collected by centrifugation (4000 × g for 10 minutes) and re-suspended in labeled M9 minimal medium (1 L, 1 g/L $^{15}NH_4Cl$ rather than 1 g/L NH_4Cl). Cells were allowed to grow at 37°C and 250 RPM for 1 hour before expression was induced with IPTG (1 mM). The culture was allowed to grow for another 3-5 hours before cell harvest by centrifugation (4000 × g for 10 min). The cell pellet was frozen and stored for at least one night at ^{-80}C .

5.2.4 Purification of AAC(6')-li

The purification of AAC(6')-Ii was achieved identically for unlabelled and labeled protein. The protocol is based on the original isolation of the protein by Wright and

Ladak [2]. All purification steps were performed at 4°C, except where mentioned explicitly.

The ice-cold cell pellet (~24 g) was shattered by impact and re-suspended in lysis buffer (100 mL for 8 L of culture; 25 mM HEPES, 2 mM EDTA, 0.05 mg/L leupeptin, 0.5 mg/L aprotinin, 0.01 mM bestatin, 0.05 mg/L pepstatin A, 1 μ M phenylmethanesulfonylfluoride, pH 7.5) with lysozyme added (10 mg/g of pellet), and stirred at 4°C for 10-20 min. The cells were further lysed by sonication (80% duty cycle, intensity of 5, 5 min) at 4°C while stirring on a stir-plate. The suspension was then centrifuged (15,000 × g for 10 min). The pellet was discarded, and the supernatant was centrifuged again (18,000 × g for 10 min). AAC(6')-Ii was purified from the supernatant.

The first column was a Q-Sepharose Fast Flow ion exchange with a bed volume of 75-100 mL and a diameter of 26 mm. It was packed with 5 volumes of buffer A (25 mM HEPES, 2 mM EDTA, pH 7.5) at a rate of 3 mL/min. After loading the bacterial supernatant, the column was washed with buffer A in a stepwise manner as follows: 200 mL at 0 M NaCl, 200 mL at 0.1 M NaCl, 100 mL 0.2 M NaCl. The protein was eluted with 100 mL at 0.3 M NaCl, 100 mL at 0.5 M NaCl, 200 mL at 1M NaCl. Fractions containing AAC(6')-Ii were identified using SDS-PAGE. AAC(6')-Ii migrates as a monomer of approximately 21 kDa. The combined fractions were concentrated (volume ≤ 50 mL) and dialyzed against HEPES buffer (5 L, 25 mM HEPES, 2 mM EDTA, pH 7.5).

The second column used was an Affi-gel 15 paromomycin-coupled agarose affinity column. A bed volume of 25 mL in a 16 mm column (for 8 L of culture) was packed at 2 mL/min with HEPES buffer (25 mM HEPES, 2 mM EDTA, pH 7.5) for 5 bed volumes. After the column was loaded with the dialyzed sample, AAC(6')-Ii was eluted with the same gradient as the one used for the Q-Sepharose Fast Flow column. Fractions containing AAC(6')-Ii were identified using SDS-PAGE. Combined fractions were concentrated (to 8-10 mL).

The third column used was XK16 Superdex 75 column on an AKTA FPLC system, elution used an isocratic mode (25 mM HEPES, 2 mM EDTA, 1 M NaCl). The column and system were kept at room temperature, but the loop and collected eluate were kept at 4°C. The purification was monitored through UV absorption, using dimer size (42 kDa) as a guideline for protein elution time. An initial fractionation step was used to determine precise retention volumes. Repeated injections (1 mL) were used until all protein solution was purified. Collected fractions were concentrated to the desired volume (protein concentration 300 μM – 1 mM) and dialyzed against the desired buffer (5 L, 25 mM HEPES, 2 mM EDTA pH 7.5 for non-NMR assays, or 100 mM Na₂HPO₄/NaH₂PO₄ pH 6.5 for NMR). Protein concentrations were determined using spectroscopic absorbance measurements using a theoretical exctinction coefficient of 33,920 M⁻¹cm⁻¹ at 280 nm (ExPASy proteomics), and Lowry-Bradford assays. Typical protein yield was 55 mg per liter of cell culture.

5.2.5 NMR:HSQC, STD, STD-TOCSY, TOCSY, ILOE

The NMR experiments were run at the Quebec/Eastern Canada High field NMR facility with the 500 MHz or the 800 MHz spectrometers described above. All samples included $10\%~D_2O$.

5.2.6 HSQC

Spectra were acquired using AAC(6')-Ii (100 μ M to 300 μ M) in sodium phosphate buffer (100 mM, pH 6.5). Spectra were acquired with 4 transients, using 64 increments in the nitrogen dimension.

5.2.7 STD and STD-TOCSY

Spectra were acquired with AAC(6')-Ii (5 µM) in sodium phosphate buffer (500 mM, pH 7.5) and ligand (5 mM). Spectra were acquired using internal spectral subtraction with 64 increments. The reference frequency used was at 30 ppm and the saturation frequency was -2 ppm.

5.2.8 ILOE

Spectra were acquired with AAC(6')-Ii (5 μ M) in phosphate buffer (500 mM, pH 7.5) and ligand (5 mM). The NOESY pulse sequence was used with mixing times of 700, 800, and 900 ms for comparison.

5.2.9 Circular Dichroism (CD)

Spectra were acquired with AAC(6')-Ii (2 μ M) in HEPES buffer (500 mM, pH 7.5) on a Jasco J-810 spectrometer, using a 0.2 mm path length cuvette. Data were collected at temperatures from 15 to 50°C, wavelengths from 200 to 300 nm, and scan rates of 50-200 nm/min in 0.5 nm increments with bandwidths of 1 nm. Each scan was performed 8

times and averaged. The thermal unfolding experiments were run in triplicate. Temperature was ramped at a rate of 0.5°C/min with 5 min equilibration time.

5.2.10 Differential Scanning Fluorimetry (DSF)

Differential scanning fluorimetry assays were performed on a Biorad MyIQ single-color real-time PCR detection system. Samples were placed in polypropylene strips with flat caps from Axygen scientific, a subsidiary of Corning life sciences (Union City, Calif., USA). AAC(6')-Ii (5 μM) was used with ligand (25 mM) in a solution buffered with HEPES buffer (200 mM, pH 7.5), using Sypro Orange (5x, Life Technologies, Carlsbad, CA, USA) as the revealing dye. Thermal melt experiments were performed from 20°C to 70°C in 0.5°C increments with 30 second dwell times. Each sample was measured in triplicate and averaged.

5.2.11 Kinetics Studies - UV-vis, Stopped-flow

Enzyme activity was monitored using a procedure described in the literature [17, 22]. Thus, the assays were performed in HEPES buffer (100 mM, pH 7.5) containing 4,4′-dithiodipyridine (DTDP, 400 μ M), neomycin (400 μ M) and various concentrations of AcCoA (10 – 100 μ M). Reaction volumes were typically 400 μ L. The assay mixtures were pre-incubated for 3 min at 37°C, and the reaction was initiated by the addition of AAC(6′)-Ii (3.6 μ M). The reaction was monitored at 324 nm ($\epsilon_{324\,nm}$ (thiopyridine) = 19,800 M⁻¹ cm⁻¹). All synthetic compounds were tested first in the absence of enzyme (control) and in the absence of aminoglycoside (to determine if they are substrates themselves). The concentration of inhibitor (0.25 – 1000 μ M) was also varied to determine the IC₅₀.

An alternative version of the assay used MES buffer (100 mM, pH 6.5) instead of HEPES (100 mM, pH 7.5). In this case, 5,5'-dithiobis-(2-nitrobenzoic acid) (DTNB) was used instead of DTDP in virtue of its much lower background hydrolysis rate. This reaction was monitored at 412 nm (ϵ_{412} (DTNB) = 14,150 M⁻¹ cm⁻¹). Otherwise this version of the assay is identical to the one above. This version of the assay was used when the tested compounds had absorbance that interfered with DTDP.

5.2.12 Docking

In silico screening was performed with the Molecular Forecaster docking suite (Montreal, Canada)[48, 64], using the 'docking 1' workflow. An unpublished crystal protein structure was used of AAC(6')-Ii bound to the bisubstrate inhibitor [22]. The coordinates were provided by Prof A.M. Berghuis at McGill.

5.3 Synthesis

5.3.1 Chemicals

Unless otherwise noted, all chemicals were obtained from Sigma-Aldrich Canada, Ltd (Oakville, Ontario, Canada). Reagents and solvents were used without further purification unless specifically mentioned.

Unless otherwise stated, all chemical reactions were performed under inert dry nitrogen atmosphere. Anhydrous THF was obtained from distillation over sodium. Anhydrous DCM was obtained from Innovative Technology Pure Solv MD-7 Solvent purification system (Port Washington, NY, USA). Anhydrous methanol was obtained by drying "anhydrous methanol" from a commercial bottle over activated molecular sieves over a period of at least 10 min.

5.3.2 Compound characterization

$$0 \xrightarrow{1} {}^{2} \underset{3}{\overset{4}{\longrightarrow}} \underset{5}{\overset{H}{\overset{6}{\longrightarrow}}} {}^{7}$$

N-(3-Morpholinopropyl)acetamide (3.8):

N-(3-Aminopropyl) morpholine (292 μL, 2 mmol) that had

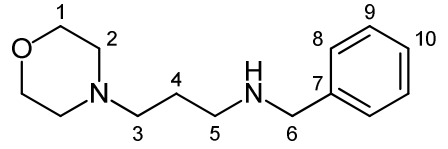
been dried by evaporation from toluene (3 × 10 mL) was dissolved in pyridine (2 mL). Acetic anhydride (378 μ L, 4 mmol) was added dropwise to the mixture before stirring overnight at room temperature under a nitrogen atmosphere. The solvent was evaporated under reduced pressure. The resulting oil was dissolved in a minimal amount of chloroform and purified by silica gel flash chromatography (chloroform/methanol, 4:1, Rf = 0.2), affording the known compound **5.1** [65] as a light orange oil (335 mg, 90% yield). ¹H NMR (300 MHz, CDCl₃) δ 3.79 (t, 4H, J = 4.5 Hz, H-1), 3.34 (dt, 2H, J = 6.6, 5.8 Hz, H-5), 2.59 (t, 4H, J = 4.5 Hz, H-2), 2.53 (t, 2H, J = 6.8 Hz, H-3), 1.86 (s, 3H, H-7), 1.68 (p, 2H, J = 6.8 Hz, H-4); ¹³C NMR (75 Hz, CDCl₃) δ 170.8 (C-6), 65.6 (C-1), 56.0 (C-5), 52.6 (C-2), 37.8 (C-3), 24.3 (C-7), 22.9 (C-4); HRMS (ESI): Calcd. for C₉H₁₉O₂N₂ (M+1): 187.14410; Found: 187.14398.

N-Ethyl-3-morpholinopropan-1-amine (3.9):

N-Ethyl-3-morpholinopropan-1-amine (3.9):

Lithium aluminum hydride (43 mg, 0.81 mmol) was dissolved in dry THF (5 mL) under a nitrogen atmosphere. Compound 3.8 (103 mg, 0.54 mmol) was dissolved in dry THF (5 mL) and added dropwise into the solution of lithium aluminum hydride. The mixture was refluxed for 2 hours. Once the reaction was complete, the solvent was evaporated under reduced pressure. The residue was dissolved in diethyl ether (10 mL) and cooled to 0°C. Water (43 μ L) was added to the solution, before 15% NaOH (43 μ L), and more water (130 μ L, Fieser workup [66]) was added.

After warming to room temperature, magnesium sulfate (1 g) was added and the precipitate was filtered off. The product was purified by Combiflash (0-30% methanol in chloroform, Rf = 0.4 in 30% MeOH, 5% NH₄OH in CHCl₃). The product was obtained as a clear oil (50.8 mg, 55% yield). Compound **3.9** is part of the claim in a patent application [67]. ¹H NMR (300 MHz, CDCl₃) δ 3.68 (t, 4H, J = 4.4 Hz, H-1), 2.63 (m, 4H, H-6, H-5), 2.41 (t, 4H, J = 4.4 Hz, H-2), 2.37 (t, 2H, J = 7.4 Hz, H-3), 1.77 (s, 1H, NH), 1.66 (p, 2H, J = 7.2 Hz, H-4), 1.08 (t, 3H, J = 7.1 Hz, H-7); ¹³C NMR (75 Hz, CDCl₃) δ 63.0 (C-1), 53.5 (C-3), 49.8 (C-2), 44.5 (C-5), 40.2 (C-6), 22.8 (C-7), 22.8 (C-4); HRMS (ESI): calcd for C₉H₂₀N₂O (M+1) 173.16484 expt 173.16505.



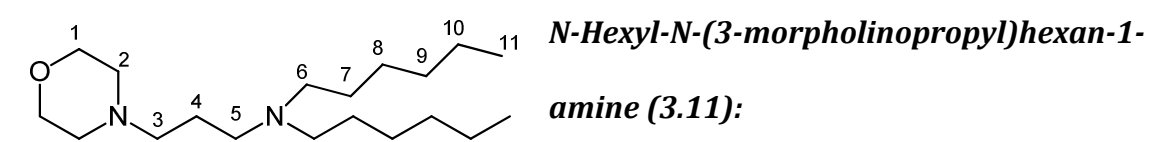
N-Benzyl-3-morpholinopropan-1-amine (3.10):

The procedure to prepare this patented compound

[68] was taken from Greene and Wutz [70] and modified as follows. N-(3-

Aminopropyl)morpholine (731 μ L, 5 mmol) was dissolved in water (10 mL) with potassium carbonate (approximately 1 g). To this mixture was added benzyl bromide (119 μ L, 1 mmol). The mixture was refluxed for 30 minutes. The mixture was extracted in chloroform (3 × 10 mL). The organic phase was dried over sodium sulfate before filtering through Celite and evaporating the solvent under reduced pressure. The product was purified by Combiflash (0-10% methanol gradient in chloroform, Rf = 0.2 in 10% methanol in chloroform) with **3.10** being the major product (75 mg, 32%). ¹H NMR (300 MHz, CDCl₃) δ 7.30 (m, 5H, H-8, H-9, H-10), 3.52 (t, 4H, J = 6.7 Hz, H-1), 2.57 (t, 2H, J = 4.1 Hz, H-5), 2.24 (m, 4H, H-2), 2.22 (t, 2H, J = 4.2 Hz, H-3), 4.48 (p, 2H, J = 4.2 Hz, H-4), 1.09 (s, 2H, H-6); ¹³C NMR (75 Hz, CDCl₃) δ 128.6 (C-7), 128.2 (C-9), 128.0

(C-8), 127.8 (C-10), 66.8 (C-1), 56.7 (C-6), 53.7 (C-3), 47.8 (C-2), 40.6 (C-5), 30.1 (C-4); HRMS (ESI): Calcd C₁₄H₂₃N₂O (M+1) 235.17915 expt: 235.17960.



N-(3-Aminopropyl)morpholine (500 μL, 3.4 mmol) was dissolved in chloroform (5 mL) along with triethylamine (150 μL, 1.0 mmol) and pyridine (500 μL, 6.2 mmol). Hexyl bromide (150 μL, 1.1 mmol) was added to the mixture before stirring the solution overnight at room temperature. The solvent was evaporated under reduced pressure and the product was purified on Combiflash (column pretreated with 1% NH₄OH in 20% methanol in chloroform, 0-50% methanol in chloroform linear gradient, Rf = 0.3 at 50% methanol in chloroform). The product was obtained as a clear oil (44 mg, 26% yield). ¹H NMR (300 MHz, CDCl₃) δ 3.67 (t, 4H, J = 4.6 Hz, H-1), 2.65 (t, 2H, J = 7.2 Hz, H-5), 2.59 (m, 4H, H-6), 2.41 (t, 4H, J = 3.8 Hz, H-2), 2.33 (t, 2H, J = 7.1 Hz, H-3), 1.75 (p, 2H, J = 7.4 Hz, H-4), 1.53 (m, 4H, H-7), 1.25 (m, 12H, H-8, H-9, H-10), 0.85 (m, 6H, H-11); ¹³C NMR (75 Hz, CDCl₃) δ 66.9 (C-1), 56.5 (C-3), 53.7 (C-5), 53.5 (C-2), 51.5 (C-6), 31.6 (C-7), 27.0 (C-4), 25.4 (C-8), 22.7 (C-9), 22.6 (C-10), 14.0 (C-11); HRMS (ESI): Calcd. C₁₄H₄₀N₂O 313.32000 expt 313.32022

3-Morpholinopropan-1-ol (3.12):

ON 3 4 5 OH Morpholine (87.5 μL, 1 mmol) was dissolved in water (1.5 mL).

3-Bromopropanol (90.4 μL, 1 mmol) and sodium hydroxide (550 μL, 2 M, 1.1 mmol) were added to the mixture before heating under microwave irradiation (95°C, 20 min).

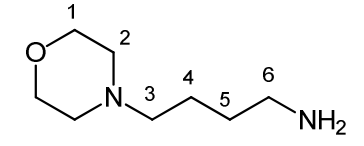
The solvent was then evaporated under reduced pressure. The product was obtained as a

clear oil (100 mg, 69%). The product is reported in the literature [74] and matches previous literature spectral values [75]. 1 H NMR (300 MHz, CDCl₃) δ 4.76 (s, 1H, OH), 3.76 (t, 2H, J = 5.4 Hz, H-5), 3.67 (t, 4H, J = 4.6 Hz, H-1), 2.58 (t, 2H, J = 5.7 Hz, H-3), 2.49 (m, 4H, H-2), 1.68 (p, 2H, J = 5.6 Hz, H-4); 13 C NMR (75 Hz, CDCl₃) δ 66.8 (C-1), 64.3 (C-5), 59.0 (C-3), 53.7 (C-2), 26.8 (C-4); HRMS (ESI): Calc for C₇H₁₅NO₂ (M+1) 146.11756 expt 146.11766

2-(4-Morpholinobutyl)isoindoline-1,3-dione (3.32): (3.32): Morpholine (96
$$\mu$$
L, 1.1 mmol) and 2-(4-

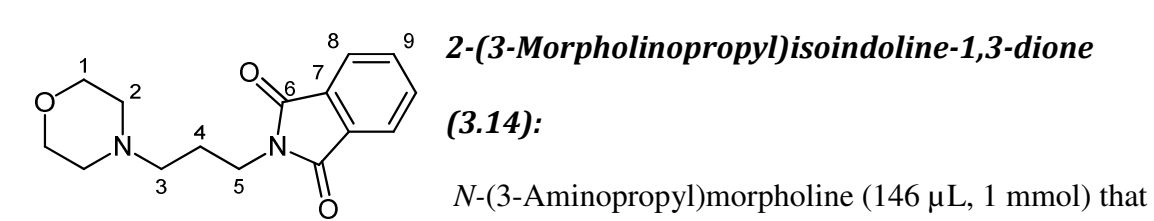
bromobutyl)isoindoline-1,3-dione (282 mg, 1 mmol) were dissolved in dimethylformamide (1.5 mL) and heated by microwave irradiation (30 min, 140°C). The solvent was evaporated under reduced pressure and the resulting oil was suspended in chloroform (10 mL) before an orange precipitate was filtered off. The desired product was purified from the solution on Combiflash (0-10% methanol in chloroform, Rf = 0.2 at 10% methanol in chloroform). The product was obtained as a clear oil (216 mg, 75% yield). Compound **5.13** was previously patented [77]. Spectral properties match previous literature [78]. ¹H NMR (300 MHz, CHCl₃) δ 7.71 (m, 2H, H-9), 7.60 (m, 2H, H-10), 3.66 (m, 6H, H-1, H-6), 2.37 (m, 4H, H-2), 2.31 (t, 4H, J = 6.8 Hz, H-3), 1.67 (p, 2H, J = 6.7 Hz, H-5), 1.48 (p, 2H, J = 6.7 Hz, H-4); ¹³C NMR (75 Hz, CDCl₃) δ 168.3 (C-7), 133.8 (C-8), 132.0 (C-9), 123.1 (C-10), 66.8 (C-1), 58.3 (C-6), 53.6 (C-3), 37.7 (C-2), 26.4 (C-5), 23.7 (C-4); HRMS (ESI): Calc for C₁₆H₂₀N₂O₃ 289.15333 expt 289.15343.

4-Morpholinobutan-1-amine (3.13):



Compound **3.32** (144 mg, 0.5 mmol) was dissolved in ethanol (6 mL) and combined with hydrazine hydrate (250

 μ L, 5.2 mmol) before the mixture was refluxed for 2 hours. The solvent was evaporated under reduced pressure. The residue was dissolved in hydrochloric acid (6 mL, 2 N) and the white precipitate was filtered off. The resulting aqueous solution was evaporated under reduced pressure. The desired product was purified from the residue on Combiflash (0-30% methanol in chloroform, Rf = 0.15 in 30% methanol in chloroform) and obtained as a clear oil (36 mg, 46% yield). Compound **3.13** has been previously patented [79]. Spectral properties matched literature values [80]. ¹H NMR (300 MHz, CD₃OD) δ 3.69 (t, 4H, J = 4.7 Hz, H-1), 2.74 (m, 2H, H-6), 2.47 (t, 4H, J = 4.3 Hz, H-2), 2.37 (t, 2H, J = 7.1 Hz, H-3), 1.56 (m, 4H, H-4, H-5); ¹³C NMR (75 Hz, CD₃OD) δ 66.2 (C-1), 58.3 (C-3), 53.3 (C-2), 40.3 (C-6), 28.6 (C-4), 23.1 (C-5).



had been dried by evaporation from toluene (3 × 10 mL) was dissolved in chloroform (10 mL). Phthalic anhydride (148 mg, 1 mmol) was added to this mixture before heating to reflux. After 10-15 min of reflux, acetic acid (114 μ L, 2 mmol) was added. The mixture was refluxed for 3 more hours. The solution was dried over sodium sulfate and filtered through Celite. The mixture was evaporated under reduced pressure to obtain the final product (268 mg, 98% yield). Characterization matched literature values [68, 69] ¹H NMR (300 MHz, CDCl₃) δ 7.81 (m, 2H, H-8), 7.71 (m, 2H, H-9), 3.76 (t, 2H, J = 6.7 Hz,

H-5), 3.56 (t, 4H, J = 3.9 Hz, H-1), 2.45 (t, 2H, J = 6.9 Hz, H-3), 2.41 (m, 4H, H-2), 1.88 (m, 2H, H-4); ¹³C NMR (75 Hz, CDCl₃) δ 168.5 (C-6), 133.9 (C-7), 132.2 (C-8), 123.2 (C-9), 66.6 (C-1), 56.3 (C-5), 53.4 (C-2), 36.5 (C-3), 24.6 (C-4). HRMS (ESI): Calcd. for $C_{15}H_{19}N_2O_3$ (M+1): 275.13902; expt: 275.13914.

N-(3-Bromopropyl)phthalimide (282 mg, 1 mmol) and 2,6-dimethylmorpholine (135 μL, 1.1 mmol, mixture of diastereomers) were dissolved in DMF (3 mL) and heated under microwave irradiation (140°C, 30 min) before being allowed to crystallize overnight. The supernatant was removed and the crystals were dissolved in ethyl acetate (5 mL) before washing with aqueous NaOH (2 M, 2 × 5 mL). The resulting product was purified by Combiflash (0-20% ethyl acetate in hexanes, Rf = 0.4 in 20% ethyl acetate in hexanes). Compound **3.26** was obtained as a clear oil (63 mg, 21%). ¹H NMR (300 MHz, CDCl₃) δ 7.62 (m, 2H, H-9), 7.53 (m, 2H, H-10), 3.92 (m, 2H, H-1), 3.73 (t, 2H, J = 7.2 Hz, H-6), 2.32 (m, 2H, H-4), 2.25 (m, 4H, H-2), 1.80 (p, 2H, J = 6.9 Hz, H-5), 1.17 (d, 6H, J = 6.4 Hz, H-3); ¹³C NMR (75 Hz, CDCl₃) δ 168.5 (C-7), 134.0 (C-8), 134.0 (C-9), 123.2 (C-10), 71.2 (C-1), 63.1 (C-2), δ 59.1 (C-6), 56.0 (C-4), 24.8 (C-5), 19.0 (C-3); HRMS (ESI): calcd for $C_{17}H_{22}N_2O_3$ 303.16898 expt. 303.16921

Mixture of 2-(3-((2R,6R)-2,6-dimethylmorpholino)propyl) isoindoline-1,3-dione and 2-(3-((2S,6S)-2,6-dimethylmorpholino)propyl) isoindoline-1,3-dione (3.27):

 $\it N$ -(3-Bromopropyl)phthalimide (282 mg, 1 mmol) and 2,6-dimethylmorpholine (135 μ L, 1.1 mmol, mixture of diastereomers) were dissolved in DMF (3 mL) and heated under microwave irradiation (140°C, 30 min) before allowing the product to crystallize overnight. The supernatant was removed and the crystals were dissolved in ethyl acetate (5

mL) before washing with aqueous NaOH (2 M, 2 × 5 mL). The desired product was purified by Combiflash (0-20% ethyl acetate in hexanes, Rf = 0.2 in 20% ethyl acetate in hexanes). Compound **3.27** was obtained as an off-white crystal (212 mg, 70%). ¹H NMR (300 MHz, CDCl₃) δ 7.83 (dd, 2H, J = 5.5 Hz, 3.2 Hz, H-12), 7.53 (dd, 2H, J = 5.5 Hz, 3.2 Hz, H-13), 3.76 (t, 2H, J = 6.9 Hz, H-9), 3.49 (t, 2H, J = 7.3 Hz, H-1, H-2), 2.72 (d, 2H, J = 10.5 Hz, H-4), 2.42 (t, 2H, J = 6.9 Hz, H-7), 1.89 (p, 2H, J = 6.6 Hz, H-8), 1.66 (d, 2H, J = 10.7 Hz, H-3), 1.10 (d, 6H, J = 6.3 Hz, H-5, H-6); ¹³C NMR (75 Hz, CDCl₃), 168.5 (C-10), 133.9 (C-11), 132.2 (C-12), 123.1 (C-13), 71.3 (C-1 or C-2), 71.3 (C-1 or C-2), 59.2 (C-9), 59.2 (C-3 or C-4), 56.0 (C-3 or C-4), 36.5 (C-7), 24.8 (C-8), 19.0 (C-5 or C-6), 19.0 (C-5 or C-6); HRMS (ESI): Calc for C₁₇H₂₂N₂O₃ (M+1) 303.16898 expt 303.16921

Mixture of 3-((2R,6R)-2,6-

6 4 7 9 NH₂

Dimethylmorpholino)propan-1-amine and 3-((2S,6S)-2,6-dimethylmorpholino)propan-1-amine (3.15 anti):

Compound **5.7** (211 mg, 0.7 mmol) was dissolved in ethanol (5 mL) with heating (50°C). Hydrazine hydrate (70.1 mg, 1.4 mmol) was dissolved in water (1 mL) and added to the

phthalimide solution before refluxing overnight. After cooling, the precipitate was filtered off and the solvent was evaporated under reduced pressure. The resulting offwhite solid was dissolved in ethanol and the solution was acidified with anhydrous HCl in ethanol (16%, 10 mL). The reaction was left to sit for 72 hours. The solvent was decanted and the precipitate was washed with methanol (5×5 mL). The product was further purified on silica (5-20% methanol, 4% ammonium hydroxide linear gradient in chloroform, Rf = 0.15 in 20% methanol 4% ammonium hydroxide in chloroform) to yield the title product as a white powder (53.9 mg, 45%). 1 H NMR (300 MHz, CDCl₃) δ 3.59 (m, 2H, H-1, H-2), 2.79 (m, 4H, H-3, H-4), 2.36 (t, 2H, J = 6.6 Hz, H-7), 1.67 (p, 2H, J = 6.6 Hz, H-8), 1.63 (t, 2H, J = 6.6 Hz, H-9), 1.09 (d, 6H, J = 6.2 Hz, H-5, H-6). 13 C NMR (75 Hz, CDCl₃) δ 67.6 (C-1), 67.6 (C-2), 55.5 (C-3), 55.5 (C-4), 52.7 (C-7), 46.1 (C-9), 36.6 (C-8), 15.2 (C-5 or C-6), 15.1 (C-5 or C-6); HRMS (ESI): Calc for C₉H₂₀N₂O 173.16484 expt 173.16511

6 5 0 1 2 3 OH

4-(2-Hydroxyethyl)phenyl acetate (3.24):

The synthetic procedure was adapted from Guo et al [72] as follows. Potassium hydroxide (0.42 g, 7.5 mmol) was dissolved in water (7 mL) and 4-(2-hydroxyethyl)phenol (690 mg, 5 mmol) was added. Ice (from MilliQ water) and

acetic anhydride (519 μ L, 5.5 mmol) were immediately added to the solution (15 g) as well as acetic anhydride (591 μ L, 6.25 mmol) and chloroform (5 mL). The mixture was stirred for 45 minutes. The product was extracted in chloroform (3 × 10 mL). The combined organic layers were dried over sodium sulfate and the solvent was evaporated under reduced pressure. The resulting oil was purified on Combiflash (0-20% ethyl acetate in hexanes, Rf = 0.2 at 20% ethyl acetate in hexanes) as a clear oil (758 mg, 84% yield). The isolated compound had matching spectral properties to literature values [73]. ¹H NMR (300 MHz, CDCl₃) δ 7.25 (d, 2H, J = 8.6, 2.2 Hz, H-2), 7.03 (d, 2H, J = 8.6, 2.2 Hz, H-3), 3.85 (t, 2H, J = 6.6 Hz, H-8), 2.86 (t, 3H, J = 6.6 Hz, H-7), 2.29 (s, 3H, H-6), 1.46 (s, 1H, OH); ¹³C NMR (75 Hz, CDCl₃) δ 169.9 (C-5), 149.1 (C-1), 136.5 (C-4), 136.0 (C-2), 121.5 (C-3), 63.3 (C-8), 38.5 (C-7), 21.1 (C-6); HRMS (ESI): Calc for C₁₀H₁₀O₃ (M+1) 203.06652 expt: 203.6701

2-(4-(Methoxymethoxy)phenyl)ethanol (3.25):

4-(2-Hydroxyethyl)phenol (276 mg, 2 mmol) was
dissolved in acetone (5 mL). Potassium carbonate (1 g) and chloro(methoxy)methane
(172 μL, 3 mmol) were added to the solution before stirring at room temperature for 1
hour. The solvent was evaporated under reduced pressure and the resulting solid was
triturated in hexanes before purification on Combiflash (0-33% ethyl acetate in hexanes,
Rf = 0.2 at 2:1 hexanes: ethyl acetate). The desired product was obtained as a clear oil
(100 mg, 55% yield). Spectral properties matched literature values [76]. ¹H NMR (300
MHz, CDCl₃) δ 7.13 (d, 2H, J = 8.5 Hz, H-2), 6.98 (d, 2H, J = 8.5 Hz, H-3), 5.14 (s, 2H, H-7), 3.80 (t, 2H, J = 6.5 Hz, H-6), 3.46 (s, 3H, H-8), 2.80 (t, 2H, J = 6.5 Hz, H-5), 2.15
(s, 1H, OH); ¹³C NMR (75 Hz, CDCl₃) δ 155.8 (C-1), 131.9 (C-4), 116.4 (C-3), 94.5 (C-

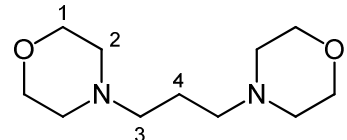
7), 63.7 (C-6), 22.9 (C-8), 38.3 (C-5); HRMS (ESI): calc C₁₀H₁₄O₃ (M+1) 205.08352 expt 205.08374

$$\begin{array}{c|c}
4 & 0 & 0 \\
\hline
N & 2 & 1 & N
\end{array}$$

1,3-Dimorpholinopropane-1,3-dione (3.28):

Morpholine (350 µL, 4 mmol) was dissolved in diethyl ether (10 mL) and malonyl chloride (100 µL, 1 mmol) was

added dropwise. The mixture was stirred at room temperature for 15 minutes. The precipitate was collected by vacuum filtration and washed with diethyl ether. The precipitate was dissolved in minimal hot methanol, and hot ethyl acetate was added until precipitation started. It was then allowed to cool. Crystals were collected by filtration and the mother liquor was evaporated under reduced pressure and more product was crystallized in the same way. Title compound was obtained as orange crystals (94 mg, 36%). Compound 3.28 has been previously synthesized [81]. ¹H NMR (300 MHz, CDCl₃) δ 3.63 (m, 8H, H-3), 3.58 (m, 8H, H-4), 3.49 (s, 2H, H-1); ¹³C NMR (75 Hz, CDCl₃) δ 165.4 (C-2), 66.8 (C-1), 66.6 (C-3), 46.8 (C-4).



1,3-Dimorpholinopropane (3.29):

Morpholine (347 μ L, 4 mmol) was dissolved in chloroform (5 mL) and cooled to 0°C in an ice bath. Propane-1,3-diol di-ptoluenesulphonate (768 mg, 2 mmol) was dissolved in chloroform (5 mL) and cooled to 0°C in an ice bath. Potassium carbonate (approximately 1 g) was added to the morpholine solution. The solution of propane-1,3-diol di-*p*-toluenesulfphonate was then added dropwise to the morpholine solution at 0°C before allowing the mixture to warm to room temperature over 3 hours. The reaction was quenched by the addition of 1 M

NaOH (10 mL). The mixture was extracted in chloroform (3 \times 10 ml). The combined organic solution was washed with water (2 \times 10 mL) and brine (1 \times 10 mL).

Evaporation of the solvent under reduced pressure yielded a beige semi-liquid-solid. The sample was lyophilized overnight. The remaining powder was dissolved in chloroform (1 mL) and purified by Combiflash (0-20% methanol in chloroform). This previously synthesized compound [71] was obtained as a clear oil (42 mg, 10% yield). ¹H NMR (300 MHz, CDCl₃) δ 3.69 (t, 8H, J = 4.1 Hz, H-1), 2.42 (t, 8H, J = 4.1 Hz, H-2), 2.36 (t, 4H, J = 7.5 Hz, H-3), 1.67 (p, 2H, J = 7.5 Hz, H-4); ¹³C NMR (75 Hz, CDCl₃) 66.9 (C-1), 53.7 (C-3), 47.6 (C-2), 30.1 (C-4); HRMS (ESI): calcd. C₁₁H₂₂O₂N₂ (M+1) 215.17406 expt 215.17458.

2-(Benzo[d][1,3]dioxol-5-yl)-N-(3-morpholinopropyl)acetamide (3.30):

3,4-Methylenedioxyphenylacetic acid (180 mg, 1 mmol) and N-(3-

dimethylaminopropyl)-N'-ethylcarbodiimide hydrochloride (288 mg, 1.5 mmol) were dissolved in dry THF (5 mL). N-(3-Aminopropyl)morpholine (146 μ L, 1 mmol) was added to the solution dropwise and stirred over 16 hours. The solvent was evaporated under reduced pressure. The residue was dissolved in chloroform (1 mL) and purified on Combiflash (0-10% methanol in chloroform, Rf = 0.2 at 10% methanol in chloroform) to yield a white solid (260.7 mg, 89% yield). 1 H NMR (300 MHz, CH₃OH) δ 6.60 (m, 3H, H-10, H-12, H-13), 5.87 (s, 2H, H-14), 3.55 (t, 4H, J = 4.4 Hz, H-1), 3.37 (s, 2H, H-7), 3.23 (m, 2H, H-5), 2.30 (m, 4H, H-2), 2.28 (t, 2H, J = 6.6 Hz, H-3), 1.56 (p, 2H, J = 6.6 Hz, H-4); 13 C NMR (75 Hz, CDCl₃) δ 171.0 (C-6), 147.9 (C-8), 146.7 (C-9), 128.8 (C-

11), 122.4 (C-12), 109.6 (C-13), 108.5 (C-10), 101.1 (C-14), 66.8 (C-1), 57.1 (C-3), 53.6 (C-2), 43.4 (C-7), 38.8 (C-5), 28.2 (C-4); calc for C₁₆H₂₂N₂O₄ (M+1) 307.16523 expt 307.16547

2-(3,4-Dihydroxyphenyl)-N-(3-

morpholinopropyl)acetamide (3.31):

3,4-Dihydroxyphenylacetic acid (168 mg, 1 mmol) was dissolved in DCM/THF (3 mL/5

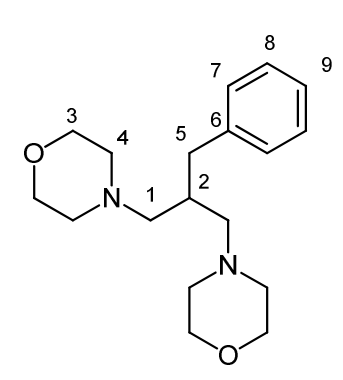
mL) and cooled to 0°C on ice. Oxalyl chloride (127 μ L, 1.5 mmol) was added dropwise to the solution over 5 minutes before stirring at room temperature for 15 minutes. Solvent and remaining oxalyl chloride were evaporated under reduced pressure. The crude acid chloride was re-dissolved in chloroform (10 mL) before combining this solution with N-(3-aminopropyl)morpholine (146 μ L, 1 mmol) and stirring for 1 hour at room temperature. The solvent was evaporated under reduced pressure. The desired product was recrystallized from acetone to afford yellowish white crystals (36 mg, 13% yield). 1 H NMR (300 MHz, CH₃OH) δ 6.49 (m, 3H, H-10, H-12, H-13), 3.64 (t, 4H, J = 4.5 Hz, H-1), 3.20 (t, 2H, J = 6.7 Hz, H-5), 2.41 (t, 4H, J = 4.5 Hz, H-2), 2.33 (t, 2H, J = 6.7 Hz, H-3), 1.56 (m, 2H, H-4).

2-Benzylpropane-1,3-diyl dimethanesulfonate (3.34):

The synthetic procedure was adapted from that of Rios-Lombardi [84]. Diethylbenzyl malonate (360 μ L, 1.5 mmol) was dissolved in dry THF (8 mL) and cooled to -78°C.

Lithium aluminum hydride (300 mg, 4.5 mmol) was added to the reaction mixture in one

portion before stirring for 1 hour. The Feiser workup [66] was performed to remove the aluminum salt. The filtrate was concentrated under reduced pressure to afford the crude intermediate Mp 65-67 °C, literature 66-68°C [85]. This diol (257 mg, 1.6 mmol) was dissolved in dry DCM (15 mL) before the addition of pyridine (160 μ L, 2 mmol) and cooling to 0°C. Methylsulfonyl chloride (160 μ L, 2.1 mmol) was added dropwise to the mixture. The reaction mixture was allowed to warm to room temperature and stirred overnight. The solvent was evaporated under reduced pressure and the product was purified on silica (0-50% linear gradient of EtOAc in hexanes, Rf = 0.3 at 50% EtOAc in hexanes). The product was obtained as a white crystalline material (90 mg, 19%). Spectral properties match literature values [84]. 1 H NMR (300 MHz, CDCl₃) δ 7.34 (m, 2H, H-7), 7.23 (m, 1H, H-8), 7.17 (m, 2H, H-6), 4.18 (m, 4H, H-1), 3.01 (s, 6H, H-3), 2.74 (d, 2H, J = 7.6 Hz, H-4), 2.47 (m, 1H, H-2); 13 C NMR (75 Hz, CDCl₃) δ 137.2 (C-5), 129.0 (C-7), 128.9 (C-6), 127.0 (C-8), 67.8 (C-1), 40.1 (C-3), 37.2 (C-4), 33.3 (C-2)

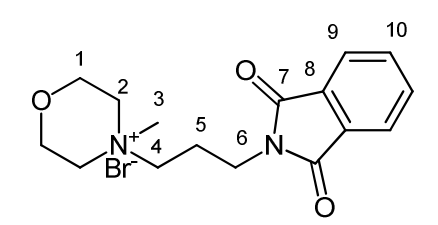


4,4'-(2-Benzylpropane-1,3-diyl)dimorpholine (3.32):

Morpholine (135 μ L, 1.7 mmol) that had been previously dried over molecular sieves was added dropwise to 3.34 dissolved in dry DMF (5 mL). The reaction mixture was heated to 50°C overnight. The solvent was evaporated under reduced

pressure. The residue was suspended in 1:1 hexanes-ethyl acetate (2.5 mL), the precipitate was filtered off, and the product was purified on neutral alumina with 0-100% ethyl acetate in hexanes to yield the product as a clear oil (27 mg, 32%). ¹H NMR (300 MHz, CDCl₃) δ 7.23 (m, 5H, H-7, H-8, H-9), 3.69 (t, 8H, J = 4.7 Hz, H-3), 2.73 (m, 2H, H-5), 2.42 (m, 8H, H-4), 2.14 (m, 4H, H-1), 1.90 (m, 1H, H-2); ¹³C NMR (75 Hz,

CDCl₃) δ 131.2 (C-6), 129.6 (C-8), 128.0 (C-7), 125.7 (C-9), 67.0 (C-3), 61.0 (C-4), 54.0 (C-1), 36.7 (C-5), 33.7 (C-2) calcd for C₁₈H₂₂N₂O₂ 305.22235 expt 305.22200



4-(3-(1,3-Dioxoisoindolin-2-yl)propyl)-4methylmorpholin-4-ium bromide (5.1):

N-Methylmorpholine (110 μ L, 1 mmol) and 2-(4-

bromopropyl)isoindoline-1,3-dione (268 mg, 1 mmol) were dissolved in acetonitrile (10 mL) and refluxed overnight. The solvent was evaporated under reduced pressure. The resulting orange powder was washed with chloroform to yield the desired product as an off-white powder (165 mg, 45%). NMR (300 MHz, D₂O) δ 7.67 (m, 4H, H-9, H-10), 3.88 (t, 4H, J = 4.6 Hz, H-1), 3.63 (t, 2H, J = 6.7 Hz, H-6), 3.39 (m, 4H, H-2), 3.04 (s, 3H, H-3), 2.07 (m, 2H, H-5).

was mixed with neutral alumina (5 g) and combined with di-*tert*-butyl dicarbonate (94 μ L, 1 mmol). Ethyl acetate (2 mL) was added and the mixture was stirred for 30 seconds before being allowed to sit for 10 min. The product was extracted in ethyl acetate (5 × 2 mL) and the organic solution was filtered through sand before evaporating the solvent under reduced pressure. The residue was dissolved in ethyl acetate (5 mL) and run through a plug of basic alumina. The solvent was evaporated under reduced pressure to afford the product as a slightly orange oil (215 mg, 88 %). Compound **5.2** has been reported previously and spectral properties match literature values [82]. ¹H NMR (300

MHz, CH₃OH) δ 5.43 (s, 1H, NH), 3.68 (t, 4H, J = 4.7 Hz, H-1), 3.16 (m, 2H, H-5), 2.40 (t, 4H, J = 4.8 Hz, H-2), 2.33 (t, 2H, J = 6.8 Hz, H-3), 1.63 (p, 2H, J = 6.7 Hz, H-4), 1.40 (s, 9H, H-8); ¹³C NMR (75 Hz, CDCl₃) δ 152.1 (C-6), 74.7 (C-7), 62.9 (C-1), 56.4 (C-5), 53.0 (C-3), 49.6 (C-2), 35.7 (C-8), 24.4 (C-4).

4-(3-Aminopropyl)-4-methylmorpholin-4-ium mixed iodide and chloride (5.3):

Compound **5.2** (244 mg, 1 mmol) was combined with iodomethane (68 μ L, 1.1 mmol) in anhydrous ethanol (10 mL). The mixture was stirred for 24 h at 50°C. The solvent was evaporated under reduced pressure to a volume of 2-3 mL. Hydrochloric acid (25 mL, 12% aqueous) was added. The reaction was stirred for 15 minutes and the product was then allowed to crystallize at room temperature for 48 h and on ice for 90 min. The resulting green crystals were collected by vacuum filtration, washed with cold ethanol and dried to yield the desired product (145 mg, 45%). Spectral properties match previously reported values [83]. ¹H NMR (300 MHz, CH₃OH) δ 3.76 (t, 4H, J = 3.7 Hz, H-1), 3.27 (m, 6H, H-2), 2.95 (s, 3H, H-3), 2.82 (t, 2H, J = 7.7 Hz, H-4, H-6), 1.94 (m, 2H, H-5).

Chapter 6 References

- 1. Jacobson, M.P., *Methods in Molecular Biology, Vol. 316: Bioinformatics and Drug Discovery*. *Edited by Richard S. Larson*. ChemMedChem, 2006. **1**(6): p. 654-655.
- 2. Forrest, R.D., *Early History of wound treatment*. Journal of the Royal Society of Medicine, 1982. **75**: p. 198-205.
- 3. Porter, J.R., *Antony van Leeuwenhoek: tercentenary of His Discovery of Bacteria.* Bacteriological Reviews, 1976. **40**(2): p. 260-269.
- 4. D'Costa, V.M., et al., *Antibiotic resistance is ancient*. Nature, 2011. **477**(7365): p. 457-461.
- 5. Baltz, R.H., *Antimicrobials form Actinomycetes: Back to the future.* Americal Society for Microbiology, 2007.

- 6. Valen, V., A New Evolutionary Law. Evol. Theory, 1973. **1**(1).
- 7. Thompson, J.N., Evolution. The role of coevolution. Science, 2012. **335**(6067): p. 410-411.
- 8. Gonzalez III, U.S. and J.P. Spencer, *Aminoglycosides: A practical Review*. Am Fam Physician, 1998. **58**(8): p. 1811-1820.
- 9. CLark, R., C. Pakiz, and M. Hostetter, *Synergystic activity of aminoglycoside-beta-lactam combinations against Pseudomonas aeruginosa with an unusual aminoglycoside antiiogram.* Med Microbiol Immunol, 1990. **179**(2): p. 77-86.
- 10. Vardakas, K.Z., et al., beta-Lactam plus aminoglycoside or fluoroquinolone combination versus beta-lactam monotherapy for Pseudomonas aeruginosa infections: a meta-analysis. Int J Antimicrob Agents, 2013. **41**(4): p. 301-10.
- 11. Marie-Paule Mingeot-Leclercq, Y.G., and Paul M. Tulkens, *Aminoglycosides: Activity and Resistance*. Antimicrob Agents Chemother, 1999. **43**(4): p. 727-737.
- 12. De Pascale, G. and G.D. Wright, *Antibiotic resistance by enzyme inactivation:* from mechanisms to solutions. Chembiochem, 2010. **11**(10): p. 1325-1334.
- 13. Wiedemann, B., Mechanisms of antibiotic resistance and their dissemination of resistance genes in the hospital environment. Infect. Control, 1983. **4**(6): p. 444-447.
- 14. NJ, L., et al., *Survey of aminoglycoside resistance patterns*. Chemioterapia, 1986. **5**(3): p. 185-190.
- 15. listed], n., The most frequency occurring aminoglycoside resistance mechanisms combined results from surveys in eight regions of the world. The aminoglycoside resistance study groups. J chemother., 1995(Suppl 2): p. 17-30.
- 16. EE, U., et al., Characterization of high-level aminoglycoside-resistance enterococci in Kuwait hospitals. Microb Drug Resist, 2004. **10**(2): p. 139-145.
- 17. Gerard D. Wright, P.L., Overexression and characterization of the chromosomal aminoglycoside 6'-N-acetyltransferase from Enterococcus faecium. Antimicrob Agents Chemother, 1997. **41**(5): p. 956-960.
- 18. Draker, K.-A., D.B. Northrop, and G.D. Wright, *Kinetic Mechanism of GCN5-Related Chromosomal Aminoglycoside Acetyltransferase AAC(6')-Ii from Enterococcus faecium: Evidence of Dimer Subunit Cooperativity.* Biochemistry, 2003. **42**: p. 6565-6574.
- 19. Burk, D.L., et al., *Structures of aminoglycoside acetyltransferase AAC(6')-Ii in a novel crystal form: structural and normal-mode analyses.* Acta Crystallogr D Biol Crystallogr, 2005. **61**(Pt 9): p. 1273-9.
- 20. Freiburger, L.A., K. Auclair, and A.K. Mittermaier, *Elucidating protein binding mechanisms by variable-c ITC*. Chembiochem, 2009. **10**(18): p. 2871-3.
- 21. Freiburger, L.A., et al., *Competing allosteric mechanisms modulate substrate binding in a dimeric enzyme.* Nat Struct Mol Biol, 2011. **18**(3): p. 288-294.
- 22. Gao, F., et al., *Regio- and chemoselective 6'-N-derivatization of aminoglycosides: bisubstrate inhibitors as probes to study aminoglycoside 6'-N-acetyltransferases.*Angew Chem Int Ed Engl, 2005. **44**(42): p. 6859-6862.
- 23. Vong, K., et al., *Inhibitors of aminoglycoside resistance activated in cells*. ACS Chem Biol, 2012. **7**(3): p. 470-475.
- 24. Shuker, S.B.h.P.M.R.F.S., *Discovering high-affinity ligands for proteins: SAR by NMR*. Science, 1996. **274**(5292): p. 1531-1534.

- 25. Erlanson, D.A., R.S. McDowell, and T. O'Brien, *Fragment-based drug discovery*. J Med Chem, 2004. **47**(14): p. 3463-3482.
- 26. Hajduk, P.J. and J. Greer, *A decade of fragment-based drug design: strategic advances and lessons learned.* Nat Rev Drug Discov, 2007. **6**(3): p. 211-219.
- 27. Ciulli, A. and C. Abell, *Fragment-based approaches to enzyme inhibition*. Curr Opin Biotechnol, 2007. **18**(6): p. 489-496.
- 28. Lombes, T., et al., *NMR-guided fragment-based approach for the design of AAC(6')-Ib ligands*. Chembiochem, 2008. **9**(9): p. 1368-1371.
- 29. Moore J, A.-M.N., Fejzo J, Jacobs M, Lepre C, Peng J, Xie X, *Leveraging structural approaches: applications of NMR-based screening and X-ray crystallography for inhibitor design.* J Synchrotron Radiat., 2004. **11**(Pt 1): p. 97-100.
- 30. Vetting, M.W., et al., *Mechanistic and structural analysis of aminoglycoside N-acetyltransferase AAC(6')-Ib and its bifunctional, fluoroquinolone-active AAC(6')-Ib-cr variant.* Biochemistry, 2008. **47**(37): p. 9825-9835.
- 31. Bodenhausen, G. and D.J. Ruben, *Natural abundance nitrogen-15 NMR by enhanced heteronuclear spectroscopy*. Chemical Physics Letters, 1980. **69**(1): p. 185-189.
- 32. Markin, C.J. and L. Spyracopoulos, *Increased precision for analysis of proteinligand dissociation constants determined from chemical shift titrations*. J Biomol NMR, 2012. **53**(2): p. 125-38.
- 33. Yu, H., *Extending the size limit of protein nuclear magnetic resonance*. Proc Natl Acad Sci U S A, 1999. **96**(2): p. 332-334.
- 34. Fernandez, C., *TROSY in NMR studies of the structure and function of large biological macromolecules*. Current Opinion in Structural Biology, 2003. **13**(5): p. 570-580.
- 35. Zerbe, O., BioNMR in Drug Research. 2002.
- 36. Dalvit, C., et al., *WaterLOGSY as a method for primary NMR screening:*Practical aspects and range of applicability. Journal of Biomolecular NMR, 2001. **21**(4): p. 349-359.
- 37. Zartler, E.R., et al., *1D NMR Methods in Ligand-Receptor Interactions*. Current Topics in Medicinal Chemistry, 2003. **3**(1): p. 25-37.
- 38. Larsson, A., et al., *Efficiency of hit generation and structural characterization in fragment-based ligand discovery.* Curr Opin Chem Biol, 2011. **15**(4): p. 482-8.
- 39. Hawe, A., M. Sutter, and W. Jiskoot, *Extrinsic fluorescent dyes as tools for protein characterization*. Pharm Res, 2008. **25**(7): p. 1487-1499.
- 40. Senisterra, G.A. and P.J. Finerty, Jr., *High throughput methods of assessing protein stability and aggregation*. Mol Biosyst, 2009. **5**(3): p. 217-223.
- 41. *IUPAC. Compendium of Chemical Terminology, 2nd ed. (the "Gold Book")*, ed. A.W. A. D. McNaught. 1997, Oxford: Blackwell Scientific Publications.
- 42. Farid, R.S. *Circular Dichroism (CD) Spectroscopy*. 2012 [cited 2013 May 6, 2013]; Available from: http://mach7.bluehill.com/proteinc/cd/cdspec.html.
- 43. Johnson, W.C., *Analyzing protein circular dichroism spectra for accurate secondary structures.* Proteins: Structure, Function, and Genetics, 1999. **35**(3): p. 307-312.

- 44. Sledz, P., et al., *Optimization of the interligand Overhauser effect for fragment linking: application to inhibitor discovery against Mycobacterium tuberculosis pantothenate synthetase.* J Am Chem Soc, 2010. **132**(13): p. 4544-4545.
- 45. Meyer, B. and T. Peters, *NMR Spectroscopy Techniques for Screening and Identifying Ligand Binding to Protein Receptors*. Angew Chem Int Ed, 2003. **42**(8).
- 46. Lepre, C.A., J.M. Moore, and J.W. Peng, *Theory and applications of NMR-based screening in pharmaceutical research*. Chem Rev, 2004. **104**(8): p. 3641-76.
- 47. Cheng, T., et al., *Structure-based virtual screening for drug discovery: a problem-centric review.* AAPS J, 2012. **14**(1): p. 133-141.
- 48. De Cesco, S., et al., *Virtual screening and computational optimization for the discovery of covalent prolyl oligopeptidase inhibitors with activity in human cells.* J Med Chem, 2012. **55**(14): p. 6306-15.
- 49. Joseph-McCarthy, D., *Computational approaches to structure-based ligand design*. Pharmacology & Therapeutics, 1999. **84**(2): p. 179-191.
- 50. Dalvit, C., NMR Methods in fragment screening: theory and a comparison with other biophysical techniques. Drug Discovery Today, 2009. **14**(21/22): p. 1051-1057.
- 51. C., G., et al., Tyrosol, the major olive oil biophenol, protects against oxidized-LDL-induced injury in Caco-2 cells. J. Nutr., 1999. **129**: p. 1269-1277.
- 52. Charrouf, Z. and D. Guillaume, *Phenols and Polyphenols from Argania spinosa*. American Journal of Food Technology, 2007. **2**(7): p. 679-683.
- 53. Tiefenbrunn, T., et al., *Small Molecule Regulation of Protein Conformation by Binding in the Flap of HIV Protease*. ACS Chem Biol, 2013.
- 54. Cala, O., et al., Virtual and Biophysical Screening Targeting the gamma-Tubulin Complex A New Target for the Inhibition of Microtubule Nucleation. PLoS One, 2013. **8**(5): p. e63908.
- 55. Brandt, T., et al., *Stability of p53 homologs*. PLoS One, 2012. **7**(10): p. e47889.
- 56. Leathen, M.L., B.R. Rosen, and J.P. Wolfe, *New strategy for the synthesis of substituted morpholines*. J Org Chem, 2009. **74**(14): p. 5107-10.
- 57. Wijtmans, R., et al., *Biological Relevance and Synthesis of C-Substituted Morpholine Derivatives*. Synthesis, 2004. **2004**(05): p. 641-662.
- 58. Khan, M.N., Suggested Improvement in the Ing-Manske Procedure and Gabriel Synthesis of Primary Amines: Kinetic Study on Alkaline Hydrolysis ofN-Phthaloylglycine and Acid Hydrolysis ofN-(o-Carboxybenzoyl)glycine in Aqueous Organic Solvents. The Journal of Organic Chemistry, 1996. **61**(23): p. 8063-8068.
- 59. Russo Krauss, I., et al., *An overview of biological macromolecule crystallization*. Int J Mol Sci, 2013. **14**(6): p. 11643-91.
- 60. Meng, X.-Y., et al., *Molecular Docking: A powerful approach for structure-based drug design.* Curr Comput Aided Drug Des, 2011. **7**(2): p. 146-157.
- 61. Shoichet, B.K., et al., *Lead discovery using molecular docking*. Current Opinion in Chemical Biology, 2002. **6**(4): p. 439-446.
- 62. Schulz, M.N., et al., *Design of a fragment library that maximally represents available chemical space*. J Comput Aided Mol Des, 2011. **25**(7): p. 611-20.
- 63. Marley J, L.M., Bracken C., *A method for efficient isotopic labeling of recombinant proteins*. J Biomol NMR, 2001. **20**(1): p. 71-75.

- 64. Corbeil, C.R., P. Englebienne, and N. Moitessier, *Docking ligands into flexible and solvated macromolecules*. 1. Development and validation of FITTED 1.0. J Chem Inf Model, 2007. 47(2): p. 435-49.
- 65. Bhattacharyya, S., O.W. Gooding, and J. Labadie, *Expedient synthesis of secondary amines bound to indole resin and cleavage of resin-bound urea, amide and sulfonamide under mild conditions*. Tetrahedron Letters, 2003. **44**(32): p. 6099-6102.
- 66. Fieser, L.F. and M. Fieser, *Reagents for Organic Synthesis*. 1967.
- 67. Aurrecoechea, N., et al., 2-[1H-Benzimidazol-2(3H)-ylidene]-2-(pyrimidin-2-yl)acetamides and 2-[benzothiazol-2(3H)-ylidene]-2-(pyrimidin-2-yl)acetamides as kinase inhibitors. 2010.
- 68. Hisashi, T., et al., *Intraocular pressure lowering agents containing phenylenediamine derivatives as the active ingredient.* 2008.
- 69. Ungwitayatorn, J., et al., *Synthesis and HIV-1 Reverse Transcriptase Inhibitory Activity of Non-Nucleoside Phthalimide Derivatives*. Chinese Journal of Chemistry, 2008. **26**: p. 379-387.
- 70. Peter G.M. Wuts, T.W.G., *Greene's Protective Groups in Organic Synthesis*. 4th ed. 2006: Wiley. 1264.
- 71. Talybov, A.G., *Alkylation of amines with 1,3-dibromopropane, epichlorohydrin and alkyl bromides in an aqueous medium.* Azarbaycan Milli Elmlar Akademiyasi, 2007. **63**: p. 75-80.
- 72. Zhao-Xia Guo, A.N.C., David C. Horwell, *Dendroid Peptide structural mimetics of w-conotoxin MVIIA based on a 2(1H)-quinolone core*. Tetrahedron, 2000. **56**: p. 5169-5175.
- 73. Shi, T., et al., *Development of a Kilogram-Scale Synthesis of Salidroside and Its Analogs*. Synthetic Communications, 2011. **41**(17): p. 2594-2600.
- 74. Gardner, J.H. and E.O. Haenni, *Some New Local Anesthetics containing the Morpholine Ring.* JACS, 1931. **53**: p. 2736-2769.
- 75. Le Sann, C., J. Huddleston, and J. Mann, *Synthesis and preliminary evaluation of novel analogues of quindolines as potential stabilisers of telomeric G-quadruplex DNA*. Tetrahedron, 2007. **63**(52): p. 12903-12911.
- 76. Buttner, A., et al., Serotonin derivatives as a new class of non-ATP-competitive receptor tyrosine kinase inhibitors. Bioorg Med Chem, 2010. **18**(10): p. 3387-402.
- 77. Luk, K.-C., et al., 4-Amino-thieno[3,2-c]pyridine-7-carboxylic acid amides in US Patent and Trademark Office. 2005: USA.
- 78. Thorat, D.A., et al., *Synthesis and biological evaluation of 2,4-diaminoquinazoline derivatives as novel heat shock protein 90 inhibitors.* Bioorg Med Chem Lett, 2011. **21**(6): p. 1593-7.
- 79. Baker, W.R., et al., *Preparation of*[[[(methoxymethoxy)piperidinyl]carbonyl](phenyl)ethoxy]hexanamide and ethyl]norleucinamide derivatives as renin inhibitors, P.I. Appl., Editor. 1992.
- 80. Ghiron, C., et al., Novel alpha-7 nicotinic acetylcholine receptor agonists containing a urea moiety: identification and characterization of the potent, selective, and orally efficacious agonist 1-[6-(4-fluorophenyl)pyridin-3-yl]-3-(4-

- *piperidin-1-ylbutyl) urea (SEN34625/WYE-103914).* J Med Chem, 2010. **53**(11): p. 4379-89.
- 81. Perez, D.G. and N.S. Nudelman, *Carbon-carbon bond formation through the carbonylation of lithium dialkylamides. One-pot synthesis of N-alkyl-substituted formamides, glyoxylamides, and hydroxymalonamides.* The Journal of Organic Chemistry, 1988. **53**(2): p. 408-413.
- 82. Caddick, S., et al., *A generic approach for the catalytic reduction of nitriles*. Tetrahedron, 2003. **59**(29): p. 5417-5423.
- 83. Singh, J., et al., A Practical Synthesis of an Anti-Methicillin ResistantStaphylococcusaureusCephalosporin BMS-247243. Organic Process Research & Development, 2000. **4**(6): p. 488-497.
- 84. Rios-Lombardia, N., et al., *Enzymatic desymmetrization of prochiral 2-substituted-1,3-diamines: preparation of valuable nitrogenated compounds.* J Org Chem, 2009. **74**(6): p. 2571-4.
- 85. Anelli, P.L., F. Montanari, and S. Quici, *Lipophilic Cage Ligands Containing Two Tightly Connected 1,7-Dioxa-4,10-diazacyclododecane Rings: Synthesis and X-ray Structure of a Sodium Perchlorate Complex* J. Org. Chem., 1988. **53**: p. 5292-5298.

Appendix A

```
#!/bin/bash
# Generate difference map cancelling noise by thresholding
and using that as a mask.
# arguments ifname1, ifname2, ofname
V = "1.15"
v = "115"
#echo ""
            NMR DiffLight v$V"
#echo "Eric Habib - McGill University Chemistry"
#echo ""
if [ "$1" = "--help" ]; then
   echo "Usage: difflight_anim$v.com FT2FILE1 FT2FILE2
OUTFILE [OPTIONS]"
    echo " or: difflight_anim$v.com --help"
    echo "Creates a two frame animation of the spectra with
the differences"
   echo "highlighted in blue for increase from FILE1 to
FILE2 or decrease in red"
   echo ""
    echo "Mandatory arguments:"
   echo "FT2FILE1 and FT2FILE2 .ft2 files of
spectra to be compared"
                                 .gif file of output
    echo "OUTFILE
animation"
   echo "Options"
   echo "-t1 pcent
                              pcent = 0-100% for noise
level cutoff"
    echo "-t2 pcent
                                  pcent = 0-100% for
difference detection cutoff"
                                   n = 0- amount of
blurring. Large values reduces contour difference
detection"
    echo "-n
                              preserves image of normalized
spectrum as test1n.png test2n.png"
   echo "-d
                              preserves image of difference
map diff.bmp"
    echo "-s
                              preserves indivitual spectra
as spectum1.gif spectrum2.gif"
   echo "-v
                             verbose, lists steps as they
are occuring"
    echo ""
    echo "Typical values for both THRESHOLD1 and THRESHOLD2
```

```
are 20-40% depending on the"
    echo "noise level and change in signal observed."
    echo "Quantification is qualitative not quantitative."
    echo "Please note that Difflight uses ImageMagick for
most operations as well as"
   echo "the script pipe2tiff.tcl which comes with the NMR
Pipe suite both of which"
    echo "are available free online at
http://www.imagemagick.org/script/download.php"
    echo "and http://www.nmrscience.com/nmrpipe.html
respectively."
   echo ""
    echo "This software is made available free under the
GNU Public License"
   echo "Report bugs to eric.habib@mail.mcgill.ca"
    exit -1
fi
if [ $# -lt 2 ]; then
  echo "Must give three file names."
  echo "If wildcard (*) was used, check that spelling was
correct, otherwise nothing may"
  echo "have been returned."
  exit -1
fi
if [ ! -r $1 ]; then
  echo "Input file 1 does not exist"
  exit -2
else
  INFILE1=$1
  if [[ $INFILE1 =~ ".fid/" ]]; then
    INF1=${INFILE1%.fid/*}
  if [[\$INF1 = \sim -]]; then
    INF1=${INF1##*-}
  fi
  shift
fi
#if [ ! -r $1 ]; then
# echo "Input file 2 does not exist"
# exit -2
#else
# INFILE2=$1
```

```
# shift
#fi
#OUTFILE=$1
#shift
BL="6"
TH0="90%"
            TH2="35%"; TH3="20%"
TH1="25%";
diff=0
norm=0
spec=0
verb=0
XMIN=4.65;
             XMAX = 12.65
XRES=512
XSCALE=2
XCUTLOW=6;
              XCUTHI=12
YMAX=135; YMIN=104
YRES=64
YSCALE=10
YCUTLOW=0;
             YCUTHI=0
POSCOLOR='#0000FF88'; NEGCOLOR='#FF0000088'
declare -i VAR1=0
declare -i VAR2=0
declare -i X
while [ -n "$1" ]; do
 case "$1" in
                     TH0=$1
    "-t0" ) shift;
                                      ;;
   "-t1" )
             shift;
                      TH1=$1
                                      ;;
                      TH2=$1
   "-t2" )
              shift;
                                      ;;
                    TH3=$1
BL=$1
    "-t3" )
            shift;
shift;
                                      ;;
   "-b" )
                                      ;;
   "-xmin" ) shift;
                      XMIN=$1
                                      ;;
   "-xmax" ) shift;
                      XMAX=$1
                                      ;;
   "-xres") shift; XRES=$1
                               ;;
    "-xscale" )
                  shift; XSCALE=$1 ;;
   "-xlowcut" ) shift; XCUTLOW=$1
    "-xhicut" )
                  shift; XCUTHI=$1 ;;
   "-ymin" ) shift; YMIN=$1
    "-ymax" ) shift;
                       YMAX=$1
                                      ;;
   "-yres" ) shift; YRES=$1
                                      ;;
    "-yscale" )
                   shift;
                            YSCALE=$1 ;;
    "-ycutlow" ) shift; YCUTLOW=$1
    "-ycuthi" ) shift; YCUTHI=$1 ;;
    "-poscolour") shift; POSCOLOR=$1
    "-negcolour")shift; NEGCOLOR=$1
                                      ;;
```

```
"-n" )
             norm=1 ;;
    "-d" )
              diff=1
                         ;;
    "-s" )
              spec=1
                          ;;
    "-v")
              verb=1
                         ;;
    * )
      if [[ "$1" =~ ".ft2" ]]; then
     if [ $verb -eq 1 ]; then
       echo $1 being processed
     fi
     INFILE2[$VAR1] = $(echo -n $1)
     if [ ! -r $1 ]; then
      "Input file $1 not readable"
      exit -1
     fi
     if [[ ${INFILE2[$VAR1]} =~ ".fid" ]]; then
      temp=${INFILE2[$VAR1]%.fid/*}
     fi
     if [[ "$temp" =~ "-" ]]; then
       NAME [\$VAR1] = \$ { temp# *- }
     fi
     OUT[$VAR1] = $(echo -n "$INF1 - ${NAME[$VAR1]}.gif")
     echo var1 $VAR1
     echo infile = ${INFILE2[$VAR1]}
     echo name = \{NAME[$VAR1]\}
     echo outfile = ${OUT[$VAR1]}
     echo
     VAR1 = \$ ( ( \$VAR1 + 1 ) )
     elif [[ "$1" =~ ".gif" ]]; then
     if [ $verb -eq "1" ]; then
       echo "Setting output file $VAR2 to $1"
     fi
     OUT[$VAR2] = $1
     VAR2 = \$ ( ( \$VAR2 + 1 ) )
      else
     echo "Unknown option '" $1 "'"
     echo "Try difflight_anim$v.com --help for more
information"
     exit
      fi
    ;;
  esac
  shift
done
```

```
# A script included with NMR Pipe that converts the nmr
data into a grayscale image.
if [ "$verb" -eq "1" ]; then
 echo "Converting Spectra for $INFILE1 and ${INFILE[*]}"
fi
tcsh -c "pipe2tiff.tcl -in ${INFILE1} -max ${TH0} -out
temp.tiff"
X=0
while [ "$X" -lt "$VAR1" ]; do
  echo X = $X
 tcsh -c "pipe2tiff.tcl -in ${INFILE2[$X]} -max $THO -out
${NAME[$X]}.tiff"
  X=$(($X + 1))
done
#rm temp.txt
# Resizing the image is for viewing ease, it is not
strictly necessary.
# Contrast stretch makes puts 2% of the darkest and
brightest pixels to their
# respective extremes, and stretches the contrast on the
rest of the image to normalize.
# Cropping removes the noise that tends to crop up in the
the low ppm of Hydrogen.
# The parameters for crop are widthxheight+Xoffset+Yoffset
if [ "$verb" -eq "1" ]; then
echo ""
echo "Resizing, normalizing, and cropping."
echo ""
fi
XRES=$( echo "$XRES*$XSCALE" | bc )
YRES=$( echo "$YRES*$YSCALE" | bc )
if [ "$XCUTHI" -ne "$XCUTLOW" ]; then
 DX=$( echo "scale=2; $XCUTHI-$XCUTLOW" | bc)
  DX=$( echo "scale=2; $XMAX-$XMIN" | bc)
fi
if [ "$YCUTHI" -ne "$YCUTLOW" ]; then
 DY=$( echo "scale=2; $YCUTHI-$YCUTLOW" | bc)
else
  DY=$( echo "scale=2; $YMAX-$YMIN" | bc)
```

```
fi
WIDTH=$( echo "$XRES*$DX/($XMAX-$XMIN)" | bc)
HEIGHT=$( echo "$YRES*$DY/($YMAX-$YMIN)" | bc)
if [ "$verb" -eq "1" ]; then
  echo "XRES= " $XRES " YRES= " $YRES
  echo "WIDTH= $WIDTH HEIGHT=$HEIGHT"
  echo "XMAX-XMIN=" $DX "YMAX-YMIN=" $DY
fi
XPPPPM=$( echo "scale=3; 1+$WIDTH/$DX" | bc)
YPP5PPM=$( echo "scale=3; 1+5*$HEIGHT/$DY" | bc)
XPPFPPM=$( echo "scale=3; $WIDTH/$DX/10" | bc)
YPPPPM=$( echo "scale=3; $HEIGHT/$DY" | bc)
\#XPPFPPM=\$(echo"1+\$WIDTH/(10*\$DX)"|bc)
#YPPPPM=$( echo "1+$HEIGHT/$DY" | bc )
#XPPPPM=$( echo "$XPPFPPM*10" | bc )
#YPP5PPM=$( echo "$YPPPPM*5" | bc )
if [ "$verb" -eq "1" ]; then
  echo "XPPPM=" $XPPPPM " YPP5PPM= " $YPP5PPM
  echo "XPPFPPM=" $XPPFPPM " YPPPPM= " $YPPPPM
fi
if [ "$XCUTLOW" -eq "0" ]; then
 XCUTLOW=$XMIN
fi
if [ "$XCUTHI" -eq "0" ]; then
 XCUTHI=$XMAX
fi
if [ "$YCUTLOW" -eq "0" ]; then
 YCUTLOW=$YMIN
fi
if [ "$YCUTHI" -eq "0" ]; then
 YCUTHI=$YMAX
fi
XOFF=$( printf %.0f $( echo "($XMAX-$XCUTHI)*$XPPPPM" |
YOFF=$( printf %.0f $( echo "($YMAX-$YCUTHI)*$YPPPPM" |
bc))
```

```
if [ "$verb" -eq "1" ]; then
 echo $WIDTH "x" $HEIGHT "+" $XOFF "+" $YOFF
fi
convert -resize "$XRES"x"$YRES"\! temp.tiff -normalize -
crop "$WIDTH"x"$HEIGHT"+"$XOFF"+"$YOFF" test1n.bmp
X=0
while [ "$X" -lt $VAR1 ]; do
  convert -resize "$XRES"x"$YRES"\! ${NAME[$X]}.tiff -
normalize -crop "$WIDTH"x"$HEIGHT"+"$XOFF"+"$YOFF"
${NAME[$X]}n.bmp
 X=$(($X + 1))
done
# Threshold removes any signal below a certain brightness.
Setting it as a percentage
# means on high noise images, a lot of the noise will show
up as signal. This percentage
# needs to be changed depending on the noise level of the
image.
if [ "$verb" -eq "1" ]; then
 echo "Removing noise."
 echo ""
fi
convert test1n.bmp -black-threshold $TH1 test1m.bmp
X=0
while [ "$X" -lt $VAR1 ]; do
  convert ${NAME[$X]}n.bmp -black-threshold $TH1
${NAME[$X]}m.bmp
 X=$(($X + 1))
done
if [ "$verb" -eq "1" ]; then
  echo "Generating difference map."
 echo ""
fi
# composite -compose difference test1m.bmp test2m.bmp - |
convert - -threshold 35% -blur 6x6 \
# -threshold 20% -fill '#55550001' -opaque white diff.bmp
X=0
while [ "$X" -lt $VAR1 ]; do
  composite -compose minus test1m.bmp ${NAME[$X]}m.bmp - |
convert - -threshold $TH2 -blur "$BL"x"$BL" -threshold $TH3
```

```
-fill $NEGCOLOR -opaque white ${NAME[$X]}dminus.bmp
  composite -compose minus ${NAME[$X]}m.bmp test1m.bmp - |
convert - -threshold $TH2 -blur "$BL"x"$BL" -threshold $TH3
-fill $POSCOLOR -opaque white ${NAME[$X]}dplus.bmp
  composite -compose Screen ${NAME[$X]}dplus.bmp
${NAME[$X]}dminus.bmp ${NAME[$X]}diff.bmp
# Superposes the difference map onto the normalized spectra
  composite ${NAME[$X]}diff.bmp -compose screen test1n.bmp
${NAME[$X]}s1.bmp
  composite ${NAME[$X]}diff.bmp -compose screen
\{NAME[X]\}n.bmp \{NAME[X]\}s2.bmp
 X=\$((\$X + 1))
done
# Gives a metric, number of pixels in the saturation map
from normal.
# Quantitates difference. Only really meaningful if
threshold values
# are absolute and identical.
if [ "$verb" -eq "1" ]; then
 echo "Calculating difference map saturation: "
fi
convert -size "$WIDTH"x"$HEIGHT" xc:black black.bmp
while [ "$X" -lt $VAR1 ]; do
  QDIFF[$X]=$(compare -metric AE black.bmp
${NAME[$X]}diff.bmp null 2>&1)
  if [ "$verb" -eq "1" ]; then
  echo "There are" $QDIFF "different pixels."
  fi
 X=$(($X + 1))
done
rm -f black.bmp
rm -f null
if [ "$verb" -eq "1" ]; then
  echo " "
  echo "Expanding to allow scale."
```

```
echo ""
fi
# Enlarges the canvas to put the gradations on the right
and bottom.
if [ ! -r "canvas.bmp" ]; then
  convert -size "$(echo "$WIDTH+100" | bc )"x"$( echo
"$HEIGHT+70" | bc )" xc:black canvas.bmp
  if [ "$verb" -eq "1" ]; then
   echo "Drawing Vertical axis"
  fi
  CURRENT=1
  COUNTI=$YCUTLOW
 OFFSET=$(printf %.0f $(echo "($YCUTLOW-$COUNTI)*$YPPPPM"
| bc))
 COUNT=$YCUTLOW
  if [ "$verb" -eq "1" ]; then
   echo "Counti=$YCUTLOW OFFSET=$OFFSET"
  fi
  while [ "$CURRENT" -lt "$HEIGHT" ]; do
    CURRENT=$(printf %.0f $(echo "($COUNT-
$YCUTLOW) *$YPPPPM+$OFFSET" | bc))
    if [ "$(($COUNT%5))" -eq "0" ]; then
      LINELENGTH=20
      convert canvas.bmp -fill yellow -font Times-Roman -
pointsize 20 -draw "text $(($WIDTH+30)),$(($CURRENT+7))
'$COUNT'" canvas.bmp
    else
      LINELENGTH=15
    fi
    convert canvas.bmp -stroke yellow -strokewidth 1 -draw
"line $WIDTH, $CURRENT $(($WIDTH+$LINELENGTH)), $CURRENT"
canvas.bmp
   COUNT=$(printf %.0f $(echo "$COUNT+1" | bc))
  done
  if [ "$verb" -eq "1" ]; then
   echo "Drawing Horizontal Axis"
  fi
  CURRENT=1
  COUNT=0
  while [ "$CURRENT" -gt "0" ]; do
```

```
CURRENT=$(printf %.0f $(echo "$WIDTH-$COUNT*$XPPFPPM" |
bc))
    if [ "$(($COUNT%10))" -eq "0" ]; then
      LINELENGTH=25
    elif [ "$(($COUNT%5))" -eq "0" ]; then
      LINELENGTH=20
    else
      LINELENGTH=15
    convert canvas.bmp -stroke yellow -strokewidth 1 -draw
"line $CURRENT, $HEIGHT $CURRENT, $(($HEIGHT+$LINELENGTH))"
canvas.bmp
    COUNT=$(($COUNT+1))
  done
  if [ "$verb" -eq "1" ]; then
    echo "XCUTLO = $XCUTLOW"
  fi
  X=$( printf %.0f $(echo "$XCUTLOW" | bc ))
  if [ "$X" != "$XCUTLOW" ]; then
    if [ "$verb" -eq "1" ]; then
     echo -n "X = $X"
    fi
    X = \{ \{ \{ \{ \{ \} \} \} \} \} \}
  fi
  XI = $X
  while [ "$X" -lt "$( printf %.0f $( echo "$XCUTHI" | bc
))"]; do
    convert canvas.bmp -fill yellow -font Times-Roman -
pointsize 20 -draw "text $(($WIDTH-5-($(printf %.0f
XPPPPM)*(X-XI)))),$((HEIGHT+45)) '$X'" canvas.bmp
    X=$[ $X+1 ]
  done
fi
X=0
while [ "$X" -lt $VAR1 ]; do
  PSAT=$( echo "scale=1; 100*${QDIFF[$X]}/$WIDTH/$HEIGHT" |
bc )
  STATS=$(echo -n ${QDIFF[$x]} "pixels or" $PSAT "%
saturation. Th1=" $TH1 "Th2=" $TH2 "Blur=" $BL)
  if [ "$verb" -eq "1" ]; then
    echo $STATS
  fi
```

```
convert canvas.bmp -fill yellow -draw "text 0,$((
$HEIGHT+62 )) '$STATS'" canvas1.bmp
  if [ "$verb" -eq "1" ]; then
   echo "Creating frames."
    echo ""
  fi
  composite -gravity NorthWest ${NAME[$X]}s1.bmp
canvas1.bmp - |\
  convert - -fill yellow -gravity "north-west" -draw "text
0,0 '$INFILE1'" ${NAME[$X]}sp1.gif
  composite -gravity NorthWest ${NAME[$X]}s2.bmp
canvas1.bmp - |\
  convert - -fill yellow -gravity "north-west" -draw "text
0,0 '${INFILE2[$X]}'" ${NAME[$X]}sp2.gif
  if [ "$verb" -eq "1" ]; then
   echo "Animating."
    echo ""
  fi
  convert -delay 80 -dispose None -page 866x700+0+0
\{NAME[X]\} sp1.gif -page +0+0 \{NAME[X]\} sp2.gif -loop 0
${OUT[$X]}
 X=$(($X + 1))
done
if [ "$verb" -eq "1" ]; then
 echo "Cleaning up."
fi
if [\$norm = 0]; then
 rm -f test1n.bmp
fi
X=0
while [ $X -lt $VAR1 ]; do
  echo ${NAME[$X]}
 rm ${NAME[$X]}.tiff
 rm ${NAME[$X]}m.bmp
  rm ${NAME[$X]}dplus.bmp
  rm ${NAME[$X]}dminus.bmp
  rm ${NAME[$X]}diff.bmp
  rm -f ${NAME[$X]}s1.bmp
```

```
rm -f ${NAME[$X]}s2.bmp
  if [ $spec = 0 ]; then
   rm -f ${NAME[$X]}spl.gif
   rm -f ${NAME[$X]}sp2.gif
  fi
  if [\$diff = 0]; then
   rm -f ${NAME[$X]}diff.bmp
  fi
  if [\$norm = 0]; then
  rm ${NAME[$X]}n.bmp
  fi
  X=$(($X + 1))
done
rm -f temp.tiff
rm -f test1m.bmp
rm -f canvas.bmp
rm -f canvas1.bmp
if [ "$verb" -eq "1" ]; then
  echo "Output in" $OUTFILE
fi
echo -n $PSAT ""
exit 0
```

Appendix B - Component Compounds of Mixtures